Università degli Studi di Sassari

Department of Biomedical Sciences

Ph.D. in Life Sciences and Biotechnologies

XXXVI cycle

Coordinator: Prof. Daria Sanna

Genome-Wide Fitness Signatures of MRSA Across Skin, Systemic, and Blood Infections

A Thesis Submitted for The Degree of Doctor of Philosophy

Ph.D. candidate: Sally Waheed Ahmed Ismail Yousief

Supervisor: Dr. Bianca Paglietti

Co-Supervisor: Prof. John Elmerdahl Olsen

Abstract

Staphylococcus aureus (particularly methicillin-resistant *S. aureus* (MRSA) is a leading cause of severe community and hospital-acquired infections worldwide. Its remarkable capacity to adapt to diverse host environments and resist multiple antimicrobials poses an urgent public health challenge. Understanding the genetic determinants that underpin MRSA fitness across distinct infection niches is essential for developing new therapeutic strategies. This thesis combines methodological innovation with *in vivo* and *ex vivo* functional genomics to map the metabolic rewiring and context-specific vulnerabilities of epidemic USA300 MRSA.

The first study **(Paper I)** focused on optimizing the construction of a highly saturated transposon mutant (tn-mutant) library of MRSA, a prerequisite for robust transposon insertion sequencing (TIS) studies. Using a *Himar1*-based two-plasmid system, we enhanced phage ϕ11 transduction efficiency via chloramphenicol pretreatment and an in-house enriched medium and implemented an optimized plasmid curing protocol. These improvements yielded a library with over 400,000 unique insertions, the most saturated to date in *S. aureus*, providing comprehensive genome coverage for downstream applications.

In the second study **(Paper II)**, we applied Transposon-Directed Insertion Site Sequencing (TraDIS) in murine models of skin, kidney, and spleen infection to identify tissue-specific fitness genes. A three-step filtering approach identified 46, 76, and 69 genes required for fitness in skin, kidney, and spleen, respectively. The gluconeogenesis genes *fbp* was essential across all tissues, while *pckA* (kidney) and *gapB* (spleen) displayed organ-specific essentiality. Skin infection uniquely depended on oxidative stress and DNA repair genes (*ahpC, ahpF, dps, uvrC, xseA*), whereas systemic infection relied on branched-chain amino acid catabolism (*bkdAB*), lipid metabolism (*SAUSA300_0355*), and putative polyamine biosynthesis (*SAUSA300_0458*).

The third study (**Accepted Manuscript III**) investigated MRSA adaptation to the intravascular environment using freshly collected human blood. TraDIS identified 76 essential genes. As proof of concept, competition assays in blood confirmed the fitness defects of *purA, purB, fbp, hssR*, and *aroA2* genes. Interestingly, disruption of certain regulators (*saeRS, σ^B*) and adhesins (*fnbA, clfA*) genes conferred a competitive advantage, revealing a potential trade-off between virulence regulation and survival in blood.

Collectively, the findings of this thesis establish a genome-scale framework of MRSA fitness requirements across tissue and blood environments, highlight conserved and niche-specific metabolic

dependencies, and identify novel vulnerabilities for therapeutic targeting. By integrating methodological advances in tn-mutant library construction with high-resolution *in vivo* and *ex vivo* functional genomics, this work expands our understanding of MRSA adaptation and paves the way for targeted interventions against this formidable pathogen.

Preface

This Ph.D. thesis was submitted to the University of Sassari to fulfill the requirements for obtaining a Ph.D. degree. The research presented in this thesis was conducted from 2022 to 2025 under the supervision of Dr. Bianca Paglietti as the main supervisor. Library construction and human blood experiments were carried out at the Department of Biomedical Sciences, University of Sassari while the sequencing and the animal experiments were conducted at the University of Copenhagen. During my Ph.D. program, I undertook three secondments at the University of Copenhagen. One was conducted under the supervision of Professor Luca Guardabassi, and the other two under the supervision of Professor John Elmerdahl Olsen. This Ph.D. project is part of the INNOTARGETS European Training Network and received funding from the European Union's Horizon 2020 Research and Innovation Program under the Marie Skłodowska-Curie Grant Agreement No. 956154.

Sally Waheed Yousief
Sassari, 2025

INNOTARGETS

This project has received funding from the European Union's Horizon 2020 research and innovation programme under the Marie Skłodowska-Curie grant agreement No 956154

Acknowledgements

I would like to express my deepest and most heartfelt gratitude to my family, whose unconditional love and support have carried me through every stage of this journey. To my mother, my brothers, and my sister: your encouragement, patience, and constant support have been the foundation of my strength. To my father, who passed away more than ten years ago, I carry your memory with me every day. I hope that, wherever you are, you are proud of this milestone and of the person I have become. Your absence has never diminished your presence in my life.

My heartfelt gratitude goes to my master's supervisor, Dr. Taha Zagloul, who sadly passed away two years ago. His belief in my potential and his early mentorship were essential in shaping the foundations of my scientific path. I carry his guidance with me in every step of my career.

I am deeply grateful to my PhD supervisor, Dr. Bianca Paglietti, for her unwavering support, guidance, and patience throughout this long journey. Thank you for standing beside me through every difficulty, for your support during the long visa process, and for your constant belief in my work and abilities. I hope that all the challenges we faced along the way now feel worth it.

A special thanks goes to my colleague Nader Abdelmalek, whose collaboration was essential in constructing the mutant library that became the foundation of this entire project. Your dedication, teamwork, and scientific rigor played a fundamental role in the success of this research.

My sincere appreciation also goes to the wonderful teams at the University of Copenhagen, Department of Veterinary and Animal Sciences, whose expertise, kindness, and collaboration made my secondment both scientifically productive and personally enriching. I am deeply grateful to Professor John Olsen and his group, especially Sajid Nisar and Tanjia, for their generous support and assistance during the *in vivo* experiments. I extend my gratitude to Professor Luca Guardabassi and his research group, with special thanks to my colleague and a brother to me Yibing Ma (Lowrence) and Assistant Professor Mattia Pirolo, whose expertise and collaboration enriched this work. I would also like to thank Assistant Professor Martin Saxtorph Bojer for his invaluable guidance and hands-on assistance during critical experimental phases.

I'm thankful for being part of INNOTARGETS, one of the MSCA programs that provided not just scientific opportunities but also the chance to connect with a wonderful team from all levels,

administration, professors, and colleagues. A special thanks to Linda, Hetti, and Jennifer. Getting to know all of you and the rest of the team was a fantastic opportunity to form friendships, experience new cultures, and share new perspectives on life.

As Ibn Khaldun once reflected, the productivity of a society comes from the collective effort and cooperation of its members. In that spirit, I recognize that this journey and its successes are not mine alone but the result of a shared endeavor.

I am also grateful to all my colleagues in Sassari, whose friendship and everyday kindness helped me adapt to a new environment. I especially thank Sepideh, who helped me greatly during when I first arrived in Sassari before moving to the United States, and Hajra, whose friendship made this journey far less lonely and far more meaningful. I would also like to extend my appreciation to Dott.ssa. Antonella Santona for her support during my early adaptation period in the lab.

Finally, at both the beginning and end of this journey, I give my deepest thanks to my Lord for all the opportunities, protection, and guidance throughout. For every moment and every person, He placed around me, or kept away for my own good, I offer my heartfelt gratitude. This accomplishment is a testament to that enduring support. **And He is with you wheresoever ye may be. And Allah sees well" (all that ye doAl Qur'aan [57:4])**".

To all of you: thank you for being part of this journey.

List of Abbreviations

ABBREVIATION	DEFINITION
AAA	Aromatic amino acid(s)
ACME	Arginine Catabolic Mobile Element
AGR	Accessory Gene Regulator (quorum-sensing system)
AHPCF	Alkyl hydroperoxide reductase system (AhpC + AhpF)
AMR	Antimicrobial resistance
ANOVA	Analysis of variance
ATP	Adenosine triphosphate
BALB/C	BALB/c inbred mouse strain
BCAA	Branched-chain amino acid(s)
BCFA	Branched-chain fatty acid(s)
BHI	Brain Heart Infusion
BHIA	Brain Heart Infusion agar
CA-MRSA	Community-associated methicillin-resistant Staphylococcus aureus
CC	Clonal complex
CCPA	Catabolite control protein A
CFU	Colony-forming unit
CFU/ML	Colony-forming units per milliliter
CI	Competitive index
CO	Outgrowth Control → Output contrast
DADO	Deoxyadenosine
DNA	Deoxyribonucleic acid
DPBS	Dulbecco's phosphate-buffered saline
ETC	Electron transport chain
EU	European Union
FASII	Type II fatty acid synthesis pathway
FDR	False discovery rate
FPP	Farnesyl diphosphate
H_2O_2	Hydrogen peroxide
HIMAR1	Himar1 mariner transposon
HRTAB	Heme-regulated transporter operon AB
HSSRS	Heme-sensing two-component system
IL-10	Interleukin-10
INNOTARGETS	Innovative Targets for Antimicrobials (MSCA-ITN program)
IO	Input → Output contrast
IP	Intraperitoneal
IPP	Isopentenyl diphosphate
JE2	USA300 JE2 MRSA strain
LA-MRSA	Livestock-associated MRSA
$LOG_{10}CI$	Base-10 logarithm of the competitive index
LOG_2FC	Log_2 fold change
LOGCPM	Log_2 counts per million
M9	M9 minimal medium
MB	Mouse B (skin sample with bottleneck)
MDSC	Myeloid-derived suppressor cell

MNTABC	Manganese ABC transporter system
MOI	Multiplicity of infection
MRSA	Methicillin-resistant Staphylococcus aureus
MSCA	Marie Skłodowska-Curie Actions
MSSA	Methicillin-susceptible Staphylococcus aureus
MVA	Mevalonate pathway
NADPH	Nicotinamide adenine dinucleotide phosphate (reduced form)
NCBI	National Center for Biotechnology Information
NE	Effective population size
NET(S)	Neutrophil extracellular trap(s)
NO·	Nitric oxide
NTML	Nebraska Transposon Mutant Library
OD_{600}	Optical density at 600 nm
PBS	Phosphate-buffered saline
PCA	Principal component analysis
PMN	Polymorphonuclear neutrophil
PPP	Pentose phosphate pathway
PRJNA	Prefix for NCBI BioProject accessions
PVL	Panton–Valentine leukocidin
QC	Quality control
Q-VALUE	FDR-adjusted p-value
RNS	Reactive nitrogen species
ROS	Reactive oxygen species
RPU	Reads per unique insertion site
RPUFC	Read-per-unique-insertion fold change
SC	Subcutaneous
SCV	Small colony variant
SN MEDIUM	Supplemented phage-transduction medium
SRA	Sequence Read Archive
ST	Sequence type
ΣB (SIGB)	Alternative sigma factor B
TCA	Tricarboxylic acid cycle
TCS	Two-component system
TIS	Transposon insertion sequencing
TMM	Trimmed Mean of M-values (edgeR normalization)
TN	Transposon
TN-SEQ	Transposon sequencing
TRADIS	Transposon-directed insertion-site sequencing
TSA	Tryptic Soy Agar
TSB	Tryptic Soy Broth
UIS	Unique insertion site
UND-PP	Undecaprenyl pyrophosphate
USA300	Community-associated MRSA lineage USA300
USA300 JE2	Epidemic MRSA strain derivative JE2
WT	Wild type
WTA	Wall teichoic acid
XSEA	Exonuclease VII large subunit

ABBREVIATION	DEFINITION
AAA	Aromatic amino acid(s)
ACME	Arginine Catabolic Mobile Element
AGR	Accessory Gene Regulator (quorum-sensing system)
AHPCF	Alkyl hydroperoxide reductase system (AhpC + AhpF)
AMR	Antimicrobial resistance
ANOVA	Analysis of variance
ATP	Adenosine triphosphate
BALB/C	BALB/c inbred mouse strain
BCAA	Branched-chain amino acid(s)
BCFA	Branched-chain fatty acid(s)
BHI	Brain Heart Infusion
BHIA	Brain Heart Infusion agar
CA-MRSA	Community-associated methicillin-resistant *Staphylococcus aureus*
CC	Clonal complex
CCPA	Catabolite control protein A
CFU	Colony-forming unit
CFU/ML	Colony-forming units per milliliter
CI	Competitive index
CO	Outgrowth Control → Output contrast
DADO	Deoxyadenosine
DNA	Deoxyribonucleic acid
DPBS	Dulbecco's phosphate-buffered saline
ETC	Electron transport chain
EU	European Union
FASII	Type II fatty acid synthesis pathway
FDR	False discovery rate
FPP	Farnesyl diphosphate
H_2O_2	Hydrogen peroxide
HIMAR1	Himar1 mariner transposon
HRTAB	Heme-regulated transporter operon AB
HSSRS	Heme-sensing two-component system
IL-10	Interleukin-10
INNOTARGETS	Innovative Targets for Antimicrobials (MSCA-ITN program)
IO	Input → Output contrast
IP	Intraperitoneal
IPP	Isopentenyl diphosphate
JE2	USA300 JE2 MRSA strain
LA-MRSA	Livestock-associated MRSA
$LOG_{10}CI$	Base-10 logarithm of the competitive index
LOG_2FC	Log_2 fold change
LOGCPM	Log_2 counts per million
M9	M9 minimal medium
MB	Mouse B (skin sample with bottleneck)
MDSC	Myeloid-derived suppressor cell
MNTABC	Manganese ABC transporter system
MOI	Multiplicity of infection
MRSA	Methicillin-resistant *Staphylococcus aureus*

MSCA	Marie Skłodowska-Curie Actions
MSSA	Methicillin-susceptible Staphylococcus aureus
MVA	Mevalonate pathway
NADPH	Nicotinamide adenine dinucleotide phosphate (reduced form)
NCBI	National Center for Biotechnology Information
NE	Effective population size

Table of contents

CHAPTER I
GENERAL INTRODUCTION

1. Introduction

Staphylococcus aureus is a major human-associated bacterium capable of existing both as a harmless colonizer and as a highly virulent pathogen. Its remarkable ability to transition from commensal carriage to invasive disease reflects rapid and coordinated adaptation to fluctuating host derived constraints, including nutrient limitation, oxidative stress, immune surveillance, and antimicrobial exposure.[1–3] These adaptations are mediated by interconnected networks governing virulence, metabolism, immune evasion, and stress tolerance, which act as coordinated systems rather than as isolated determinants.[1] Understanding these interactions requires approaches that resolve gene function within the physiological contexts in which they operate. This thesis therefore applies genome-wide functional genomics to define the tissue-specific fitness architecture that enables methicillin-resistant *S. aureus* (MRSA) to survive in the skin, deep tissues, and bloodstream.

1.1 Biology and Ecological Distribution of *S. aureus*

S. aureus is a Gram-positive, coagulase-positive coccus of the Firmicutes phylum that divides along multiple planes, forming the characteristic grape-like clusters first noted in early clinical descriptions.[2] It is carried asymptomatically by a substantial fraction of the population. Persistent nasal carriage occurs in roughly one quarter to one third of individuals, whereas others show intermittent or absent carriage depending on immune status, microbial competition, and environmental exposures.[4,5] The anterior nares constitute the principal reservoir, but colonization also occurs at the throat, axillae, groin, and perineum.[4,5] Although colonization is typically benign, it increases the risk of subsequent infection following barrier breach, surgery, trauma, or immunosuppression.[2,3] Transition to disease involves coordinated deployment of surface adhesins, secretable toxins, proteases, and immune-modulatory factors that facilitate adherence, immune evasion, and host tissue damage.[6,7] Surface proteins such as clumping factors and fibronectin-binding proteins promote adhesion, protein A interferes with opsonophagocytosis, and leukocidins target phagocytes, together forming redundant and synergistic mechanisms that enable survival in the face of intact host defenses.[1,3] Expression of these factors is governed by global regulatory circuits including Agr quorum sensing, the SaeRS two-component system, and nutrient responsive regulators such as CodY and CcpA, which link virulence output to nutrient availability and cellular metabolic state.[8]

Recent work demonstrates that *S. aureus* biofilms, particularly in device-associated infections, remodel local immunity by inducing Interleukin 10 (IL-10) dominated, granulocytic myeloid-derived suppressor cells (G-MDSCs) rich microenvironments that suppress macrophage effector function, thereby promoting persistence despite immune infiltration.[9–11]

1.2 Emergence and Global Spread of Methicillin-Resistant *S. aureus* (MRSA)

Shortly after the introduction of penicillin, β-lactamase-mediated resistance emerged in *S. aureus*, driving the development of methicillin in 1959.[12] However, resistance to methicillin appeared rapidly with the acquisition of *mecA*, encoding the low-affinity penicillin-binding protein PBP2a, which confers broad β-lactam resistance.[13] For decades, methicillin-resistant *S. aureus* (MRSA) circulated primarily in hospitals, where heavy antibiotic use and vulnerable hosts favored sustained transmission and accumulation of multidrug resistance, giving rise to what became known as hospital-associated MRSA (HA-MRSA).[14]

In the late 1990s and early 2000s, community-associated MRSA (CA-MRSA) emerged independently of healthcare environments.[15,16] Among these, the USA300 lineage (ST8), often carrying the arginine catabolic mobile element (ACME), became the dominant strain in North America and subsequently spread globally.[14,16,17] Genomic analyses revealed that USA300 combines potent cytolytic toxins, regulatory tuning, and enhanced metabolic fitness in skin and soft tissue environments, facilitating epidemic success.[14,16,17] Although MRSA remains a major contributor to global antimicrobial resistance (AMR), recent epidemiological analyses indicate that the overall burden of methicillin-susceptible *S. aureus* (MSSA) infection remains equal or greater in many regions, underscoring that epidemic success in *S. aureus* is driven not solely by resistance but by efficient host adaptation, colonization, and survival traits.[1,18]

Concerns about rising resistance persist. Ceftaroline resistance arising through PBP2a mutations has been documented in clinical MRSA isolates,[19,20] and daptomycin resistance involves complex cell envelope remodeling detectable through transcriptomic and proteomic changes.[21] Reduced susceptibility to glycopeptides and lipoglycopeptides, including dalbavancin, has also emerged in *Staphylococcus epidermidis* and *S. aureus* during treatment,[22,23] highlighting the precariousness of current therapeutic options.

1.3 USA300 JE2 as a Platform for Functional Genomics

USA300 JE2 is a widely used laboratory-adapted derivative of the epidemic USA300 lineage that preserves key virulence and metabolic features while enabling efficient genetic manipulation. [24] It serves as the background for the Nebraska Transposon Mutant Library (NTML), a comprehensive single-insertion library covering most nonessential genes, which facilitates rapid functional screening. [24] The strain's amenability to phage-mediated transduction, tolerance of chromosomal insertions, and reproducible pathogenesis in murine infection models make it an advantageous platform for constructing saturated transposon mutant libraries and performing genome-wide fitness profiling under host-like conditions.[24] Because *S. aureus* persists within immune niches and abscess-like microenvironments that diverge markedly from laboratory media, *in vivo* functional genomics is essential for identifying genes required for survival under physiologically relevant constraints.[1] This thesis leverages these tools to map the tissue-specific fitness architecture of MRSA.

1.4 Clinical Burden and Public Health Significance

S. aureus is a leading cause of both community- and hospital-acquired infections, spanning superficial abscesses, osteomyelitis, pneumonia, endocarditis, and bacteremia.[2,3] Bloodstream infection remains associated with high morbidity, extended hospitalization, and mortality rates of 15–30% despite optimized supportive care.[3] MRSA contributes substantially to the global AMR crisis, with *S. aureus* ranked among the highest-burden bacterial pathogens worldwide.[18] Although new agents such as ceftaroline, daptomycin, and dalbavancin have broadened therapeutic options, emerging resistance and treatment failures underscore the importance of targeting pathways that are required for survival *in vivo* rather than relying solely on classical susceptibility testing. [19–23] Accumulating clinical and experimental evidence highlights that treatment failure often results not from stable genetic resistance but from antibiotic tolerance and persistence.[1,3] This shifts therapeutic focus toward understanding physiological mechanisms of survival within host tissues.

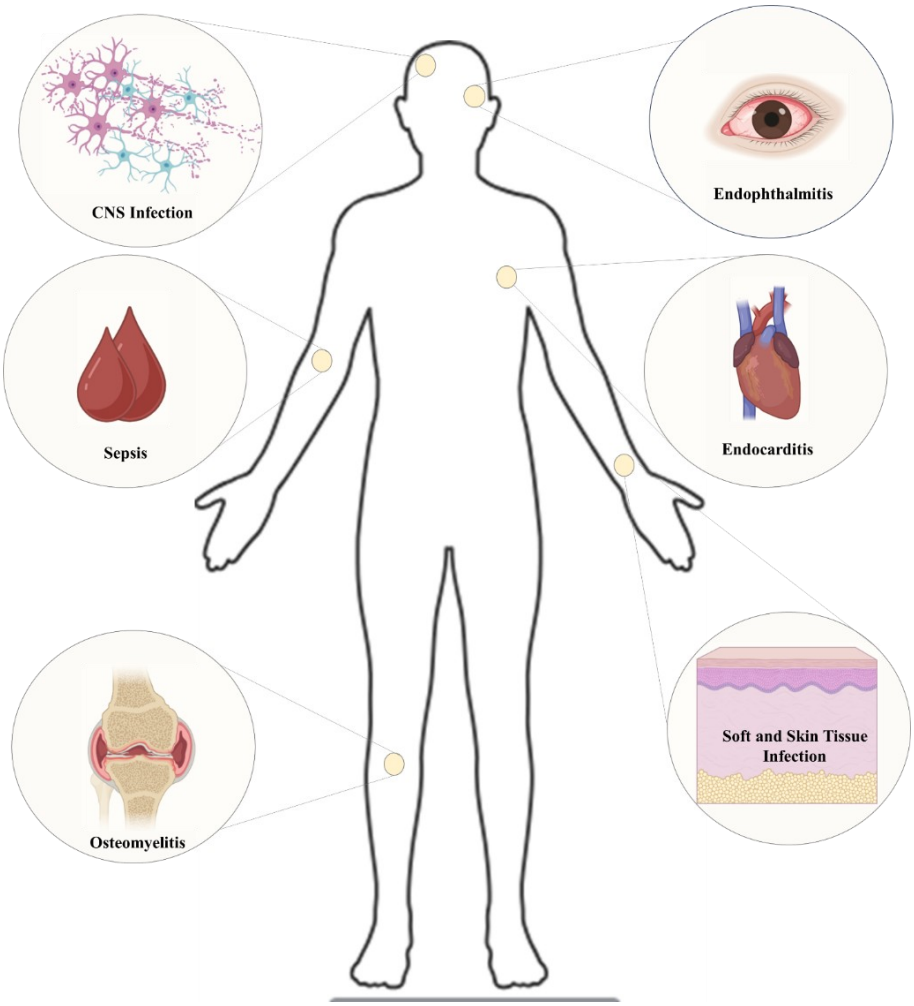

Figure 1*: *Illustration of S. aureus Infections in Different Organs.

1.5 Physiological Variation Across Infection Niches

During infection, *S. aureus* encounters diverse host environments, including the skin, mucosa, deep tissues, and bloodstream, each imposing distinct constraints on pH, osmolarity, oxygen tension, nutrient availability, and immune pressure.[25–27] These conditions shape bacterial physiology and drive niche-specific patterns of gene expression, virulence deployment, and metabolic behavior. [26,27]

On skin and mucosal surfaces, *S. aureus* must withstand low pH, high salt, desiccation, host lipids, and competition with microbiota, while evading antimicrobial peptides, pattern recognition receptors, and neutrophil recruitment.[25,28,29] During skin and soft-tissue infection, massive neutrophil influx, neutrophil extracellular trap (NET) formation, and antimicrobial peptide (AMP) release create an inflammatory milieu that selects for expression of adhesins, leukocidins, and other immune evasion factors.[28–30]

LukMF, for example, directly targets neutrophils and promotes tissue damage *in vivo*. [30] Colonization and infection are further shaped by host lipid composition and AMP–microbiome interactions.[25,28,29]

In deep tissues (bone, kidney, liver, spleen) and abscesses, bacteria reside within structured lesions characterized by hypoxia, nutrient gradients, and metal sequestration driven by nutritional immunity.[26,27,31–36] Spatially proteomics reveals altered central metabolism, increased expression of metal acquisition systems, and activation of stress responses in these niches.[31–34] In bone infection, aspartate biosynthesis becomes essential despite transport capabilities, demonstrating that tissue-specific nutrient constraints redefine metabolic requirements. [32] Osteomyelitis additionally involves dysregulated neutrophil and macrophage responses, immune checkpoint upregulation, and bone destruction, producing a chronic inflammatory environment that fails to eradicate infection.[33,37]

In the bloodstream, *S. aureus* is exposed to shear forces, complement activation, phagocytic killing, and severe metal restriction.[34–36,38] Successful dissemination requires surface adhesins (clumping factors, fibronectin-binding proteins, protein A, capsule) and coagulase-mediated fibrin shielding that support endothelial adhesion and immune evasion. [3,26,39] Nutritional immunity imposes iron and manganese starvation, countered by high-affinity bacterial uptake systems.[35,36] Macrophages function simultaneously as key immune effectors and intracellular reservoirs that permit survival, replication, or persistence.[38–40]

Across these niches, host stresses can drive antibiotic tolerance. Reactive oxygen species (ROS) produced in inflamed tissues suppress bacterial respiration and ATP, enabling survival of tolerant subpopulations despite susceptibility *in vitro*.[41,42] Macrophage derived ROS produce broad tolerance in systemic infection models,[3,41] while immune metabolites such as itaconate induce aminoglycoside tolerance.[43] Niche environments further push bacteria into metabolically slowed, stress-adapted states that reduce bactericidal antibiotic efficacy despite preserved *in vitro* susceptibility.[1] These same environments can also drive convergence of tolerance phenotypes across genetically distinct isolates,[37] while biofilms, intracellular residence, and metabolic remodeling collectively sustain persister-like populations.[42,44] For instance, biofilm associated infections can establish IL-10–rich, G-MDSCs dominated microenvironments that impair macrophage and neutrophil activity.[9,11,45]

These context-dependent physiological pressures explain why *in vitro* essentiality and susceptibility often fail to predict *in vivo* fitness.[3,25–27,37,41–44]

1.6 Metabolic and Regulatory Plasticity

Adaptation to diverse host environments requires reorganization of bacterial metabolism and regulation. Under carbohydrate limitation, *S. aureus* activates gluconeogenesis and reroutes carbon from amino acids to sustain central precursors.[31,32] Hypoxia and respiratory restriction alter tricarboxylic acid (TCA) cycle function and promote the use of alternative electron acceptors or fermentative pathways to maintain redox balance and ATP.[31,32] These shifts reflect the metabolic consequences of the nutrient and oxygen limitations described above.[25–27]

Global regulators integrate these cues; CodY couples nutrient sufficiency to repression of biosynthetic and virulence pathways, CcpA enforces carbon catabolite repression, Agr orchestrates quorum regulated transitions in secreted virulence factors, SaeRS modulates toxin and immune evasion genes, and σ^B promotes resistance to oxidative and environmental stresses.[6,8] Together, these systems coordinate metabolism, virulence, and stress responses in a manner tuned to local environmental signals.

Antibiotic tolerance is increasingly understood as a physiological outcome of this metabolic regulatory coupling rather than a fixed genetic trait. Perturbations in respiration, ATP levels, and global stress-response activation transiently shift bacterial subpopulations into less susceptible states.[1,3,31,32,41–44] These reversible tolerance phenotypes underscore the importance of genome-wide strategies that can resolve gene contributions across multiple physiological landscapes.

Biofilm-associated environments provide a clear example of how metabolic remodeling shapes immune interactions. Lactate production inhibits histone deacetylase 11 (HDAC11), driving elevated IL-10 production in macrophages and G-MDSCs and promoting immune suppression. [46] ATP synthase activity contributes to biofilm persistence by maintaining metabolic stability within structured communities,[47] while alterations in formate metabolism affect biofilm architecture and diminish toxin-induced immune modulation.[48]

Although not the analytical focus of this thesis, these mechanisms exemplify how local environmental signals can reshape metabolic pathways and immunomodulatory outcomes during infection, reinforcing the broader conceptual framework of niche driven adaptation. Together, these connections bridge the immunosuppressive microenvironments introduced in Sections 1.1 and 1.5 with the metabolic plasticity that sustains chronic infection, persistence, and tissue-specific survival strategies.

1.7 Genome-Wide Functional Genomics and TraDIS

Traditional genetic approaches such as allelic replacement mutants, conditional knockdowns, and complementation studies have been fundamental for defining the role of individual virulence factors, metabolic enzymes, and regulatory components in *S. aureus* and other bacteria. These methods have been particularly important for dissecting regulatory networks and virulence circuits in *S. aureus* but are inherently low-throughput and usually interrogate one locus at a time.[49] Because infection phenotypes emerge from coordinated, pathway level responses rather than isolated single gene effects, understanding *S. aureus* pathophysiology requires approaches that can probe the contributions of thousands of genes in parallel under physiologically relevant constraints.[50]

High density transposon mutant libraries enable genome-scale fitness analysis by generating large populations of mutants in which each non-essential gene is disrupted by a transposon insertion. This strategy was established in several bacterial pathogens using transposon-insertion sequencing (TIS) methods such as Tn-Seq (transposon sequencing), HITS (high-throughput insertion tracking by deep sequencing), and INSeq (insertion sequencing) and TraDIS.[51–54] When these libraries are exposed to *in vivo* or stress-defined conditions, changes in mutant representation provide a quantitative measure of each gene's contribution to survival.[55] This approach captures not only genes that are required for fitness under the tested conditions, but also genes whose disruption confers a competitive advantage, thereby revealing regulatory costs, immune visibility trade-offs, and metabolic burden states that would be undetectable with classical loss of function genetics.[50,55–57]

Transposon-Directed Insertion-site Sequencing (TraDIS) and related TIS methods map insertion sites at (near) base-pair resolution and allow robust quantification of mutant abundance across conditions. The original TraDIS implementation in *Salmonella Typhi* and subsequent work established dense libraries ($>10^5$–10^6 mutants) that can be queried across many environments.[54] TraDIS-style approaches have since been adapted to *S. aureus*, where ultra high-density *Himar1*-based libraries have been used to define essential genes and virulence regulators and to perform *in vivo* infection screens.[58] In infection studies, TraDIS is particularly powerful because libraries can be recovered directly from infected tissues or *ex vivo* host milieus, minimizing out-of-host passaging that might erase niche specific fitness signatures.[59] Importantly, TIS readouts capture both decreases and increases in mutant frequency, allowing the simultaneous identification of essential pathways and condition-specific anti-fitness genes within the same experiment.[50]

However, *in vivo* infection experiments often impose strong population bottlenecks in which only a fraction of the initial library establishes infection, particularly in deep organs or highly restrictive niches. Experimental factors such as suboptimal library saturation, loss of diversity during storage or inoculum preparation, and severe host-imposed bottlenecks can all cause stochastic extinction of mutants and thereby spuriously mimic gene essentiality.[55] Careful experimental design, including very high library complexity, controlled inoculum sizes, biological replicates, and appropriate *in vivo* outgrowth periods, combined with post-hoc analysis of insertion site distributions, read depth metrics, and population-genetic modelling is therefore critical to distinguish true biological essentiality from bottleneck driven artifacts and to ensure that TraDIS-based fitness maps faithfully represent the underlying infection biology.[55] Together, these methodological advances create the foundation required for the high-saturation, *in vivo* focused functional genomics framework developed in this thesis.

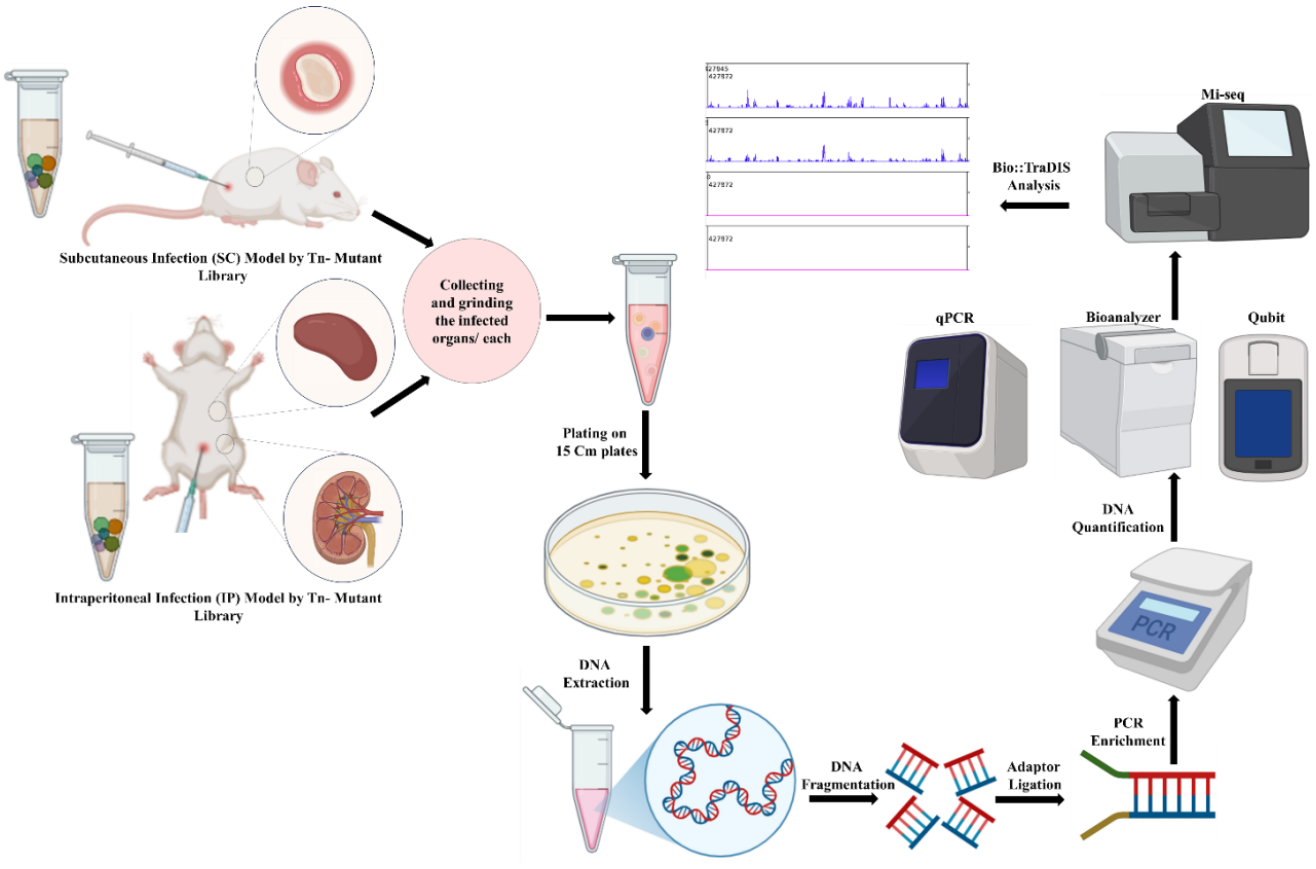

Figure 2: Overview of In Vivo Screening and TraDIS Analysis Steps.

1.8 Rationale for High-Saturation TraDIS in USA300 JE2

Understanding how *S. aureus* survives within the diverse microenvironments of the host requires experimental strategies that resolve gene function under physiologically relevant constraints. Although *in vitro* studies have clarified many aspects of *S. aureus* metabolism and regulation, they cannot reproduce the spatial, metabolic, and immunological heterogeneity of skin, deep tissues, and the bloodstream.[60–62] These physiological gradients reshape bacterial behavior in ways that fundamentally alter survival requirements.[1,61–64]

High-saturation transposon mutagenesis combined with TraDIS provides a systematic framework to overcome these limitations. By testing tens of thousands of mutants in parallel, TraDIS identifies conditionally essential genes and mutations that confer a competitive advantage capabilities unattainable with classical one gene at a time genetics, while genes that cannot tolerate insertions are inferred as essential.[50,55,57,59] The USA300 JE2 background offers a clinically relevant and genetically tractable platform for this approach. As a representative CA-MRSA lineage, it retains epidemic virulence properties while supporting efficient phage transduction, plasmid curing, and high-density mutagenesis.[24] High-quality functional genomic resources, including the NTML and recent ultra dense *Himar1* libraries, demonstrate the suitability of JE2 for genome-scale interrogation of virulence, metabolism, and stress survival.[24,58]

By integrating a high-saturation *Himar1* library with *in vivo* and *ex vivo* TraDIS profiling, this thesis defines the genetic architecture that supports MRSA fitness across skin, kidney, spleen, and human blood. This unified framework identifies both conserved metabolic dependencies and niche specific adaptive modules shaped by nutrient limitation, oxygen tension, and immune pressure. In doing so, it provides insight into the physiological logic of *S. aureus* survival within host environments and highlights vulnerabilities that may be exploited for therapeutic intervention.

CHAPTER II

AIMS AND OBJECTIVES

2. Aims and Objectives

The primary objective of this Ph.D. project was to investigate the contribution of non-essential genes to MRSA survival and fitness in skin, systemic, and human-blood environments using high-throughput functional genomics. To address this overarching goal, the research was organized into two published papers and one accepted manuscript, each examining a distinct component of MRSA pathophysiology:

- **Paper I – "Optimizing Phage-Based Mutant Recovery and Minimizing Heat Effects in the Construction of Transposon Libraries in *Staphylococcus aureus*"**: This study establishes an optimized workflow for generating highly saturated *S. aureus* transposon mutant libraries suitable for robust transposon insertion sequencing analyses.
  This chapter is based on a published article in *Scientific Reports* (2024), published by Springer Nature. This material is used in accordance with the publisher's self-archiving and thesis inclusion policies.10.1038/s41598-024-73731-y

- **Paper II – "Genome-Wide Identification of Tissue-Specific Fitness Genes in Murine Models of *Staphylococcus aureus* Infection"**: This work defines the organ-specific genetic requirements that enable MRSA survival in skin, kidney, and spleen during *in vivo* infection in mice.
  This chapter is based on a published article in *iScience* (2025), published by Cell Press (an imprint of Elsevier). This material is used in accordance with the publisher's self-archiving and thesis inclusion policies. https://doi.org/10.1016/j.isci.2025.114261

- **Accepted Manuscript III – "Profiling Genetic Determinants Required for Fitness of Community-Associated Methicillin-Resistant *Staphylococcus aureus* During Growth in Human Blood"**: This manuscript characterizes the fitness landscape of MRSA in fresh human blood, identifying genes required to withstand immune pressure and nutrient limitation.
  This chapter is based on accepted for publication in Microbiology Spectrum 2026, publishing by America Society for Microbiology.

Together, these three studies provide an integrated, genome-wide framework that maps how MRSA reprograms its physiology across distinct infection environments, defining the tissue- and condition-specific genetic signatures that underpin its success as a pathogen.

CHAPTER III
MANUSCRIPTS

Optimizing phage-based mutant recovery and minimizing heat effect in the construction of transposon libraries in *Staphylococcus aureus*

Sally W. Yousief [1] †, Nader Abdelmalek [1] †, Bianca Paglietti [1] *

[1] Department of Biomedical Sciences, University of Sassari, Sassari, 07100, Italy

†These authors contributed equally to this work

*Corresponding author: Bianca Paglietti, Email: biancap@uniss.it

Published in Scientific Reports. October 2024 10.1038/s41598-024-73731-y

Abstract

Staphylococcus aureus (S. aureus), particularly Methicillin-resistant *S. aureus* (MRSA), poses a significant global public health threat, necessitating advanced methodologies to enhance our understanding of this organism at the omics levels. This study introduces a refined protocol for constructing and curing high-density transposon mutant (tn-mutant) libraries in *S. aureus*, addressing the challenges associated with low transductant yields, and the complex genetic manipulation mechanism in Gram-positive bacteria. Our methodology employs a *HimarI* transposon based on a two-plasmid system, leveraging Himar1's high insertional efficiency in AT-rich organisms. Enhanced transduction efficiency was achieved through chloramphenicol pre-treatment and the use of modified enriched media. Complementing this, an optimized plasmid curing procedure ensured a representative and stable tn-mutant library. The protocol was successfully applied to multiple *S. aureus* strains, demonstrating an increase in mutant recovery and reduced post-curing impact. The method offers a robust approach for Transposon Insertion Sequencing (TIS) applications in *S. aureus*, enabling deeper insights into survival, resistance, and pathogenicity mechanisms. This protocol holds a significant potential for accelerating the construction of tn-mutant libraries in various *S. aureus* strains.

Keywords: Transposon insertion sequencing, *Staphylococcus aureus*, Himar1, Transduction, High-density Transposon mutant library, Plasmid cure

Introduction

Staphylococcus aureus (*S. aureus*), in particular, Methicillin-resistant *S. aureus* (MRSA), represents a significant global public health challenge. This bacterium is responsible for a broad spectrum of concerning diseases, including bacteremia, endocarditis, skin and soft tissue infections, bone and joint infections[1]. Given the significant health threat posed by this bacterium, there is a pressing need for advanced, high-throughput methodologies to augment our understanding and knowledge at the omics levels.

Since the discovery of the first well-characterized transposable element, Tn551, by Novick et al., transposon mutagenesis has revolutionized the field of *S. aureus* biology[2,3]. This began with the use of Tn917 in the early 90s and the construction of the first tn-mutant library containing 1248 mutants and led to the development of high-density transposon mutant (tn-mutant) libraries[4,5].

Over the last decade, there has been a growing focus on exploring the relationship between bacterial genotype and phenotype on a large scale. This exploration has been facilitated by Transposon Insertion Sequencing (TIS), a revolutionary technology that has significantly broadened our understanding of gene-behavior connections on a genome-wide scale[6,7].

A thorough understanding of these genes is crucial for the comprehension of the genetic mechanisms affecting survival, infection, resistance, and adaptation[8]. A central prerequisite for TIS is to establish robust; and saturated tn-mutant libraries[9]. A successful TIS experiment requires a comprehensive library of transposon insertions at all possible genomic sites[10]. However, constructing such libraries for *S. aureus* and other Gram-positive bacteria presents a significant challenge, in contrast to Gram-negative bacteria where kits such as EZ-tn5 can be easily employed[11,12]. The application of these methods to *S. aureus* is considerably less effective[13]. A two-plasmid system for transposition has proven to be effective in generating *S. aureus* tn-mutant libraries[13]. However, constructing such a library using this system involves several challenges[14,15]. The first critical step is the efficient insertion of the transposition system into the bacterial genome. The phage-based delivery system has proven to be a successful approach for recovering mutants, which is essential for generating a high-density tn-mutant library[12]. The second step is curing the transposition system plasmids without affecting the representation of the mutants, which can be particularly challenging for temperature-sensitive mutants[13]. This step is necessary to ensure plasmid-free mutants, thereby maintaining the stability of the transposon insertions within the tn-mutant

library. These challenges highlight the need to refine this approach to obtain a stable, high-saturated tn-mutant library.

Our work aims to optimize the above key steps involved in constructing a tn-mutant library in *S. aureus*, by boosting transduction efficiency and minimizing the heat-induced effect during plasmid curing. This protocol, successfully applied to various *S. aureus* strains with different phylogenetic backgrounds; is expected to accelerate the generation of highly saturated tn-mutant libraries for TIS screening.

Results

We optimized a protocol for constructing and curing a tn-mutant library as shown in Figure 1. We focus on enhancing transduction efficiency by fine-tuning the multiplicity of infection, pre-treating with chloramphenicol, and adjusting the transduction medium composition. Additionally, we validate the efficacy of the Himar1 transposition system in increasing the complexity and diversity of tn-mutant libraries using Transposon directed insertion sequencing (TraDIS). Furthermore, we compare our plasmid curing protocol to the conventional method, demonstrating its effectiveness in reducing heat-induced bias and ensuring stable mutant recovery. The following subsections provide detailed insights into our findings, highlighting the improvements achieved through these optimizations.

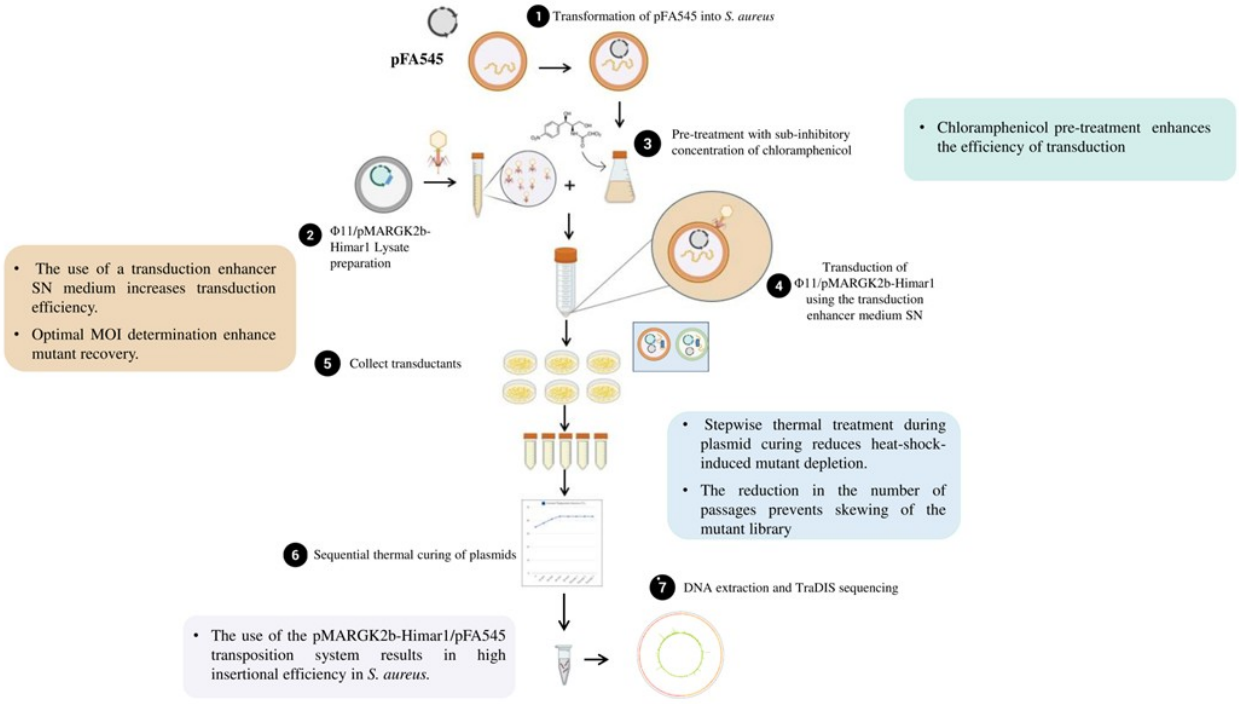

***Figure 1*: Schematic workflow of proposed optimizations for constructing tn-mutant libraries in *S. aureus*.** This figure illustrates the optimized workflow for constructing tn-mutant libraries in *S. aureus*. The key steps are sequentially numbered, beginning with the introduction of pFA545 into the strain of interest (1). This is followed by phage-based mutant recovery using ϕ11/pMARGK2b after pretreatment with chloramphenicol and the use of a transduction enhancer medium (2,3,4,5). The process continues with a stepwise thermal increase and passage reduction during the plasmid curing process (6), concluding with TraDIS (7). Details of the optimization are included in the annotation boxes.

Enhancing mutant recovery by optimizing multiplicity of infection in *S. aureus* strains

The multiplicity of infection (MOI), defined as the ratio of infecting phages to host bacterial cells, can significantly affect the infection process. We conducted experiments to determine the optimal MOI to enhance mutant recovery. A range of MOI from 0.1 to 0.6 was explored for various *S. aureus* strains, including JE2, ST398, Newman, COL, and MW2. It was observed that a high MOI was associated with an increased cell lysis, while a very low MOI was associated with reduced transduction efficiency. As depicted in Figure 2, most of the tested *S. aureus* strains showed an optimal MOI within the investigated range, with minor variations. These variations in optimal MOI among different *S. aureus* strains could be linked to several factors, such as the presence and abundance of specific phage receptors on the bacterial cell surface and the effectiveness of bacterial immune mechanisms against phages.

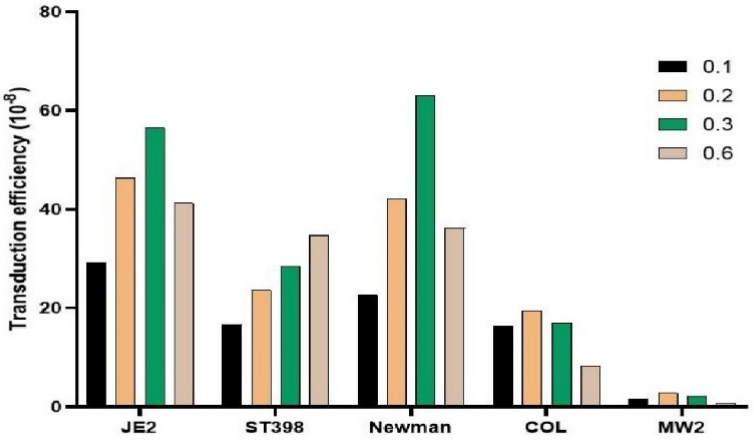

***Figure 2:* Optimal MOI for maximal transduction efficiency in *S. aureus* strains.** A significant variation in transduction efficiency across *S. aureus* strains was noted at different MOI (0.1, 0.2, 0.3, 0.6). The most substantial number of transductants is observed at an MOI of 0.2 for COL strain, MOI of 0.3 for JE2 and Newman strains, and MOI of 0.6 for ST398 strain. Although the MW2 strain generally exhibits a lower number of transductants, its highest efficiency is achieved at a MOI of 0.2.

Chloramphenicol pre-treatment and transduction medium composition improve ϕ11 transduction efficiency in *S. aureus*

Phage ϕ11 binds to its receptor on the wall teichoic acid (WTA) of bacterial cells. To increase the bacterial WTA content, a sub-inhibitory concentration of chloramphenicol was employed in parallel with tunicamycin and fosfomycin, known to inhibit WTA and decrease cell wall content, respectively. An increase in transduction efficiency of JE2 was observed in the cultures pre-treated with chloramphenicol while a significant reduction was observed with fosfomycin or tunicamycin (Figure 3). Pre-treatment with chloramphenicol showed a consistent enhancement in transduction efficiency across all tested strains (Figures 3, 4).

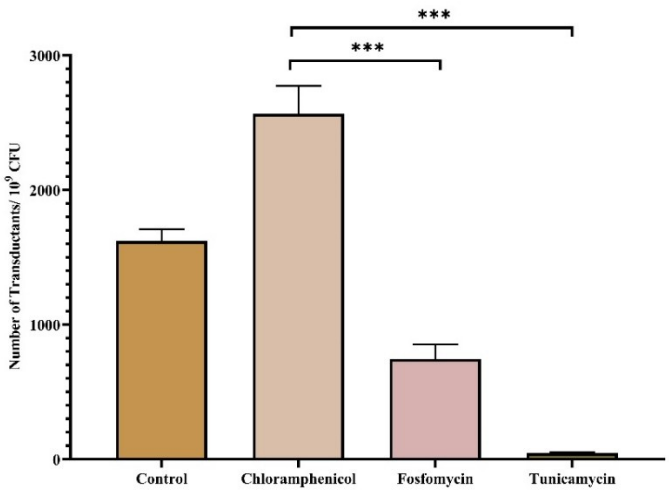

Figure 3*: Differential impact of antibiotics pre-treatment on bacterial transduction efficiency.** Comparison of the number of *S. aureus* JE2 pMARGk2b-Himar1/pFA545 transductants obtained using SN transduction medium, following cultures pre-treatment with chloramphenicol, fosfomycin, or tunicamycin. The highest yield of transductants was obtained after chloramphenicol pre-treatment. The statistical significance of these differences was determined using one-way ANOVA, followed by Tukey's multiple comparisons test. The three asterisks '' corresponds to an adjusted p-value < 0.001.

The transduction efficiency of phage ϕ11 in *S. aureus* was also significantly influenced by the composition of the transduction SN medium with 5 mM $CaCl_2$. A significant increase in transduction efficiency was observed across all tested strains, except Newman strain (Figure 4).

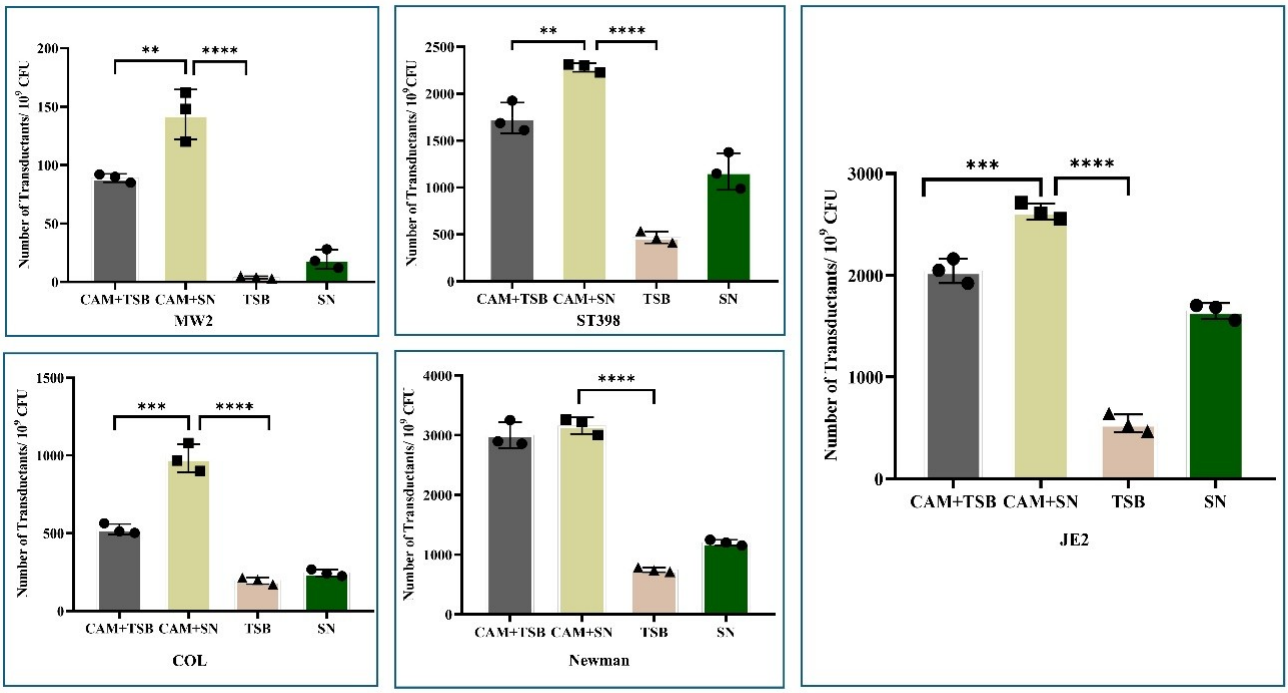

Figure 4: **Variations in transduction efficiency in TSB and SN media among *S. aureus* strains with or without chloramphenicol pre-treatment.** The use of SN medium with sub-inhibitory concentrations of chloramphenicol (SN+CAM) showed a significant increase in the number of transductants in strains JE2, MW2, ST398, and COL compared to TSB alone, TSB supplemented with chloramphenicol (TSB+CAM), and SN medium used independently. The Newman strain did not exhibit a significant difference in transductant numbers between SN+CAM and TSB+CAM conditions. However, all *S. aureus* strains tested demonstrate higher transduction efficiency in presence of SN medium plus chloramphenicol compared to SN alone. Statistical analysis was performed using one-way ANOVA, adjusted by Tukey's multiple comparison test. The significance levels are indicated as follows: * corresponds to a p-value < 0.01, ** corresponds to a p-value < 0.001, *** corresponds to a p-value < 0.0001, and **** corresponds to a p-value < 0.00001.

Himar1 transposition system enhances complexity and diversity in *S. aureus* Tn-mutant libraries

To measure the library complexity and transposition efficiency of the Himar1 transposition system. (TraDIS) was employed for both the optimized and conventional plasmid curing approaches of JE2 tn-mutant libraries (Tn-Library 1 and Tn-Library 2, respectively (Figure 5).

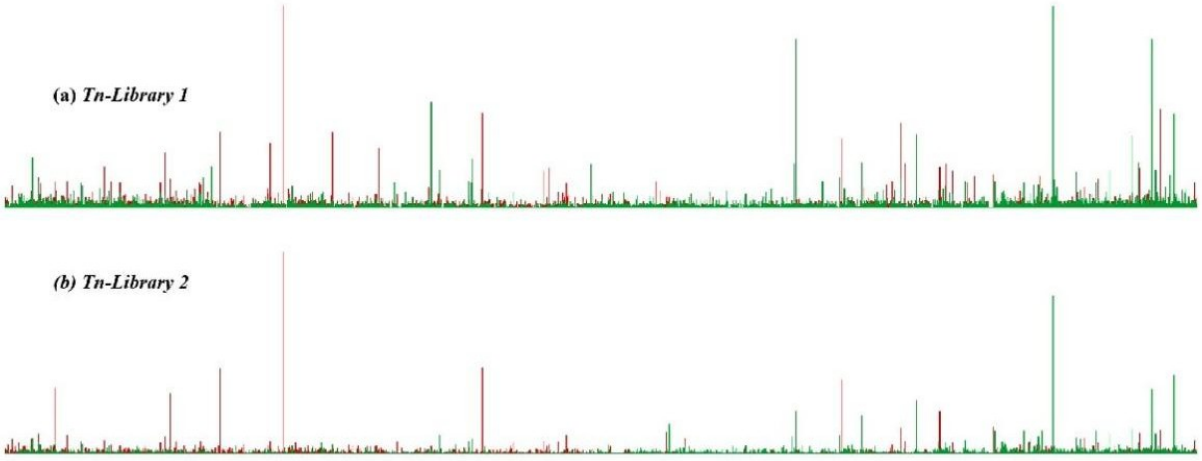

***Figure 5*: Mapping of mariner transposon insertions in *S. aureus* JE2 genome.** The plot was generated using Artemis 18.2.0. The two tracks represent the frequency and location of transposon insertions in Tn-Library 1 **(a)** and Tn-Library 2 **(b)**, in both sense and antisense orientations, which are colored in green and red, respectively. The raw transposon junction sequences were mapped and processed onto the USA300_FPR3757 reference genome.

No significant differences were observed in the quantitative aspects such as plasmids cure percentage, library size, and number of unique insertion sites (UISs) (Table 1). Linker PCR confirmed the presence of unique transposon insertions in ten randomly selected mutants prior to sequencing (data not shown).

Table 1: Library size, plasmids removal and UISs for both transposon mutant libraries.

	Library Size	% pFA545 Cure	% pMARGK2b-Himar1 cure	No. of reads	No. Of mapped reads	UISs
Tn- Library 1	2.7 x 10^9	99.99	100	24865224	19622134	446053
Tn- Library 2	1.2 x 10^9	99.93	99.99	14331985	13326649	420490

The number of unique transposon mutants in both libraries was significantly high, with more than 400,000 UISs and a coverage of more than 75% of all possible insertion sites. This was significantly higher than the two previous studies [16,17], with at least a more than 1.5-fold increase. In Tn-Library 1 and Tn-Library 2, 317 and 401 essential genes were respectively identified using the tradis_essentiality.R script, with a shared set of 310 genes (Figure 5). A total of 281 genes were common between both libraries and the essential genes reported by Grosser et al. [16] (Figure 6, Supplementary Table S2).

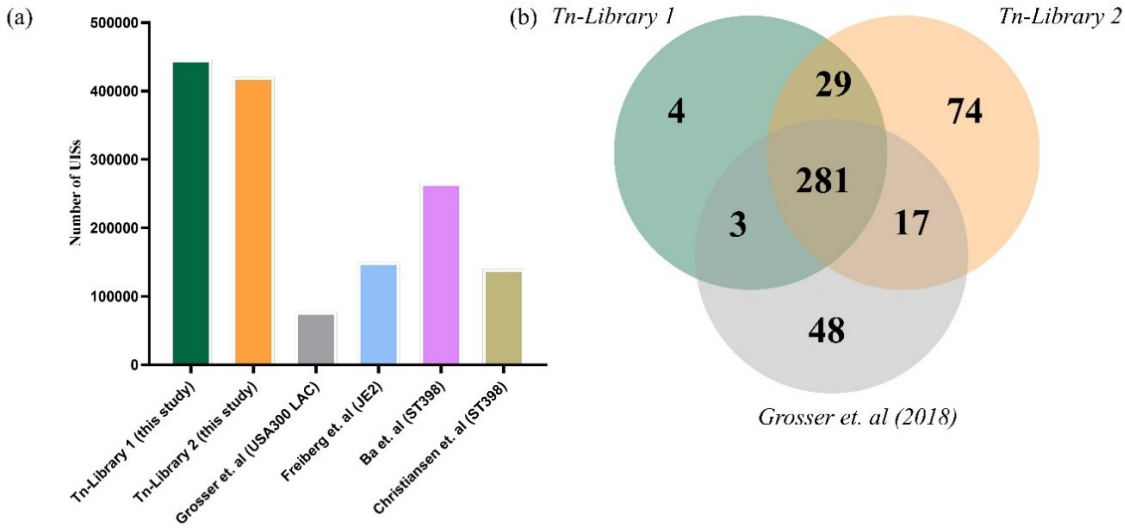

***Figure 6*: Comparative analysis of the number of UISs and essentiality in JE2. (a)** This part of the Figure presents a comparative analysis of the number of UISs in Tn-Library 1 and 2, along with other studies [16-18]. **(b)** This part of the Figure shows a Venn diagram that illustrates the distinct and shared essential genes among Tn-Library 1 (represented in green), Tn-Library 2 (represented in orange), and the study conducted by Grosser et al. [13] (represented in blue).

Gradual thermal increase and passage limitation reduce heat-induced bias in *S. aureus* tn-mutant library

After normalizing and comparing the read numbers from Tn-Library 1 and Tn-Library 2, a significant mutant depletion in Tn-Library 2 was observed compared to the slight depletion in Tn-Library 1 (Figure 7).

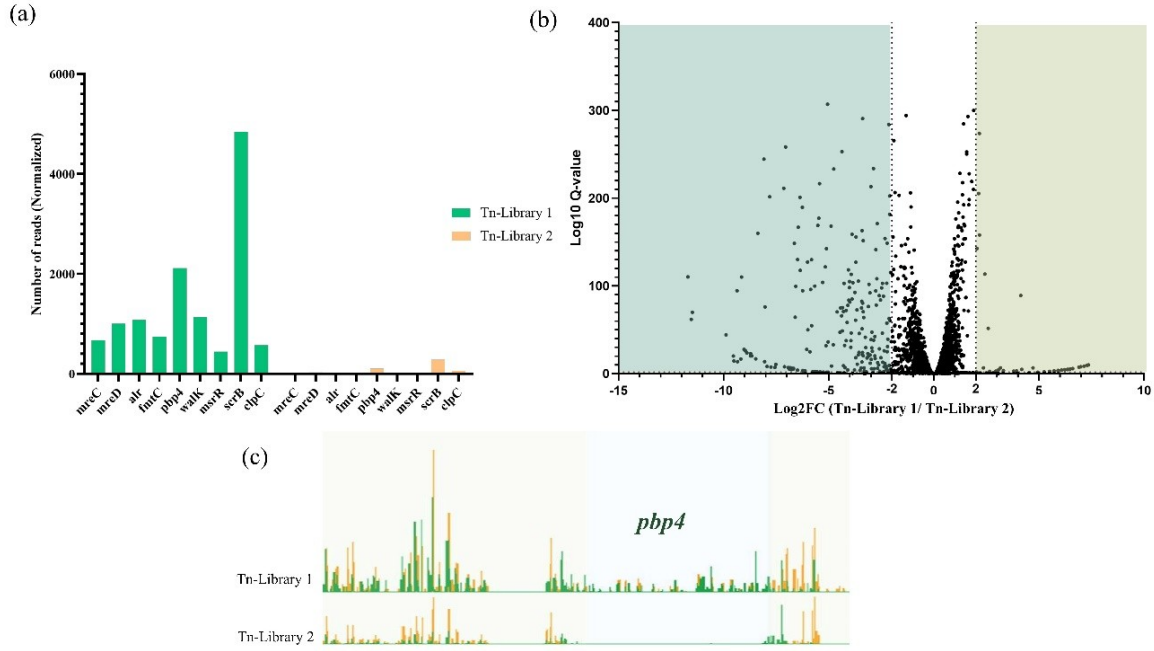

***Figure 7*: Differential gene abundance and essentiality between Tn-Library 1 and Tn-Library 2**. **(a)** This chart displays the differential abundance of normalized reads for genes identified by Santiago et al.[13], as being depleted at high temperatures, comparing Tn-Library 1 (green) and Tn-Library 2 (orange). Each gene is represented by a pair of bars showing its relative abundance in each library. **(b)**The volcano plot represents the comparative analysis of Tn-Library 1 and Tn-Library 2. Mutants that were depleted in Tn-Library 2, with a log2 fold change (log2FC) less than -2, are highlighted in jungle green. Conversely, those in Tn-Library 1 with a log2FC greater than 2 are highlighted in sage green. **(c)** Numerous transposon insertions were present in *pbp4* in Tn-Library 1, whereas they were almost absent in Tn-Library 2.

By using the *tradis_essentiality*.R script, 91 genes were identified as conditionally essential in Tn-Library 2; but not in Tn-Library 1, under their respective curing conditions. This substantial depletion of mutants in Tn-Library 2 particularly affected mutants mainly involved in cell wall biosynthesis and homeostasis (*pbp3*, *pbp4*, *fmtC*, and *auxA*) and heme biosynthesis pathway (*hemB, hemC, hemD, hemE, hemL*) (Figure 7, Supplementary Table S3).

Conversely, other genes were more enriched in Tn-Library 2 such as serine protease *htrA*, *lyrA*, *sgtB* and regulators such as the membrane two-component system member *srrB*, *rot*, *SarS* (Supplementary Table S3).

Discussion

TIS was pioneered by emerging tn-mutant libraries using high-throughput sequencing, providing a comprehensive perspective on a range of bacterial species[6]. Numerous studies on both human and livestock strains of *S. aureus* have used various TIS methodologies, including Transposon Sequencing (Tn-seq), and TraDIS[18,19,20]. Despite its promising potential, TIS has continually encountered obstacles due to the strict restrictions imposed on the genetic manipulation of multiple *S. aureus* strains[10,21]. This demonstrates the necessity for continued improvements, particularly in the generation of highly saturated and unbiased libraries to ensure the success of TIS *in vitro* and *in vivo* screens.

In this study, we present an enhanced methodology for constructing tn-mutant libraries and validate this approach in commonly studied *S. aureus* strains. The efficiency of mutagenesis protocols is influenced by several factors, including the type of transposon, the transposition system employed, transduction efficiency, and curing method to generate highly cured, comprehensive tn-mutant libraries. Although the Tn5 transposon was used to create tn-mutant libraries in *S. aureus*, enabling insertion at diverse genomic sites, it demonstrated a bias for regions with high GC content[22]. In contrast, the Himar1 transposon is constrained to insertions specifically at TA dinucleotides[23]. In *S. aureus*, the AT content constitutes approximately 67% of the entire genome, underscoring the significance of employing the Himar1 transposon to study AT-rich organisms[24].

We tested five *S. aureus* strains representing three clonal complexes (CC): CC8 (JE2, Newman, and COL), CC1 (MW2), and CC398 (ST398). These strains included both methicillin-resistant and methicillin-sensitive variants. Considering that *S. aureus* possesses a thick cell wall, a robust restriction system, and lacks an efficient delivery system via conjugation[13,25], we used a phage-based system to achieve higher transposition efficiency. The phage ϕ11-based delivery method has been successfully used to construct *S. aureus* transposon libraries[13,26,27]. Consequently, we optimized the transduction protocol for this phage to enhance the transduction efficiency across different *S. aureus* strains.

Phage ϕ11, one of the most thoroughly characterized staphylococcal phages, is frequently used as a laboratory tool for genetic manipulations. The interaction between *S. aureus* and phage ϕ11 occurs via its receptor-binding protein, which binds to α- or β-N-acetylglucosamine moieties on the cell wall WTA[28,29]. To enhance transduction efficiency, we conducted transduction experiments following pre-treatment with three different antibiotics: chloramphenicol, tunicamycin, and fosfomycin, in comparison with a no-treatment control. Our results showed a significant improvement in transduction efficiency

with a sub-inhibitory concentration of chloramphenicol compared to other pre-treatments. Tunicamycin and fosfomycin were used as negative controls, known for reducing cellular WTA levels and polysaccharide cell-wall content, respectively, at sub-inhibitory concentrations[30]. Our findings align with Nygaard et al., who demonstrated using whole-cell NMR spectroscopy, that exposure to chloramphenicol results in a relative increase in the content of polysaccharides, which constitute the primary component of the staphylococcal WTA[31,32]. This increase in cell wall WTA content augments the surface area available for phage ϕ11 attachment to its receptor, thereby enhancing the transduction process.

Another aspect that we opted for optimizing the transduction step, is the use of the appropriate MOI for each strain. This helps maintain a balance between maximizing the recovery of tn-mutants and minimizing negative impacts on the bacterial cells.

Moreover, to facilitate the accessibility of the phage to bacterial cells and increase the transduction efficiency, we prepared an in-house transduction SN medium that contains extra carbon and nitrogen sources, along with divalent cations. We observed a significant increase in the number of transductants in JE2, ST398, COL, and MW2 when SN medium with 5 mM $CaCl_2$ was employed in the transduction step compared to TSB. This enhancement can probably be attributed to the addition of carbon and phosphorus sources, such as β-glycerophosphate disodium salt, which induces physical changes to the surface area of *Staphylococcus*, positively influencing phage adsorption[33]. Additionally, it acts as a chelating agent for calcium residuals[34], preventing reinfection and interrupting the infectious cycle of the phages. Furthermore, we included divalent cations (Ca^{2+} and Mg^{2+}) in the transduction medium to facilitate phage attachment by neutralizing the charge between the host cell surface polymer and the phage surface[33,35] Evaluating transduction enhancers, that suit the specific phage and strain in use, is an essential process that can greatly influence the process of generating a tn-mutant library.

Beyond transduction, the cure process of temperature-sensitive plasmids is considered the tipping point in the construction of a successful tn-mutant library. Specifically, this event can introduce significant bias into the library representation, potentially leading to the underrepresentation of certain mutants that are sensitive to high-temperatures[13]. To evaluate this, we chose JE2 as a model strain to evaluate this process. We initially implemented a gradual increase in temperature and skipped passage after a brief time at 43°C to mitigate the bias introduced during the curing step. Parallelly, we imitated the conventional plasmid curing process employed in previous studies[36,18]. We found that numerous genes became defective due to a sudden temperature change and a short exposure at 43°C before the first

overnight incubation. This intensifies the defective effects of slow mutants at high temperatures during the curing process, resulting in a skewed library. Transposon reads of 91 genes were depleted in Tn-Library 2 compared to Tn-Library 1. Defining essential or fitness genes can be challenging, as it depends on the medium, conditions, and the competition-based approach used in tn-library construction. However, within the context of our tn-library construction, these genes may play a role in responding to high-temperature treatment under the conventional curing protocol. This observation aligns with Santiago et al. findings, who showed that a sudden temperature rise to 43°C resulted in a significant depletion of mutants, especially those involved in heat-shock response[13]. These heat survival genes were reported to significantly impact cell wall biosynthesis and signaling systems, protein folding, and c-di-AMP metabolism[13,37]. For instance, transposon insertions in cell wall biosynthesis genes, such as *pbp3, pbp4, mreC, ssaA, lcpA, lytH, fmtC, auxA* and *auxB* were found in Tn-Library1 but not in Tn-Library 2. This indicates that, despite the reduced fitness of these genes at high temperatures, the adjustments in the curing process led to better recovery of these genes. Nonetheless, no or few transposon insertions were detected in genes involved in protein folding such as *dnaJ*, *grpE*, and *dnaK*[13,37,38]. Previous reports indicate that these genes are non-essential at 37°C and essential at 43°C. Our findings show that transposon insertions in these genes were detrimental in both libraries. Furthermore, it has been observed that certain mutants in the menaquinone biosynthesis pathway (including *menC*, *menF*, *aroB*, *aroF*, and *ubiE*) and in the pyrimidine pathway (such as *pyrB*, *pyrC*, and *carB*) were significantly enriched in both libraries. These genes have been reported to be essential at 30°C[13]. Previous studies have established a connection between mutations in these pathways and the small colony variant phenotype[39]. Interestingly, Tn-Library 2 showed an enrichment of certain genes, including serine protease *htrA*, *lyrA*, and *sgtB*, and regulators, such as the membrane two-component system members *srrB*, *rot*, and *sarS*[13,40]. This implies that the curing process of the plasmids can qualitatively influence the representation of mutants in the tn-mutant library.

It's important to note that this process did not significantly impact the quantitative aspects of the tn-mutant library. For instance, the unique number of transposon insertions in both libraries represents a coverage of nearly 76% of all TA sites (with ca. 6 bp distance between transposon insertions). This coverage was significantly higher in both libraries compared to previous studies conducted on the USA300 background, where the coverage of insertions was around 55% and 28%[16,17].

To summarize, our optimized protocol offers a reliable basis for constructing tn-mutant libraries in *S. aureus*, which is considered the rate-limiting step of a successful TIS application. This will accelerate

functional genomics studies enabling more efficient exploration of bacterial survival, resistance, and pathogenicity mechanisms in *S. aureus* and other staphylococcal pathogens.

Methods

Bacterial strains, plasmids, phage and culture conditions

In this study, we used MRSA strains (JE2, MW2, COL, ST398, Mu50) and methicillin-susceptible *S. aureus* (MSSA) strains (Newman, SH1000, SH1000 pMARGK2b-Himar1, SH1000 pFA545, SH1000 pFA545gen), and *Escherichia coli* (*E. coli*) IM08B strain (Supplementary Table S1). All wild-type (WT) strains of *S. aureus* were cultured in Brain Heart Infusion (BHI) broth or BHI agar (BHI-A), and Tryptic Soy broth (TSB) or Tryptic Soy agar (TSA), at 37°C. *E. coli* IM08B was cultured in Luria broth (LB) or Luria agar (LA) agar at 37°C. Additionally, BHI, TSB, BHI agar, and TSA were used as well for growing SH1000 strains harboring temperature-sensitive plasmids at 30°C. The appropriate antibiotics used included tetracycline, chloramphenicol, erythromycin, tunicamycin, gentamicin and fosfomycin (Sigma Aldrich). Two temperature-sensitive plasmids transposition system were used: pMARGK2b-Himar1, carrying Himar1 transposon and 33 base pairs (bp) mariner mosaic ends (GAGACCGGGGACTTATCAGCCAACCTGTTAATC), and pFA545, which contains a mariner transposase. Transduction experiments were conducted using phage ϕ11. For propagation and transduction, an in-house medium, designed SN [TSB supplemented with filtered components: 1 mg/mL gelatin (Sigma Aldrich), 13.48 mg/mL β-glycerophosphate disodium salt (Sigma Aldrich), and 72 mg/mL MgSO4 was used] and $CaCl_2$ (Sigma Aldrich). Transductants were selectively grown on BHI agar plates supplemented with 5 µg/mL erythromycin, and either 5 µg/mL tetracycline or 5 µg/mL gentamicin.

Plasmid-based transposase introduction into *S. aureus* strains

The temperature-sensitive pFA545 plasmid containing mariner transposase was introduced into the *S. aureus* strain of interest, following two rounds of transformation via the *E. coli* IM08B shuttle strain. First, pFA545 plasmid was extracted from an overnight culture of *S. aureus* SH1000 at 30°C using the Qiagen mini-prep plasmid DNA extraction Kit (Qiagen) according to the manufacturer's instructions. The extracted pFA545 plasmid was used for heat shock transformation of chemically competent cells of *E. coli* IM08B according to the method described by Monk et al.[41]. *E. coli* IM08B pFA545 transformants were then selected on LA plates containing 5 mg/l of tetracycline following 48 hours incubation at 30°C.

Once again, the pFA545 plasmid was isolated from *E. coli* IM08B transformant using the Qiagen Midi-Prep Plasmid DNA Extraction Kit (Qiagen). This plasmid was then used for the electroporation of electrocompetent *S. aureus* strains (JE2, MW2, COL, ST398, and Newman), following the method described by Monk et al.[42].

High concentration pFA545 DNA (up to 5µg) was then added to 50 µl of freshly competent cells, followed by electroporation under specific conditions (18 kV/cm, 200 Ω, 25 µF). Subsequently, the cells were incubated in preheated BHI at 30°C for two hours. Ultimately, the transformed cells were plated on BHI agar supplemented with 5 mg/l of tetracycline and incubated at 30°C for 48 hours.

Due to the resistance of ST398 to tetracycline, the selection marker cassette was replaced with *aac6′-aph2′* gene, which encodes gentamicin resistance and was obtained from the Mu50 strain. This was done to construct pFA545gen, following the method of Christiansen et al.[18]. For colony screening and the subsequent experiments, tetracycline was substituted with gentamicin.

Introduction of Himar1 transposon into *S. aureus* strains containing transposase using phage ϕ11

The propagation and harvest of phage ϕ11/pMARGK2b-Himar1 were conducted using freshly prepared SN medium with 5 mM $CaCl_2$. SH1000 pMARGK2b-Himar1 strain containing the Himar1 transposon, was cultured overnight at 30°C on TSA agar and a single colony was resuspended in 1 mL of SN medium with 5 mM $CaCl_2$. The phage ϕ11 stock (approximately 10^{10} pfu/mL) was then serially diluted in SN medium with 5 mM $CaCl_2$. A mixture of 10 µL of SH1000 pMARGK2b-Himar1 resuspended cells and 100 µL of phage ϕ11 serial dilutions (up to 10^{-9}) was prepared in 4 mL of pre-maintained TSA soft agar at 50°C and poured onto TSA plates supplemented with 5 mM $CaCl_2$ followed by incubation at 30°C for 24 hours.

For lysate ϕ11/pMARGK2b-Himar1 harvest and titer determination, plates exhibiting near confluent lysis were selected. The lysate was harvested by adding 3 mL of SN medium to the plates, centrifuged for 10 min at 10,000 x g. The supernatant was filtered through a 0.22 µm filter and titrated using the aforementioned propagation method and then stored at 4°C.

The introduction of ϕ11/pMARGK2b-Himar1 into *S. aureus* strains (JE2, MW2, COL, ST398 and Newman) was performed with high efficiency using transduction, following the Krausz and Bose

protocol with modifications[43]. An overnight culture of the recipient strains was diluted 1:100 in 400 mL TSB with 1.5 µg/mL chloramphenicol and incubated at 30°C with shaking (200 rpm) until reaching the mid-exponential phase (OD_{600} 0.2 :0.3). The culture was then transferred to eight 50-mL conical tubes and centrifuged at 4,500 x g for 10 min. The supernatant was discarded, the pellets of each tube were resuspended in 0.5 mL of freshly prepared SN medium with 5 mM $CaCl_2$, and an appropriate aliquot of phage ϕ11/pMARGK2b-Himar1 was added to achieve the desired MOI for each strain. The tubes were incubated at room temperature for 10 min and then at 30°C for 35 min without shaking. An additional 2.5 mL of TSB was added to each tube, followed by centrifugation at 4,500 x g for 10 min to pellet the cells. After discarding the supernatant, the pellets of each tube were resuspended in 5 mL of TSB, incubated with shaking (200 rpm) for 2 h at 30°C, and then centrifuged at 4,500 x g for 10 min. Finally, the pellets from each tube were resuspended in 250 uL of TSB and plated each on 15 cm Ø BHI Agar supplemented with 5 mg/L erythromycin and 5 mg/L tetracycline and incubated at 30°C for 48 hours. This process was repeated 20 times, resulting in 160 plates. Colonies were harvested from each plate by adding 3 mL of BHI supplemented with 5 mg/L erythromycin. All aliquots were then combined into a single pool, distributed into 1 mL glycerol stocks, and stored at -80°C for future use.

To optimize this process, transduction experiments were conducted in SN medium with 5 mM $CaCl_2$, with and without a pre-treatment of TSB containing sub-inhibitory concentration of chloramphenicol, tunicamycin (4 µg/mL), or fosfomycin (4 µg/mL) as above. Additionally, a range of MOI ratios (from 0.1 to 0.6) with approximately 10^9 CFU/mL of *S. aureus* JE2, ST398, Newman, COL, and MW2 strains, to identify the optimal MOI that yields the highest number of transductants.

Curing of temperature-sensitive plasmids from transposon mutants

JE2 was chosen as a model to investigate the thermal effects of plasmid curing on the tn-mutant library. An aliquot of glycerol stock of an uncured tn-mutant library of JE2 was thawed on ice and subsequently inoculated into 600 mL of BHI medium containing three antibiotics (chloramphenicol, tetracycline, and erythromycin). The culture was then subjected to a stepwise temperature increase starting at 35°C for 20 min, then increased to 38°C for 20 min, further to 41°C for 20 min, and finally a step at 43°C for 20 min. The OD_{600} was monitored for the subsequent 100 min until it reached 0.4. A 30 mL aliquot of the culture was then recovered by centrifugation (4000 rpm for 10 min), resuspended in 600 mL of pre-warmed BHI (43°C) containing 5 mg/L erythromycin, and incubated with aeration overnight at 43°C. This procedure was repeated for two days to yield a third generation tn-mutant library, designed as Tn-Library 1. In

parallel, an aliquot of the uncured library of JE2 was subjected to a conventional curing process without the gradual increase to 43°C and included an extra passage before the first overnight incubation at 43°C. This library was assigned as Tn-Library 2. For both libraries, cells were plated, each day, on mono-antibiotic BHI plates containing 5 mg/l of erythromycin, chloramphenicol, or tetracycline and incubated at 37°C overnight. The curing percentage was calculated for each step. Aliquots of the cured transposon libraries containing 20% glycerol were stored at -80°C.

Verification of tn-mutant library complexity by Linker PCR

The complexity of the tn-mutant library was confirmed using a method known as Linker PCR, as described by Christiansen et al[18]. Random selection of ten colonies from BHI plates containing 5 mg/l erythromycin, were cultured in BHI broth at 37°C overnight. DNA was extracted from these overnight cultures using the DNeasy Blood & Tissue kit (Qiagen), with the addition of 0.5 mg/mL (250 units/mL) of lysostaphin (Sigma Aldrich). The DNA was then digested with the *RsaI* restriction enzyme (Thermo Fisher Scientific) at 37°C for 16 h, followed by purification using the GenJet PCR Purification Kit (Thermo Fisher Scientific).

Oligo 254 and 256 adaptors (Supplementary Table S4) were prepared by resuspending them in an annealing buffer composed of 100 mM Tris-HCl (pH 8), 500 mM NaCl, and 20 mM EDTA, and then diluting each adaptor to a concentration of 100 µM. The adaptor solutions were combined in a 1:1 ratio and denatured at 95°C for 3 min, followed by an hour-long incubation at room temperature. The annealed adaptors were then ligated to the digested DNA using T4 ligase (Thermo Fisher Scientific) at 22°C for an hour. Post-ligation, DNA was purified using the GenJet PCR Purification Kit (Thermo Fisher Scientific) and subjected to PCR using Phusion high-fidelity DNA Polymerase (Thermo Fisher Scientific) with specific primers (forward TnL and reverse primer 258) (Supplementary Table S4). The PCR conditions were as follows: an initial denaturation for 3 min, followed by 30 cycles of 45-sec denaturation at 94°C, 1 min annealing at 53°C, and 2 min elongation at 72°C, with a final 10 min elongation at 72°C. PCR products were then visualized on a 1% agarose gel run at 90 volts for 30 min.

TraDIS sequencing and data processing

DNA was extracted from two aliquots of the previously mentioned two cured libraries, separately. Two µg of each extracted DNA sample in 100 µL H_2O were sheared to an average fragment size of 300-400 bp using a sonication device (Bioruptor® Pico, Diagenode) with the following profile: 10 cycles of 30 s

ON, 90 s OFF at low frequency. Following the methodology outlined by Barquist, et al.[44], these fragmented DNA samples were prepared for TraDIS with adapters and primers previously designed[18]. The libraries were sequenced on an Illumina MiSeq platform using Miseq V2 50 cycles kit resulting in reads with the initial 10 bp (CAACCTGTTA) being transposon insert-specific followed by the junction region.

The resulting data were subsequently processed for bioinformatic analysis using the Bio-Tradis pipeline (https://github.com/sanger-pathogens/Bio-Tradis). This analysis generated files that facilitated the determination of the number of reads and the accurate enumeration of UISs for each gene within the JE2 reference genome (Genbank: CP000255.1). To compare output reads of the optimized curing method with those of the conventional method, the Tradis_comparison.R script was used. The UISs were visualized at both the individual gene level and within a circular representation of the genome using Artemis (version 18.2.0) and Artemis DNAPlotter (version 18.2.0), respectively.

Acknowledgments

This study has received funding from the European Union's Horizon 2020 research and innovation program under the Marie Sklodowska-Curie grant agreement No. 956154.

Special thanks are extended to Prof. Simon Foster (University of Sheffield, UK) for kindly providing the transposon and transposase plasmids and phage. We would also like to thank Prof. John Elmerdahl Olsen (University of Copenhagen, Denmark) for providing the wild-type strains and for reviewing the manuscript. We extend our profound gratitude to the OHAR group led by Prof. Luca Guardabassi (University of Copenhagen, Denmark), for hosting and providing access to the sequencing platform.

Data availability

Raw sequencing data and metadata will be available in the NCBI Sequence Read Archive (SRA) upon publication, under BioProject accession no. PRJNA1137847.

References

1. Turner, N. A. *et al.* Methicillin-resistant Staphylococcus aureus: an overview of basic and clinical research. *Nat. Rev. Microbiol.* **17**, 203–218 (2019).

2. Novick, R. P., Edelman, I., Latta, P. D., Swanson, E. C. & Pattee, P. A. Translocatable elements in Staphylococcus aureus. *Contrib. Microbiol. Immunol.* **6**, 41–55 (1979).

3. Berger-Bächi, B. Insertional inactivation of staphylococcal methicillin resistance by Tn551. *J. Bacteriol.* **154**, 479–487 (1983).

4. Mani, N., Tobin, P. & Jayaswal, R. K. Isolation and characterization of autolysis-defective mutants of Staphylococcus aureus created by Tn917-lacZ mutagenesis. *J. Bacteriol.* **175**, 1493–1499 (1993).

5. Mei, J., Nourbakhsh, F., Ford, C. W. & Holden, D. W. Identification of *Staphylococcus aureus* virulence genes in a murine model of bacteraemia using signature-tagged mutagenesis. *Mol. Microbiol.* **26**, 399–407 (1997).

6. Cain, A. K. *et al.* A decade of advances in transposon-insertion sequencing. *Nat. Rev. Genet.* **21**, 526–540 (2020).

7. Champie, A. *et al.* Enabling low-cost and robust essentiality studies with high-throughput transposon mutagenesis (HTTM). *PLoS ONE* **18**, e0283990 (2023).

8. Shields, R. C. & Jensen, P. A. The bare necessities: Uncovering essential and condition-critical genes with transposon sequencing. *Molecular Oral Microbiology* **34**, 39–50 (2019).

9. Cho, H. Transposon insertion site sequencing (TIS) of Pseudomonas aeruginosa. *J. Microbiol.* **59**, 1067–1074 (2021).

10. Yajjala, V. K., Widhelm, T. J., Endres, J. L., Fey, P. D. & Bayles, K. W. Generation of a Transposon Mutant Library in Staphylococcus aureus and Staphylococcus epidermidis Using bursa aurealis. in *The Genetic Manipulation of Staphylococci* (ed. Bose, J. L.) vol. 1373 103–110 (Springer New York, New York, NY, 2014).

11. Khatiwara, A. *et al.* Genome Scanning for Conditionally Essential Genes in Salmonella enterica Serotype Typhimurium. *Appl. Environ. Microbiol.* **78**, 3098–3107 (2012).

12. Maliszewski, K. L. Batch Transduction of Transposon Mutant Libraries for Rapid Phenotype Screening in Staphylococcus. in *The Genetic Manipulation of Staphylococci* (ed. Bose, J. L.) vol. 1373 75–81 (Springer New York, New York, NY, 2015).

13. Santiago, M. *et al.* A new platform for ultra-high density Staphylococcus aureus transposon libraries. *BMC Genomics* **16**, 252 (2015).

14. Bowring, J. Z. *et al.* Screening for Highly Transduced Genes in Staphylococcus aureus Revealed Both Lateral and Specialized Transduction. *Microbiol. Spectr.* **10**, e02423-21 (2022).

15. Mašlaňová, I., Stříbná, S., Doškař, J. & Pantůček, R. Efficient plasmid transduction to Staphylococcus aureus strains insensitive to the lytic action of transducing phage. *FEMS Microbiology Letters* **363**, fnw211 (2016).

16. Grosser, M. R. *et al*. Genetic requirements for Staphylococcus aureus nitric oxide resistance and virulence. *PLoS Pathog.* 14, e1006907 (2018).

17. Freiberg, J. A. *et al*. Restriction of arginine induces antibiotic tolerance in Staphylococcus aureus. *Nat Commun* **15**, 6734 (2024).

18. Christiansen, M. T. *et al.* Genome-Wide High-Throughput Screening to Investigate Essential Genes Involved in Methicillin-Resistant Staphylococcus aureus Sequence Type 398 Survival. *PLoS ONE* **9**, e89018 (2014).

19. Lo, H.-Y. *et al.* Transposon sequencing identifies genes impacting *Staphylococcus aureus* invasion in a human macrophage model. *Infect. Immun.* **91**, e00228-23 (2023).

20. Monk, I. R. Genetic manipulation of Staphylococci—breaking through the barrier. *Front. Cell Inf. Microbiol.* **2**, (2012).

21. Chaudhuri, R. R. *et al.* Comprehensive Identification of Salmonella enterica Serovar Typhimurium Genes Required for Infection of BALB/c Mice. *PLoS Pathog.* **5**, e1000529 (2009).

22. Herron, P. R. Transposon Express, a software application to report the identity of insertions obtained by comprehensive transposon mutagenesis of sequenced genomes: analysis of the preference for in vitro Tn5 transposition into GC-rich DNA. *Nucleic Acids Research* **32**, e113–e113 (2004).

23. Choudhery, S. *et al.* Modeling Site-Specific Nucleotide Biases Affecting Himar1 Transposon Insertion Frequencies in TnSeq Data Sets. *mSystems* **6**, e00876-21 (2021).

24. Bossé, J. T. *et al.* Rationally designed mariner vectors for functional genomic analysis of Actinobacillus pleuropneumoniae and other Pasteurellaceae species by transposon-directed insertion-site sequencing (TraDIS). *Animal Diseases* **1**, 29 (2021).

25. Pajunen, M. I. Generation of transposon insertion mutant libraries for Gram-positive bacteria by electroporation of phage Mu DNA transposition complexes. *Microbiology* **151**, 1209–1218 (2005).

26. Coe, K. A. *et al.* Multi-strain Tn-Seq reveals common daptomycin resistance determinants in Staphylococcus aureus. *PLoS Pathog.* **15**, e1007862 (2019).

27. Lee, W. Construction of high-density transposon mutant library of Staphylococcus aureus using bacteriophage ϕ11. *J. Microbiol.* **60**, 1123–1129 (2022).

28. Ingmer, H., Gerlach, D. & Wolz, C. Temperate Phages of *Staphylococcus aureus*. *Microbiol. Spectr.* **7**, 7.5.1 (2019).

29. Li, X. *et al.* An essential role for the baseplate protein Gp45 in phage adsorption to Staphylococcus aureus. *Sci. Rep.* **6**, 26455 (2016).

30. Zhu, X. *et al.* Tunicamycin Mediated Inhibition of Wall Teichoic Acid Affects Staphylococcus aureus and Listeria monocytogenes Cell Morphology, Biofilm Formation and Virulence. *Front. Microbiol.* **9**, 1352 (2018)

31. Nygaard, R., Romaniuk, J. A. H., Rice, D. M. & Cegelski, L. Spectral Snapshots of Bacterial Cell-Wall Composition and the Influence of Antibiotics by Whole-Cell NMR. *Biophysical Journal* **108**, 1380–1389 (2015).

32. Van Dalen, R., Peschel, A. & Van Sorge, N. M. Wall Teichoic Acid in Staphylococcus aureus Host Interaction. *Trends in Microbiology* **28**, 985–998 (2020).

33. Kim, S. G. *et al.* Strategy for mass production of lytic Staphylococcus aureus bacteriophage pSa-3: contribution of multiplicity of infection and response surface methodology. *Microb. Cell Fact*. **20**, 56 (2021)

34. Ding, G.-J. *et al.* Amorphous calcium phosphate nanowires prepared using beta-glycerophosphate disodium salt as an organic phosphate source by a microwave-assisted hydrothermal method and adsorption of heavy metals in water treatment. *RSC Adv.* **5**, 40154–40162 (2015).

35. Li, X. *et al.* Exploring the Benefits of Metal Ions in Phage Cocktail for the Treatment of Methicillin-Resistant Staphylococcus aureus (MRSA) Infection. *Infect. Drug Resist.* **15**, 2689–2702 (2022).

36. Ba, X. *et al.* High-Throughput Mutagenesis Reveals a Role for Antimicrobial Resistance- and Virulence-Associated Mobile Genetic Elements in Staphylococcus aureus Host Adaptation. *Microbiol. Spectr.* **11**, e04213-22 (2023).

37. Singh, V. K. *et al.* An insight into the significance of the DnaK heat shock system in Staphylococcus aureus. *Int. J. Med. Microbiol.* **302**, 242–252 (2012)

38. Matthews, T., Baumann, R. G. & Domanski, T. L. Analysis and Characterization of Staphylococcus aureus ClpB and Associated Co-Chaperone Proteins dnaK, dnaJ and grpE. *FASEB j*. **21**, (2007).

39. Proctor, R. A. *et al*. Small colony variants: a pathogenic form of bacteria that facilitates persistent and recurrent infections. *Nat. Rev. Microbiol.* **4**, 295–305 (2006).

40. Kim, D. Y., Kwon, E., Shin, Y.-K., Kweon, D.-H. & Kim, K. K. The Mechanism of Temperature-Induced Bacterial HtrA Activation. *J. Mol. Biol.* **377**, 410–420 (2008).

41. Monk, I. R., Tree, J. J., Howden, B. P., Stinear, T. P. & Foster, T. J. Complete Bypass of Restriction Systems for Major Staphylococcus aureus Lineages. *mBio* **6**, e00308-15 (2015).

42. Monk, I. R. & Stinear, T. P. From cloning to mutant in 5 days: rapid allelic exchange in Staphylococcus aureus. *Access Microbiology* **3**, (2020).

43. Krausz, K. L. & Bose, J. L. Bacteriophage Transduction in Staphylococcus aureus: Broth-Based Method. in *The Genetic Manipulation of Staphylococci* (ed. Bose, J. L.) vol. 1373 63–68 (Springer New York, New York, NY, 2014).

44. Barquist, L. et al. The TraDIS toolkit: sequencing and analysis for dense transposon mutant libraries. *Bioinformatics* **32**, 1109–1111 (2016).

Authors' Contributions

SY and NA were involved in the conception and design of the study, acquisition of data, and data analysis and interpretation, drafted the manuscript and revised it critically for important intellectual content. BP provided overall supervision, contributed to the study's design and coordination, and was responsible for the final approval of the version to be published. All authors read and approved the final manuscript.

Additional Information

The authors declare no competing interests.

Supplementary materials

Further details can be found at the following links:

Supplementary Table S1: Bacterial strains and plasmids used in this study.

https://static-content.springer.com/esm/art%3A10.1038%2Fs41598-024-73731-y/MediaObjects/41598_2024_73731_MOESM1_ESM.xlsx

Supplementary Table S2: Fitness genes identified in Tn-Library 1 and Tn-Library 2 following the plasmid curing process, compared with a previous study in *S. aureus*
https://static-content.springer.com/esm/art%3A10.1038%2Fs41598-024-73731-y/MediaObjects/41598_2024_73731_MOESM2_ESM.xlsx

Supplementary Table S3: Output of tradis_comparison.R for Tn-Library 1 versus Tn-Library 2**.**
https://static-content.springer.com/esm/art%3A10.1038%2Fs41598-024-73731-y/MediaObjects/41598_2024_73731_MOESM3_ESM.docx

Supplementary Table S4: List of primers used in this study.

https://static-content.springer.com/esm/art%3A10.1038%2Fs41598-024-73731-y/MediaObjects/41598_2024_73731_MOESM4_ESM.xlsx

Genome-Wide Identification of Tissue-Specific Fitness Genes in Murine Models of *Staphylococcus aureus* Infection

Sally W. Yousief [1], Nader Abdelmalek [1], Martin S. Bojer [2], Yibing Ma [2], Priscila R. Guerra [2], Sajid Nisar[2], John E. Olsen [2], Bianca Paglietti [1,3 *]

[1] Department of Biomedical Sciences, University of Sassari, Sassari, Italy
[2] Department of Veterinary and Animal Sciences, Faculty of Health and Medical Sciences, University of Copenhagen, Frederiksberg, Denmark
[3] Lead contact
*Correspondence: biancap@uniss.it
Published in iScience. December 2025 https://doi.org/10.1016/j.isci.2025.114261

Summary

Staphylococcus aureus must dynamically rewire its metabolism to persist within distinct host tissues during infection. We applied *in vivo* transposon-directed insertion site sequencing (TraDIS) in murine models of skin, kidney, and spleen infections to define tissue-specific fitness landscapes for the epidemic USA300 lineage. We identified 46, 76, and 69 fitness genes in the skin, kidney, and spleen, respectively. The core gluconeogenesis gene *fbp* was essential across all tissues, whereas *pckA* and *gapB* showed organ-specific essentiality in the kidney and spleen. Skin infection required oxidative stress and DNA repair genes (*ahpC*, *ahpF*, *dps*, *uvrC*, *xseA*), consistent with elevated genotoxic pressure. In contrast, kidney and spleen relied on branched-chain amino acid catabolism (*bkdAB*), lipid metabolism (*SAUSA300_0355*), and putative polyamine biosynthesis (*SAUSA300_0458*). Competition assays *in vivo* and under oxidative (H_2O_2) and gluconeogenic (M9) conditions validated these tissue-specific dependencies. These results reveal how *S. aureus* remodels metabolic networks and identifies context-specific vulnerabilities for therapeutic targeting.

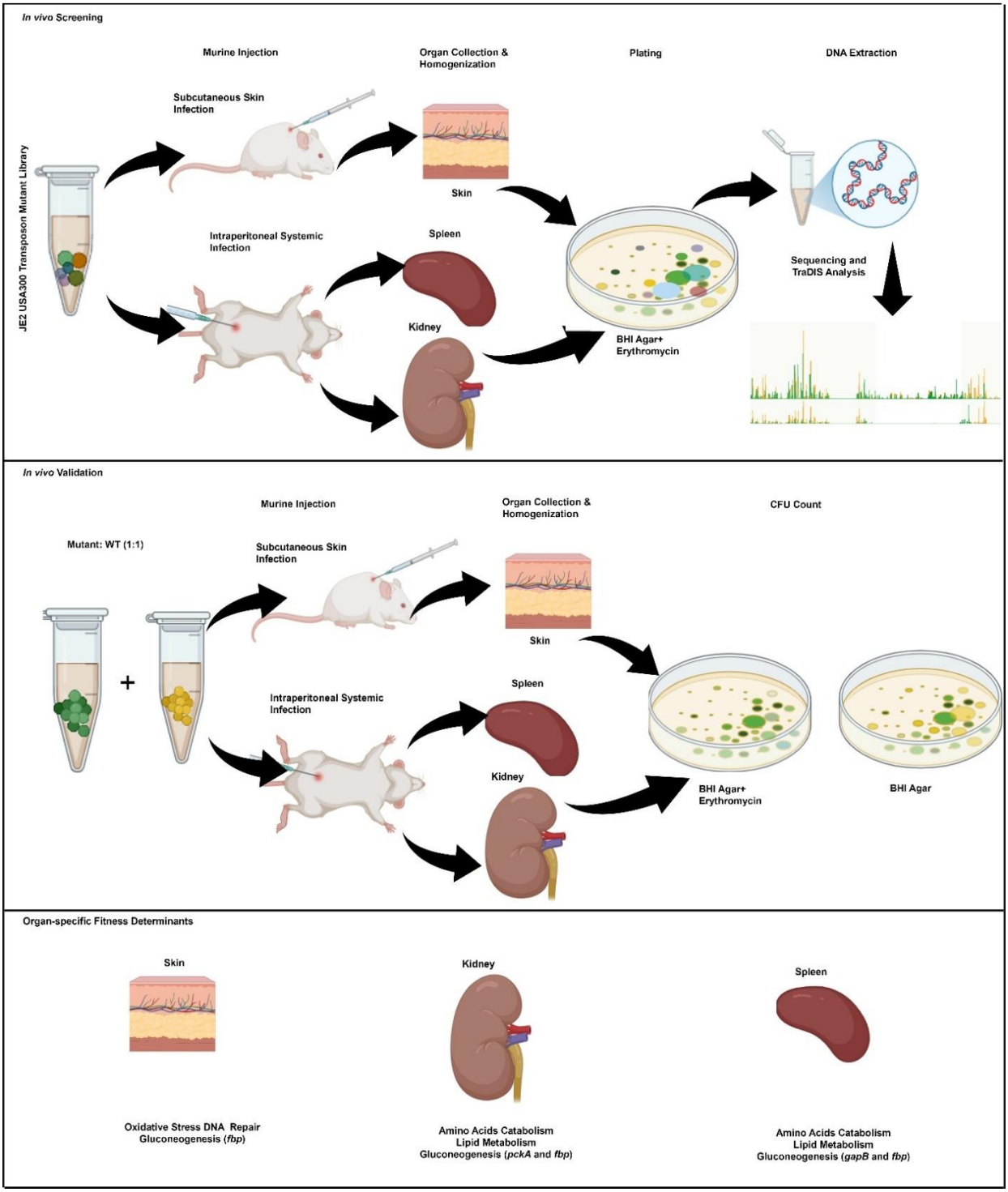

Keywords:

Staphylococcus aureus, TraDIS (transposon-directed insertion site sequencing), Tissue-specific fitness, oxidative stress response, DNA repair, gluconeogenesis, amino acid catabolism, murine infection models

Introduction

Staphylococcus aureus is a versatile pathogen capable of causing infections ranging from superficial skin abscesses to life-threatening systemic disease.[1] Its success across diverse host environments relies not only on a wide array of virulence factors but also on robust metabolic adaptability and stress resilience.[2–4] Although virulence regulation is well characterized, the genetic and metabolic strategies that underpin tissue-specific survival remain incompletely understood.[3,4]

Under nutrient and oxygen limitations, *S. aureus* reprograms central metabolism to maintain redox balance and energy production. This includes the suppression of the tricarboxylic acid cycle (TCA), activation of fermentative pathways, and reliance on amino acid catabolism.[5–8] These responses are tightly regulated by global regulators, such as CodY and CcpA, which integrate carbon and nitrogen availability with biosynthetic demand.[9] Studies have shown tissue-dependent transcriptional changes; for instance, during bone infection, *S. aureus* upregulates gluconeogenic and proteolytic genes,[10] whereas glycolytic pathways predominate in glucose-rich lungs.[11] Despite multiple *in vivo* Tn-seq studies, cross-tissue analyses within one coherent framework remain less common, especially when replicates and bottlenecks are systematically handled.

To address this, we applied Transposon-Directed Insertion Site Sequencing (TraDIS) and a previously published, highly saturated *S. aureus* USA300 JE2 transposon mutant library[12] to identify genes that contribute to bacterial fitness in a tissue-specific manner during murine models of skin and systemic infection. TraDIS offers a high-throughput approach enabling identification of fitness genes under defined conditions,[13] providing insights into the regulatory and metabolic networks that support *S. aureus* survival across these distinct host niches. These findings offer a foundation for targeting context specific vulnerabilities during infection.

Results

S. aureus population bottlenecks are minimized during in vivo library screening

To minimize bottlenecks, i.e., the loss of mutant diversity due to a sharp reduction in the number of mutants successfully establishing infection, mice were inoculated with a high dose of *S. aureus* (3×10^9 colony forming units (CFU) per mouse) for both the skin (SC) and systemic (IP) models, as determined in predesigned pilot experiments. Bacterial burdens were consistently high across organs, with average

CFU/organ counts of 8×10^{11} in skin, 7.4×10^{10} in kidney, and 4.4×10^{12} in spleen. Each organ was represented by three samples: two from individual mice and one pooled sample derived from eight mice, enabling both inter-individual comparison and robust signal detection. Mutant diversity was well maintained, with 85,000 to 300,000 unique insertion sites (UISs) recovered from output libraries. To evaluate the post-infection diversity, we applied two complementary metrics. The effective population size (N_e) reflects the evenness of mutant representation within each tissue-specific population, while the insertion reduction percentage quantifies loss of insertional diversity relative to the input library.

Post-infection diversity analysis showed that kidney and spleen samples, whether from individual mice or pooled groups, maintained high effective population sizes (*Ne* ~90,000–100,000) with <30% insertion reduction, indicating minimal bottleneck effects. In contrast, skin samples exhibited greater variability (*Ne* ~15,000–90,000). One individual sample (Mouse B, MB) showed the lowest diversity, with a high insertion reduction (>70%). The other individual skin sample (Mouse A, MA) had a moderate reduction (~55%) but retained a relatively high *Ne* of 67,808, indicating a relatively even distribution of mutants despite some loss. For this analysis, insertion reductions <50% were interpreted as mild bottlenecks, while values above that threshold reflected more substantial diversity loss[14] **(Table 1)**. Overall, the population structure remained sufficiently balanced to support robust genome-wide analysis. These findings are consistent with previous observations in host-associated microbial systems, where effective population sizes are typically 10–20 times smaller than total bacterial loads due to clonal expansion and stochastic bottlenecks.[15]

Insertion profiles were directly compared across the two individual mice and the pooled sample within each organ. Gene-level depletion patterns were highly concordant among the three replicates, supporting the decision to combine data per organ for genome-wide fitness analysis.

Table 1: Statistical overview of TraDIS analysis of output screening profiles.

Sample	No. of Reads	No. of Mapped Reads	% of Mapped Reads	UISs	N_e	Insertion Reduction (%)
Skin Infection Screening						
M_A	5207936	4754884	91.3%	178366	67808.29	55.41%
M_B	8540154	7498355	87.8%	84996	15397.69	78.75%
P_{Skin}	9455334	8293759	87.7%	205820	90288.78	48.56%

Systemic Infection Screening (Kidney)						
M_C	7157160	5346875	74.7%	299974	99769.27	25%
M_D	7930996	6994453	88.1%	298045	98490.25	25.49%
P_{Kidney}	9122370	8008825	87.79%	303906	102401.9	24%
Systemic Infection Screening (Spleen)						
M_E	7611438	6551695	86.07%	288322	99910.91	27.92%
M_F	7557340	5144540	68.07%	296786	105863	25.8%
P_{Spleen}	5981364	5237243	87.55%	246929	73282.72	38.26%

(M= individual mouse, P= pooled sample)

Multi-stage filtering identifies fitness and anti-fitness genes across infection sites

To identify fitness genes, we compared each output library to the input library and filtered for mutants that were significantly depleted, yielding 106, 122, and 113 condition-specific essential genes for skin, kidney, and spleen infections, respectively **(Table S1)**. As a post comparison proof reading step, we applied a read depth aware quality control (QC) to all depleted calls.[14,16] This QC addresses limits of read count based (edgeR) calls[17] by incorporating UIS counts alongside reads per UIS (RPU) to catch unusual read shifts not accompanied by proportional UIS changes. We compared UIS and RPU between combined inputs and organ outputs.[17,18] A mutant was flagged as false depleted when insertion diversity was stable ($\Delta UIS\% \leq 20$ with UIS_{in} and $UIS_{out} \geq 5$) but RPU fell at least two-fold (RPU fold-change, $RPU_{FC} \leq 0.5$). In the input vs output contrast this QC flagged 0 genes in skin, 2 in kidney, and 0 in spleen **(Table S2)**. Next, we refined these results by intersecting them with mutants depleted in comparison to the outgrowth control (input library grown at 37°C in Brain Heart Infusion),[19] identifying 46, 81, and 73 condition-specific essential genes in the skin, kidney, and spleen infections, respectively **(Table S1)**, that were specifically lost under *in vivo* selection pressure. Applying the same QC to this outgrowth control vs output contrast flagged 0 genes in all organs; therefore, no additional exclusions were required at this step. Finally, we excluded genes for which mutants were also depleted during *in vitro* outgrowth **(Table S1)**, resulting in 46, 76, and 69 genes **(Table S3A-G)** in the skin, kidney, and spleen, respectively **(Figure 1).**

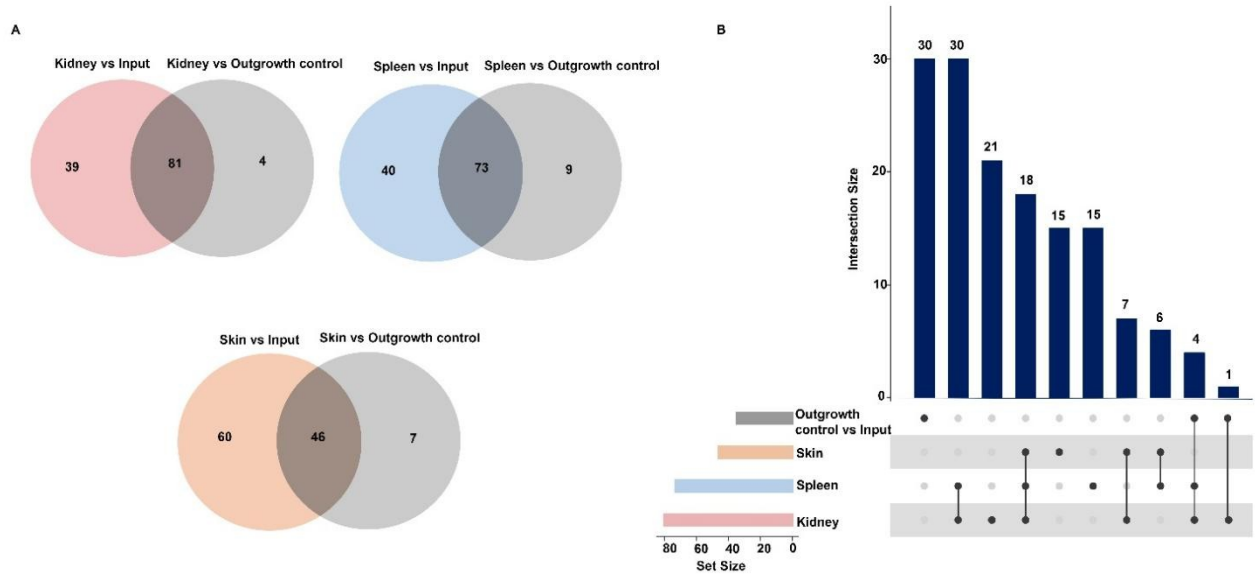

Figure 1: Comparative analysis of fitness genes in USA300 JE2 in skin and systemic infection models. **(A)** Venn diagrams showing the overlap between mutants depleted in each infected organ (the kidney, spleen, skin) relative to the input and outgrowth control at 37°C. Each diagram illustrates organ-specific and shared sets of fitness genes. **(B)** UpSet plot visualizing the intersections of fitness genes required for *in vivo* survival across the kidney, spleen, skin, and outgrowth control versus input groups **(Table S3A-G)**. The left bar chart shows the total number of fitness genes for each group, whereas the top bar chart quantifies the number of genes in each intersection. The analysis was conducted using the following criteria: log fold change (log_2FC) ≤ -2, log counts per million (logCPM) > 2, and q-value < 0.01.

To identify enriched (anti-fitness) genes, we mirrored the depletion workflow and applied the same read depth aware QC. QC removed flagged genes from the input vs output and outgrowth control vs output contrasts (skin: 47, 95; kidney: 4, 118; spleen: 8, 31). We then intersected the curated contrasts and excluded genes enriched in outgrowth control vs input, yielding the final organ-specific enriched sets **(Figure 2, Table S2).**

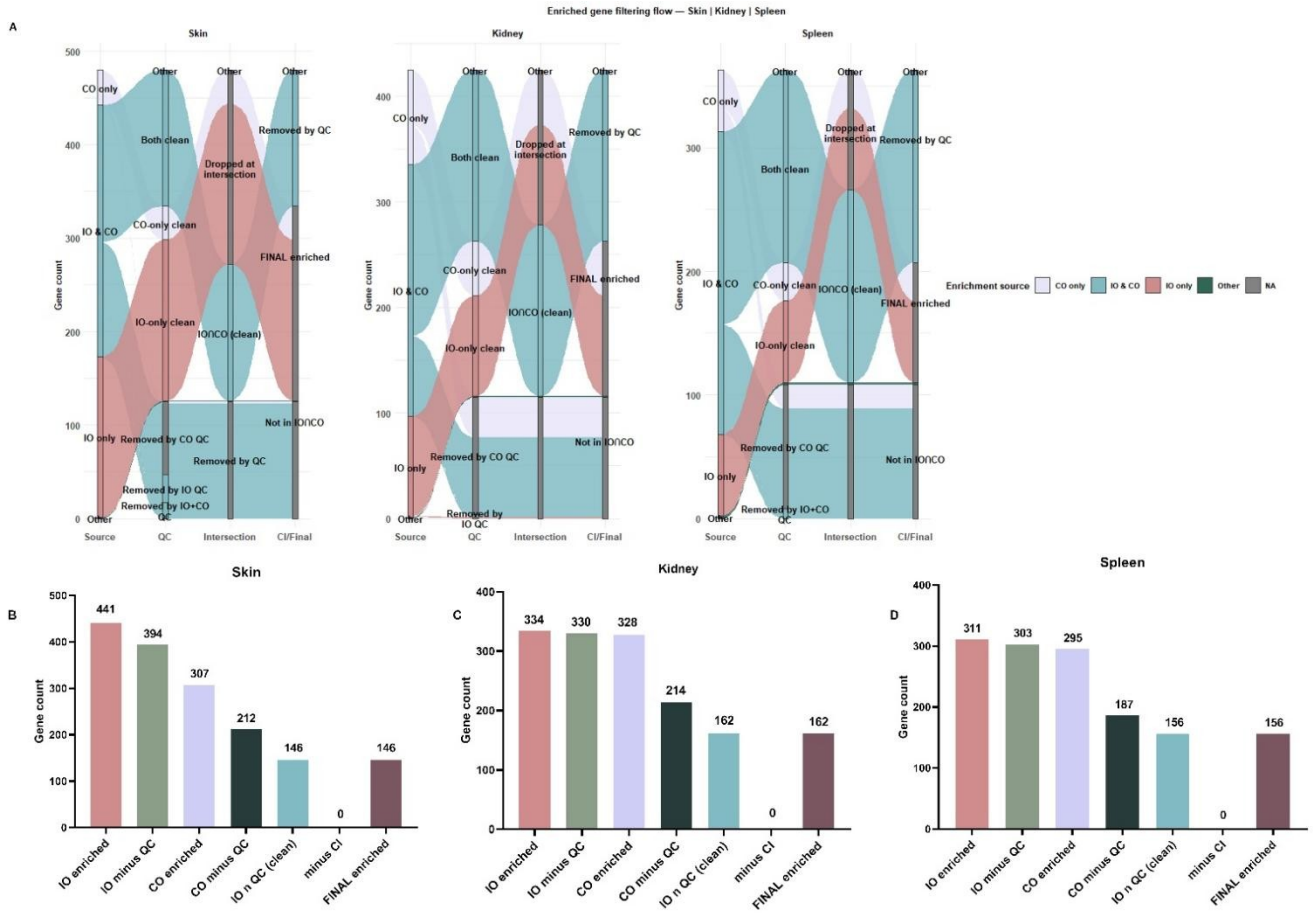

Figure 2: Provenance and curation of enriched (anti-fitness) genes across infection sites. **(A) Alluvial overview.** For skin, kidney, and spleen (left to right), four stages are shown: Source → QC → Intersection → CI/Final. Band width is proportional to gene count. Colors indicate enrichment origin at Source (IO & CO, IO only, CO only, other; see key). QC filter removes likely read-depth artifacts, namely genes with stable insertional diversity (ΔUIS ≤20% with UIS_{in} ≥5 and UIS_{out} ≥5) but ≥2-fold change in reads per insertion (RPU). Intersection retains genes enriched and QC-clean in both contrasts (IO ∩ CO). CI/Final excludes genes also enriched in the outgrowth-control vs input contrast (CI); the remainder constitutes the Final enriched set **(Table S4)**. **(B-D) Stepwise bar chart.** For each organ, bars report gene counts at each step: IO enriched → after IO QC → CO enriched → after CO QC → IO∩CO (clean) → after CI exclusion → Final enriched. Exact counts are shown above bars; "0" at "after CI exclusion" indicates no removals at that step. **Abbreviations:** IO, input→output; CO, outgrowth control→output; CI, outgrowth control→input; QC, quality control; UIS, unique insertion sites; RPU, reads per unique insertion site.

This conservative three-tiered approach and the QC approach enhanced result specificity and reduced the risk of false positive results, enabling robust identification of tissue-specific fitness genes that reflect the physiological challenges encountered by *S. aureus* in distinct host environments. Thus, these genes constitute sets of high-confidence, organ-specific fitness genes.

Distinct metabolic and stress response requirements shape tissue-specific fitness

Analysis of fitness genes during *S. aureus* infection in the skin, kidney, and spleen revealed distinct patterns of metabolic and stress response gene depletion. Mutants of genes involved in purine and pyrimidine biosynthesis *(purA, purE, pyrC, and pyrE)* were consistently depleted in the kidney, spleen, and skin. However, mutants of *purB* were flagged enriched in the skin **(Figure 3A)**. Prophage genes encoding PVL-like proteins (e.g., *SAUSA300_1959*, *SAUSA300_1962*) were depleted in skin, whereas the PVL toxin genes *lukS-PV*/*lukF-PV* (*SAUSA300_1382*/*1381*) were not.

A pronounced depletion of oxidative stress response mutants (*ahpC, ahpF, and dps*) and DNA repair mutants, including (*uvrA, uvrB, uvrC, recD* and *xseA*) were observed in the skin infection, Mutants such as *ahpC* and *dps,* and *uvrC* were also depleted in the spleen **(Figure 3B)**.

Mutants of gluconeogenic genes *pckA, gapB* (*SAUSA300_1633*), and *fbp* (*SAUSA300_2455*) **(Figure 3C and 4A)** were also strongly depleted in the kidney, spleen, and skin. Notably, mutants in *glk* (spleen), *gpmI* (skin), and *pyk* (kidney and spleen) were enriched, *glk* functions in upper glycolysis, whereas *gpmI* and *pyk* act in lower glycolysis.

Mutants of genes associated with aromatic amino acid biosynthesis (*aroA2* and *aroE*) and menaquinone biosynthesis (*SAUSA300_1470, menH, menC, menE* and *ubiE*) were enriched in the skin but depleted in the kidney **(Table S1)**. Mutants of genes involved in branched-chain amino acid metabolism (*bkdAA, bkdAB, bkdB, ilvE,* and *lpdA*) were strongly depleted in the kidney and spleen, along with *SAUSA300_0355* mutants*,* an uncharacterized gene positioned at a key junction of the mevalonate pathway **(Figure 3D and 4B)**. Notably, mutants of other genes in this pathway, *SAUSA300_2483 (mvaA)* and *SAUSA300_2484 (mvaS)* **(Table S1)**, were also significantly depleted in systemic tissues. In the same organs, mutants of *SAUSA300_0458*, annotated as a putative ornithine/lysine/arginine decarboxylase, was also required for the fitness during systemic infection.

Finally, mutants of genes related to central carbon metabolism and oxidative energy production (*pdhA, pdhB,* and *SAUSA300_0995*) were enriched in the skin, whereas heme detoxification system mutants (*hrtA, hrtB, hssR,* and *hssS*) were specifically depleted in the spleen **(Figure 3C)**.

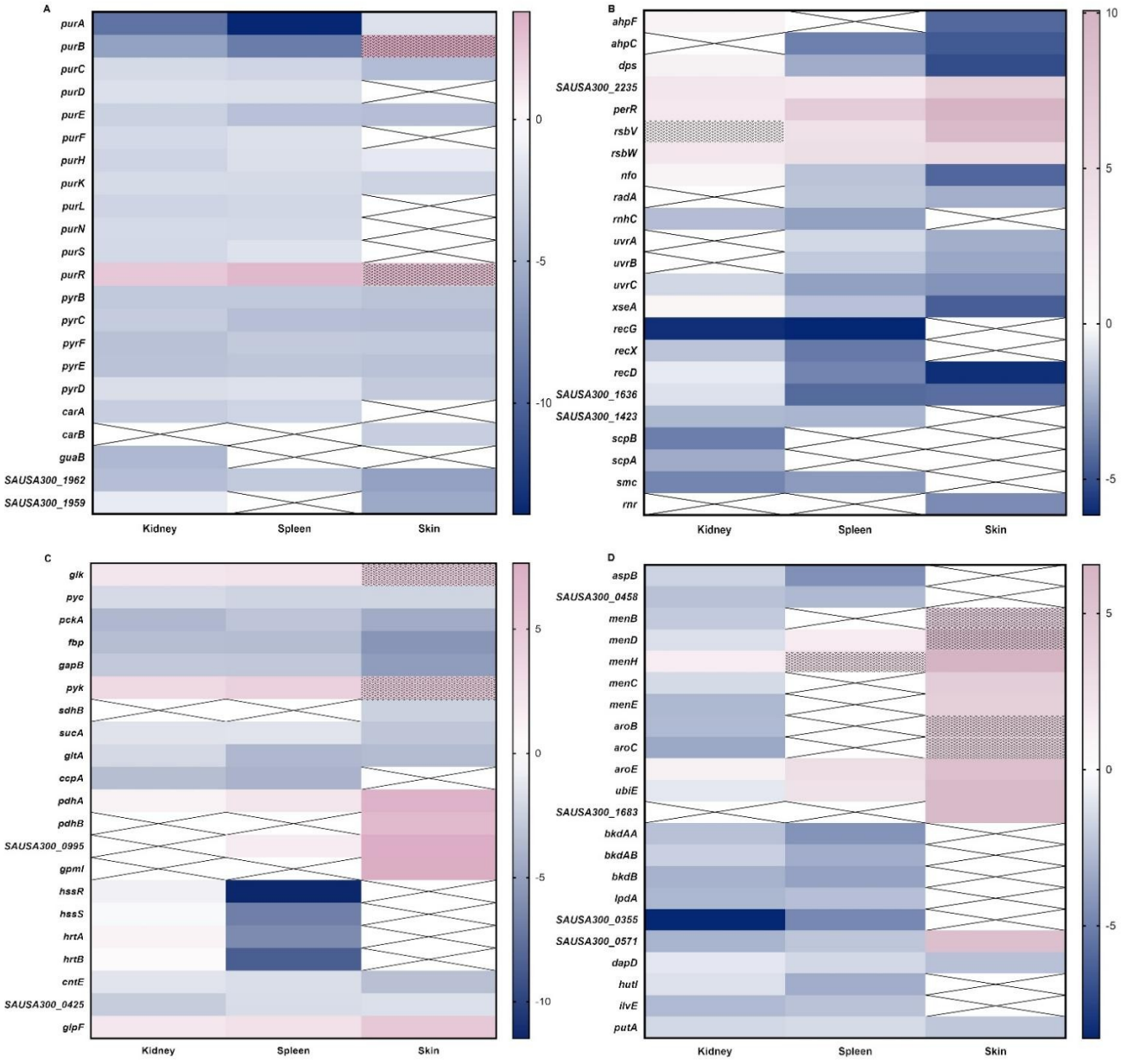

Figure 3: Tissue-specific essentiality of metabolic and stress-response pathways across skin, kidney, and spleen infection models. Heatmaps illustrate the $\log_2$FC values of USA300 JE2 mutants during skin and systemic infection (kidney, and spleen), grouped into various biologically relevant pathways: **(A)** purine and pyrimidine biosynthesis, **(B)** oxidative stress response and DNA repair systems, **(C)** central carbon metabolism, gluconeogenesis, and heme detoxification system, **(D)** BCAA-associated and connected metabolic pathways. Each heatmap represents genes on the y-axis, and tissue sites on the x-axis. Blue shading indicates gene depletion ($\log_2$FC $\leq$ -2; survival fitness genes), and pink shading indicates gene enrichment ($\log_2$FC $\geq$ 2; dispensable or advantageous when inactivated). Dotted fill denotes enriched calls that were QC-flagged (read-depth/UIS criteria) and not carried forward into the final call set. A cross (×) within a cell indicates that the gene was not detected as significantly depleted or enriched in that tissue.

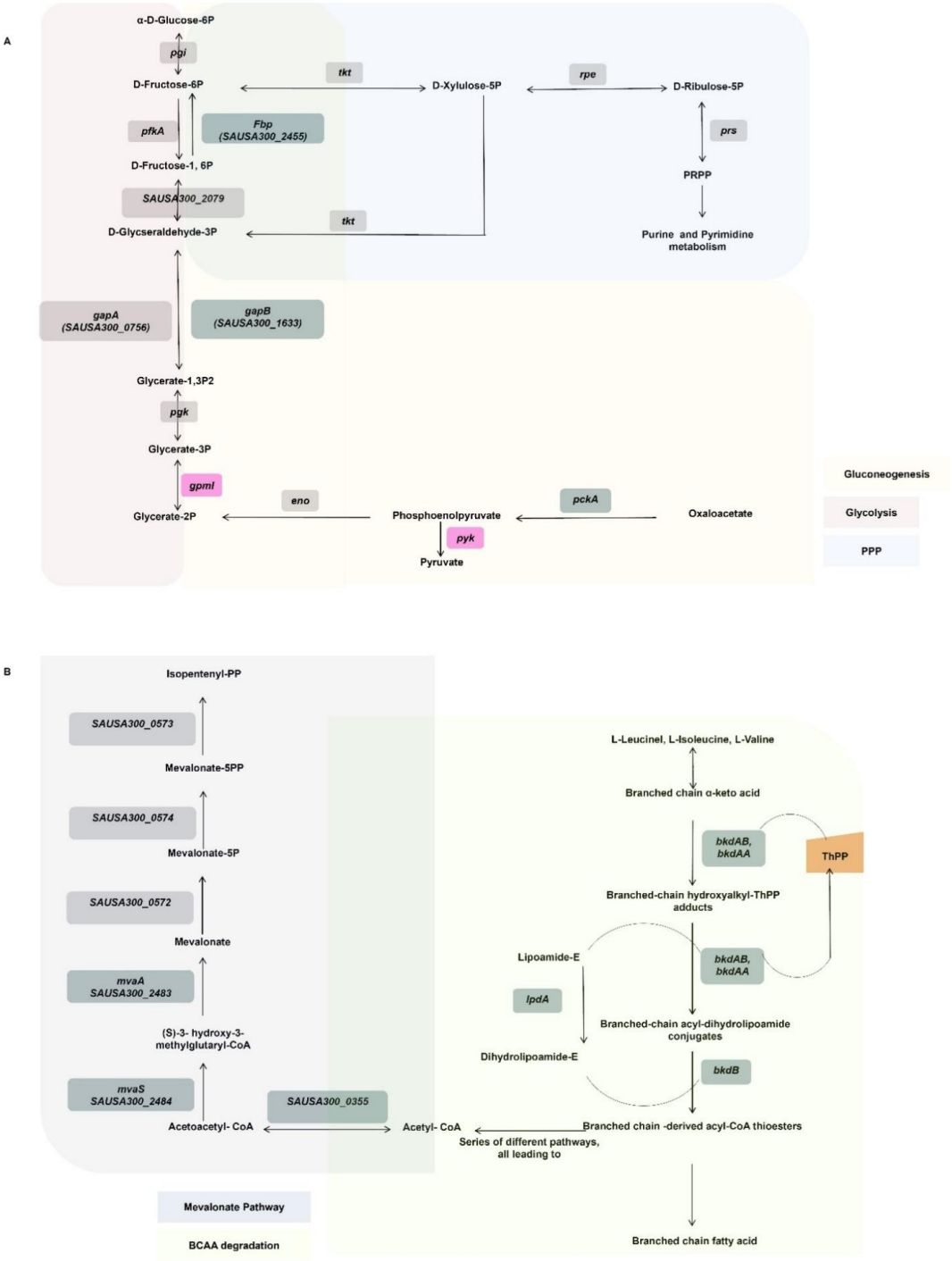

Figure 4: Metabolic pathway vulnerabilities identified by TraDIS during S. aureus infection. **(A)** Overlay of gluconeogenesis, glycolysis, and the pentose phosphate pathway (ppp), highlighting the genes required across both systemic (kidney, spleen) and skin infection models. **(B)** Branched-chain amino acid degradation and the mevalonate pathway, depicting genes specifically required during systemic infection. Universally essential genes are shown in gray, gene whereas survival fitness genes, identified by TraDIS ($\log_2$FC ≤ -2, logCPM > 2, $q < 0.01$), are shown in dark teal. *The pyk* and *gpmI* genes, which were enriched with transposon insertions in systemic sites and skin niche respectively, are shown in pink.

Cross-study benchmark of our USA300 JE2 TraDIS with explicit bottleneck control

To contextualize our organ-resolved calls, we intersected our filtered gene sets ($log_2FC \leq -2$, $q \leq 0.01$) with the published final significant lists from prior *in vivo* Tn-seq studies **(Figure S1, Table S5).** In skin, applying our thresholds recovered 10/153 of Valentino *et al*., (MSSA HG003/NCTC8325) overall abscess-specific essentials (~6.5%) and confirmed 10/46 of our benchmark calls; versus Grosser *et al*., (MRSA USA300 LAC/JE2) we observed 7 shared genes at day 3 and day 7.[20,21] In systemic screens, we compared our datasets to the recent datasets of Chang *et al*., (MRSA USA300-HOU-MR, TCH1516) who reported single-replicate liver (~6M reads; $log_2FC \leq -2$, $P \leq 0.01$,) and lung (~3M reads; $log_2FC \leq -4$, $P \leq 0.01$) datasets and noted bottlenecks that prevented kidney/spleen discovery. Overlap with their liver set comprised 12 genes with our kidney calls and 6 with our spleen; overlap with their lung set comprised 10 with our kidney and 4 with our spleen.[22] Li *et al*., (MSSA Newman) reported >90% loss of mutant population despite 12 liver and 6 kidney mono-infection replicates.[23] Despite a different infection route, Kim *et al*., (MRSA USA300 LAC) showed strong concordance with our data: 29 shared genes with kidney and 22 with spleen.[24] Calls here are made using a replicate-paired IO∩CO rule (significant in Output vs Input *and* Output vs Outgrowth control) with prespecified q value, log_2FC, and logCPM thresholds.

Validation of tissue-specific fitness genes in skin and systemic infections

To validate fitness genes required for *S. aureus* survival *in vivo*, as identified via bio:: TraDIS analysis, we performed *in vivo* competition assays using 11 selected mutants from the Nebraska Transposon Mutant Library (NTML)[25] and the USA300 JE2 wild type (WT) in murine skin and systemic infection models. In the skin infection model, *ahpC, ahpF, dps, xseA, and uvrC* mutants were significantly outcompeted by the WT **(Figure 5A)**. Similarly, during systemic infection, three mutants *SAUSA300_0355*, *SAUSA300_0458*, and *SAUSA300_1465 (bkdAB)* displayed significant attenuation in in the kidney and spleen **(Figure 5B and 5C)**. Notably, among the genes predicted by TraDIS analysis to be fitness genes in both the skin and systemic sites, only the *fbp (SAUSA300_2455)* mutant exhibited a significant fitness defect across all organs tested. *In vivo* validation suggested a kidney biased requirement for *pckA* and a spleen biased requirement for *gapB* **(Figure 5B and 5C)**. In rich medium (BHI), NTML monocultures showed no sustained growth-rate defect, a subset displayed only a modest lag **(Figure S2A–C)**. In 24 h mixed-culture BHI competitions against WT, competitive indices (log_{10} CI) were centered near zero, consistent with neutrality in rich media **(Figure S2D).**

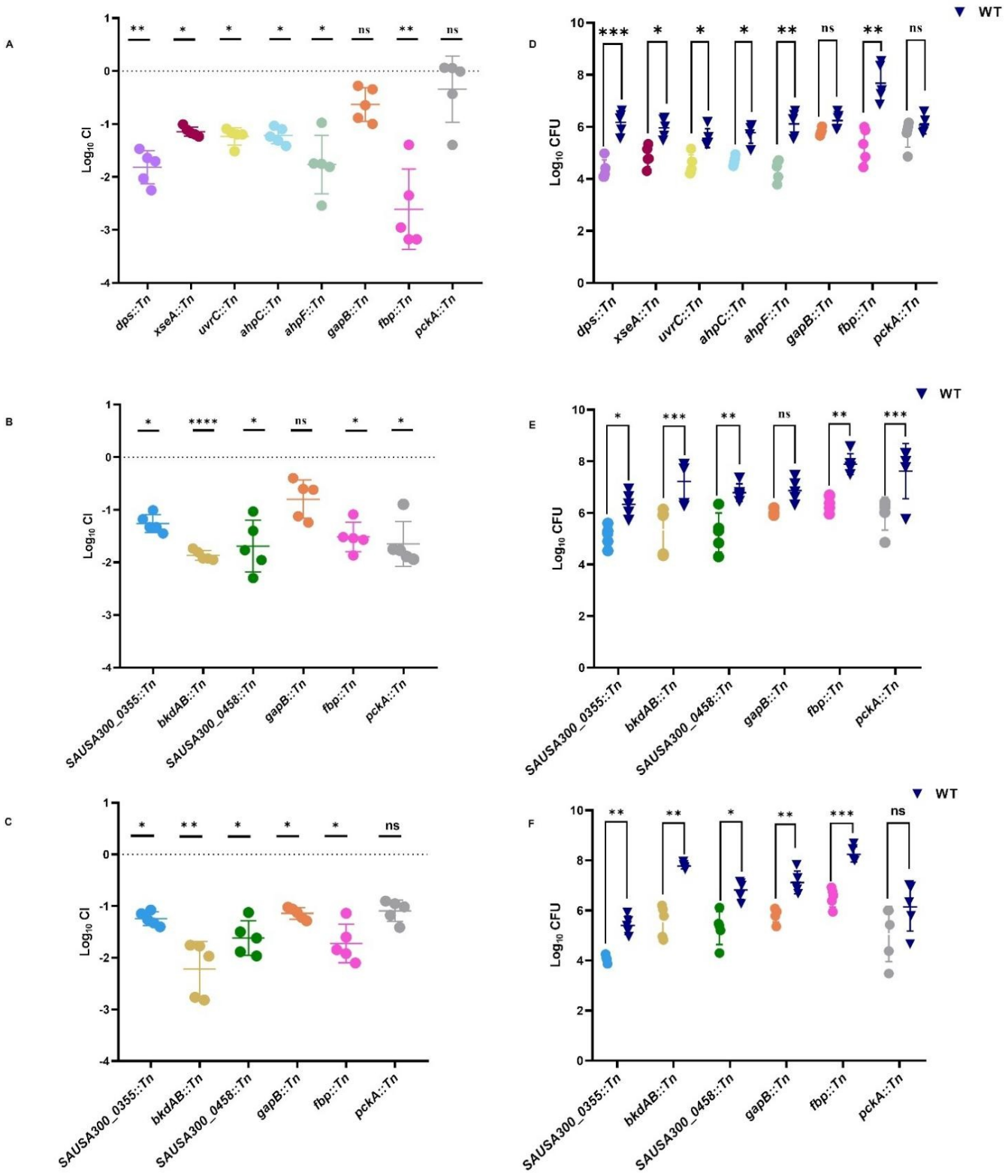
A
B
C
D
E
F
WT
Log10 CI
Log10 CFU
dps::Tn
xseA::Tn
uvrC::Tn
ahpC::Tn
ahpF::Tn
gapB::Tn
fbp::Tn
pckA::Tn
SAUSA300_0355::Tn
bkdAB::Tn
SAUSA300_0458::Tn

Figure 5: In vivo validation of fitness defects in S. aureus mutants via competitive co-infection in murine skin and systemic infection models. One experiment; single mixed inoculum with independent biological replicates (n=5 mice). Mice were co-infected with a 1:1 mixture of WT and individual mutant strains. **(A-C)** The competitive index (CI), representing relative mutant fitness compared to WT, was determined following co-infection in murine skin (A), kidney (B), and spleen (C) infection models. CI values are $\log_{10}$-transformed; a $\log_{10}$ (CI) of 0 indicates equal fitness, while $\log_{10}$ (CI) < –1 was considered biologically depleted based on a hypothetical 10-fold attenuation threshold. **(D-F)** Bacterial burden expressed as $\log_{10}$-transformed CFU recovered from the corresponding abscess (D), kidney (E), and spleen (F) samples. Organ homogenates were plated on BHI agar (total CFU) and BHI agar supplemented with 5 mg/l erythromycin (mutant-selective) to quantify relative abundance. Statistical analysis was performed using one-sample, two tailed t-tests against a theoretical mean of -1 for CI comparisons (A-C), two-way ANOVA with repeated measures, and Sidak's multiple comparisons test for CFU data (D-F). Each data point represents an individual mouse. Bars indicate group means. P-values are indicated as follows: $P < 0.05$ (*), $P < 0.01$ (**), $P < 0.001$ (***); ns, not significant.

Validation of oxidative and gluconeogenic fitness determinants by in vitro competition assays

To functionally validate genes associated with oxidative stress and central carbon metabolism, competitive assays were performed under short H_2O_2 exposure and in glucose-free M9 (gluconeogenic) medium. Mutants of *ahpC, ahpF, dps, uvrC, xseA* and *fbp* were all significantly depleted following H_2O_2 challenge. Similarly, mutants in gluconeogenesis linked genes (*fbp*, *pckA*, and *gapB*) were significantly depleted during growth in M9 medium containing glycerol as the sole carbon source **(Figure 6A-B)**. Interestingly, the *fbp* mutant displayed an even stronger depletion under H_2O_2 exposure than in M9 **(Figure 6C)**.

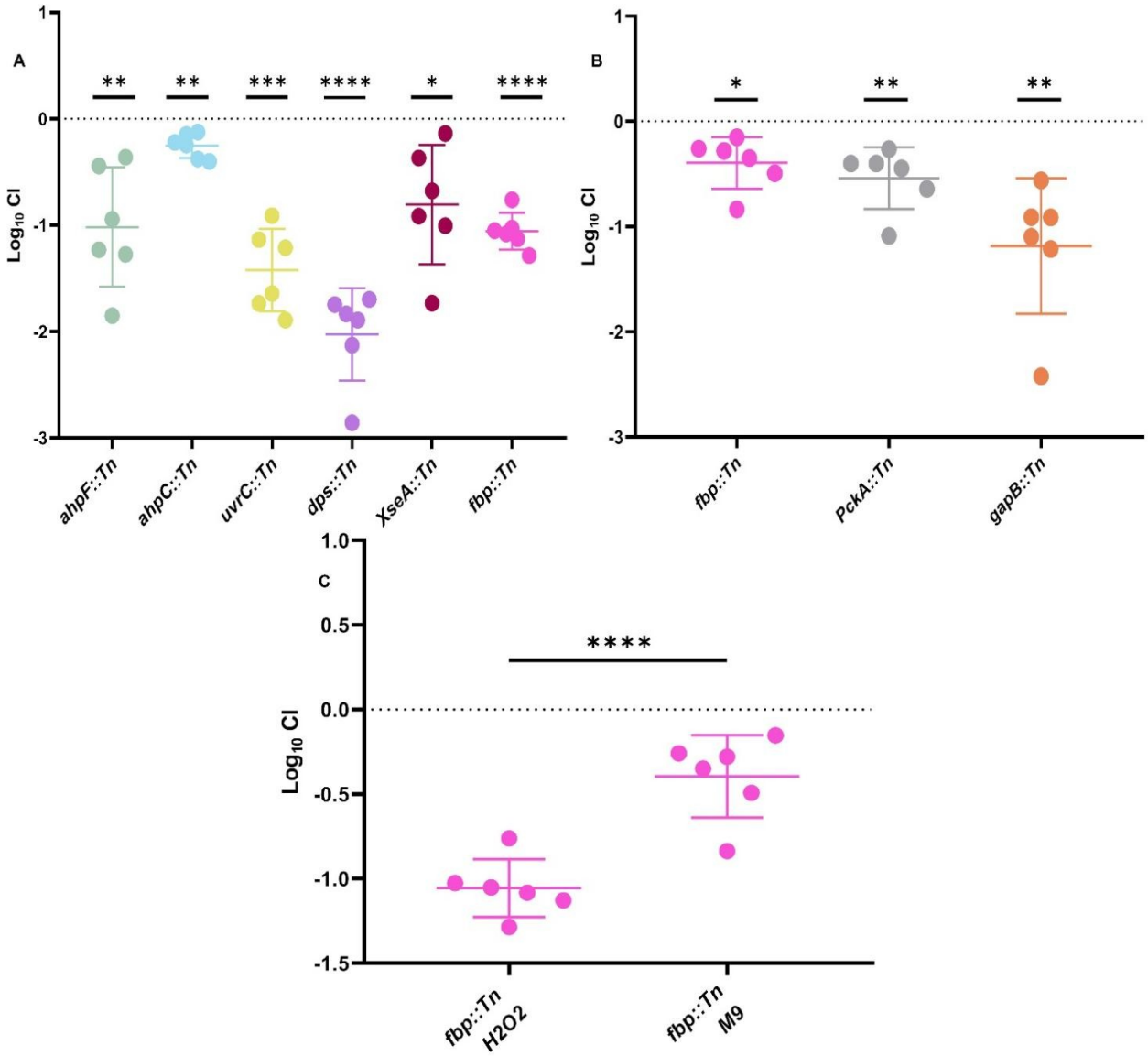

Figure 6: In vitro competitive assays under oxidative stress and gluconeogenic conditions. **(A)** Log_{10} CI of oxidative-stress mutants after short H_2O_2 exposure. **(B)** Log_{10} CI of gluconeogenesis-pathway mutants in glucose-free M9 medium. **(C)** Comparison of log_{10} CI for a representative gluconeogenic mutant under H_2O_2 versus M9 conditions. Statistical significance was assessed by one-sample two-tailed t-test vs zero for (A) and (B), and by unpaired two-tailed t-test (parametric) for (C). Two independent experiments were performed, each with three independent replicates (n = 6 per group). Each point represents one replicate and bars indicate group means. P-values are indicated as follows: $P < 0.05$ (*), $P < 0.01$ (**), $P < 0.001$ (***); ns, not significant.

Discussion

This study provides a comprehensive view of the tissue-specific genetic requirements for *S. aureus* growth and survival across distinct host environments. By leveraging a highly saturated transposon mutant library and *in vivo* TraDIS screening across skin and systemic infection models, we identified both conserved and niche-specific fitness and anti-fitness genes that support infection.

A major strength of this study was the use of high-dose infection strategies to minimize bottlenecks, allowing for robust library retention and meaningful assessment of mutant fitness.[16,26] As recommended previously, the inoculum should contain between 10-100 cells per insertion mutant.[27] This approach led to high organ-specific bacterial burdens and supported the recovery of complex mutant libraries with UIS counts that exceeded those reported in comparable *in vivo* TraDIS studies.[28,29] Effective population size and insertion retention metrics confirmed that mutant diversity was preserved across all samples; however, one mouse (MB in the skin infection model) showed a strong bottleneck **(Table 1)**. While this sample showed reduced complexity, it was retained in the initial step of analysis as the mutant depletion profile was highly concordant with the other skin samples, preserving biological signal. For subsequent read depth aware QC post proof and curation which assume stable insertion diversity UIS and can be distorted when severe bottlenecks decouple read depth from diversity, we excluded MB to avoid coverage driven artifacts.[14,16–18] *In vivo* Tn-seq/TraDIS is vulnerable to infection bottlenecks and PCR "jackpots," which can distort readouts independent of true fitness effects.[16] Accordingly, read counts were used for differential testing, while UIS tracked library complexity and skew.[17,18] We then applied a post-hoc, read depth aware QC that flags loci with stable UIS_s but ≥2× shifts in RPU, removing "read depth only" enrichments and "false depletions" to increase specificity without losing genuine signal.[14,18] This strategy follows field guidance and aligns with community pipelines (TRANSIT; Bio-TraDIS).[17,18] To further improve the reliability of our findings, we applied a stringent three-tiered filtering pipeline to define fitness and anti-fitness genes during skin and systemic infection. By excluding mutants that were also depleted and enriched under *in vitro* conditions, we minimized background noise and isolated *in vivo* specific fitness genes hits. This conservative approach was chosen to increase the specificity of gene discovery and enable the robust identification of tissue-specific vulnerabilities.

Our replicate-resolved design with explicit bottleneck accounting (per-sample UIS_s and CFU) and the filtration decision rule yields conservative yet stable TraDIS inferences across skin and systemic niches. In skin, Valentino *et al*. and Grosser *et al.* evaluated replicate correlation but did not pair input and output

within the same replicate, preventing direct bottleneck quantification (e.g., UIS_s retention, N_e).[20,21] In systemic models, Chang *et al*., used a heterogeneity (HTR) score with organ-specific cutoffs and reported strong kidney/spleen bottlenecks, while Li's >90% post-recovery loss shows replication alone cannot offset severe bottlenecks.[22,23] Conversely, substantial overlap with the independent airway model of Kim *et al*. supports a conserved *in vivo* fitness core when low bottlenecks are maintained.[24] By requiring concordant significance in both contrasts (IO∩CO) and enforcing logCPM/coverage and replicate-stability filters, we remove CO-only and IO-only artifacts and mitigate bias from the standardized, replicate outgrowth control. Together, these contrasts emphasize that our replicate-resolved design, high CFU recovery, filtration decision rule, and UIS_s based bottleneck accounting yield conservative yet robust cross study comparisons.

S. aureus navigates a complex landscape of host-imposed stresses that necessitate the dynamic reorganization of its metabolic, regulatory, and stress-response networks for effective infection. Our analysis showed that nucleotide biosynthesis is required for *S. aureus* survival during skin and systemic infections, in agreement with previous studies.[30–32] This agreement further supports the validity of the results produced. Consistent depletion of pyrimidine biosynthesis mutants across the skin, kidney, and spleen suggests that this pathway is broadly essential for *in vivo* fitness, regardless of the specific tissue environment. In parallel, several purine biosynthesis mutants also showed widespread depletion across the three tissues, albeit with slightly more variability. Notably, *purB and purR* mutants were flagged as enriched in the skin, suggesting that *S. aureus* may have a local availability of host-derived purines or engagement of salvage pathways. As previously described, cutaneous infection is neutrophil-dominated with abundant Neutrophil Extracellular Traps (NETs),[33–35] where *S. aureus* nuclease (Nuc) and adenosine synthase A (AdsA) convert NET DNA into deoxyad enosine (dAdo) that engages host purine salvage and triggers caspase-3 apoptosis.[36,37] Taken together, these observations may suggest reduced reliance on strict pathway control in environments where host-derived purines may be available. By contrast, kidneys at 24 h post-infection are PMN-rich but not yet mature abscesses with organized architecture typically evident at 48h.[38,39] Splenic macrophage subsets specialize in rapid filtration/clearance of blood-borne microbes.[40]Choueiry *et al*. demonstrated that purine metabolism in *S. aureus* is tightly regulated by nutrient availability and Li *et al.* showed that strains with impaired purine biosynthesis can persist *in vivo*, likely through compensatory virulence mechanisms or alternative metabolic routes.[41,42] Nevertheless, the overall pattern reinforces that *de novo* purine synthesis remains essential, particularly during systemic infection. As previously described, *de novo* guanine biosynthesis is essential in systemic

infection, and salvage alone is insufficient (*guaB*/*guaA* required, *xpt*/*pbuX* dispensable).[43] Supporting this, mutants disrupted in *purR*, a transcriptional repressor of the purine biosynthesis pathway, were enriched in systemic infection model.[31,44,45]

TraDIS screening of the skin abscess model highlighted the essential roles of the stress response pathways in promoting *S. aureus* survival within the hostile skin microenvironment. Mutants in genes encoding antioxidant defenses, including *ahpC, ahpF,* and *dps* were significantly depleted in the skin, reflecting the oxidative and genotoxic pressures imposed by host immunity. *In vivo* and *in vitro* competitive index assays, including a short H_2O_2 exposure variant confirmed that the disruption of *ahpC, ahpF,* and *dps* impairs bacterial fitness, pointing to their importance in counteracting oxidative stress and maintaining genome integrity at the host pathogen interface. In the inflamed skin niche, ROS oxidatively inactivate PerR, de-repressing redox defenses (e.g., *ahpC, ahpF, dps*).[46,47] Alkyl-hydroperoxidases (AhpC, AhpF) mitigate ROS toxicity by detoxifying peroxides, while Dps sequesters iron and protects DNA from oxidative damage.[48] Excess iron drives Fenton chemistry, escalating DNA-damaging hydroxyl radicals.[49–51] Interestingly, mutants in *perR* were highly enriched, particularly during skin infection, suggesting that repression of oxidative stress genes may be disadvantageous in this niche, possibly because constitutive de-repression of antioxidant systems enhances survival.

Moreover, several mutants in DNA repair genes involved in the SOS response and mismatch repair systems were significantly depleted in the skin model, including *uvrA, uvrB, uvrC, recD,* and *xseA*, suggesting they are critical for survival under genotoxic stress. *In vivo* and *in vitro* competitive assays - including an H_2O_2 exposure mimicking oxidative DNA damage- confirmed that disruption of *uvrC* and *xseA* significantly reduced *S. aureus* fitness in the skin infection model, emphasizing the importance of DNA repair mechanisms in promoting bacterial persistence within the abscess microenvironment. Genotoxic stress typically activates the SOS response via RecA-mediated cleavage of the LexA repressor, thereby inducing the expression of nucleotide excision repair genes such as *uvrC*.[52] This inducible system plays a broader role in promoting bacterial persistence and population-wide stress tolerance.[53] The mismatch repair pathway, which includes *recJ* and the ExoVII complex (*xseA*, *xseB*), contributes to maintaining genome integrity under oxidative and host-imposed stress, and has been shown to be critical for repairing immune-mediated DNA damage in *S. aureus*.[54]

TraDIS analyses identified the genes *fbp, pckA,* and *gapB*, which encode fructose-1,6-bisphosphatase (FBPase), phosphoenolpyruvate carboxykinase (PckA), and glyceraldehyde-3-phosphate dehydrogenase

(GapB) as fitness genes during *S. aureus* infection in the skin, kidney, and spleen, implicating gluconeogenesis as a core metabolic requirement across infection sites. Mutants in *pyk* were consistently enriched in systemic sites where *gpmI* in skin niche. and *eno* (enolase) is essential under basal conditions, these patterns collectively suggest a metabolic bias toward gluconeogenesis over glycolysis during infection. *In vitro* competition in glucose-free M9 (gluconeogenic) likewise showed depletion for *fbp*, *pckA*, and *gapB*. However, subsequent validation using competitive assays revealed striking tissue-specific dependencies. In the kidney, both *pckA* and *fbp* were indispensable, whereas *gapB* was dispensable, indicating reliance on canonical gluconeogenesis from oxaloacetate, with the potential bypass of GapB through host-derived glycerol or redundant enzymatic activity. In contrast, in the spleen, *S. aureus* required both *gapB* and *fbp*, but not *pckA*, consistent with gluconeogenic flux driven by substrates that enter downstream of oxaloacetate, such as glycerol or amino acids, allowing *S. aureus* to flexibly reroute carbon into hexose biosynthesis under tissue-specific nutrient constraints.[55] In the skin, only *fbp* was essential, implying a restricted but targeted use of gluconeogenesis, likely sustained by triose intermediates and a glucose-depleted abscess milieu.[56] The common essentiality of *fbp* emphasizes its pivotal role in maintaining fructose-6-phosphate (F6P) pools, thereby fueling anabolic pathways and redox homeostasis. Although not a constituent of the pentose phosphate pathway (PPP) *per se*, *fbp* enables F6P regeneration, which could sustain PPP flux, an indispensable process in *S. aureus* for NADPH production, energy metabolism, nucleotide biosynthesis, and oxidative stress resistance.[57] In line with this model, an *in vitro* short H_2O_2 exposure variant competitive assay showed the *fbp* mutant was significantly outcompeted by the wild type. This depletion under short H_2O_2 exposure was even stronger than in M9. Disruption of this pathway compromises these functions, ultimately impairing biofilm formation and reducing virulence *in vivo*.[58] While our findings emphasize the importance of gluconeogenic flux, there is compelling evidence that glycolysis is also vital, particularly for counteracting nitric oxide ($NO\cdot$) stress.[59] Consistent with this, our TraDIS analysis revealed that multiple glycolytic genes including *pfkA*, *SAUSA300_2079*, *gapA*, *pgk*, and *eno* were essential for growth in both input and output libraries, indicating that glycolysis is likewise indispensable under infection conditions. This metabolic adaptability aligns with prior findings that *S. aureus* requires both glycolytic and gluconeogenic activities to endure host-imposed pressures.[60] Our findings underscore the importance of tissue-specific metabolic flexibility, with *fbp* emerging as a central node linking carbon flux to redox balance and biosynthesis. Further research is needed to elucidate how *S. aureus* coordinates glycolysis and gluconeogenesis during infection and how this balance is modulated by the immune environment and nutrient availability *in vivo*.

Notably, aromatic-amino-acid (AAA) biosynthesis mutants, *aroA2* (*SAUSA300_1683*) and *aroE*, were enriched in the skin but depleted in the kidney; this pattern may reflect glucose depletion and peptide availability in skin abscesses and the role of *aroE* in shikimate flux, whereby peptides/free amino acids could buffer AAA biosynthesis in skin, whereas the kidney niche may require greater *de novo* shikimate-pathway activity.[7,56,61]

Furthermore, mutants in genes involved in branched-chain amino acid (BCAA) catabolism (*bkdAA, bkdAB, bkdB, ilvE,* and *lpdA*) and the uncharacterized *SAUSA300_0355* gene were strongly depleted in the kidney and spleen, but not in the skin, underscoring a compartmentalized metabolic requirement and a critical, tissue-specific role for amino acid catabolism in supporting *S. aureus* survival during systemic infection. Mechanistically, this systemic pattern is most consistent with a membrane-centric requirement in which the IlvE (branched-chain aminotransferase, BCAT), BKD (branched-chain α-keto acid dehydrogenase; subunits E1α bkdAA, E1β bkdAB, E2 bkdB, E3 lpdA) and FabH (β-ketoacyl-ACP synthase III; ACP, acyl carrier protein) route supplies branched acyl-CoA primers for the type II fatty-acid synthesis (FASII) pathway to produce branched-chain fatty acids (BCFAs) **(Figure 4)**. In *S. aureus*, FabH initiates fatty-acid synthesis using branched primers derived from BCAA catabolism.[62–64] Disrupting BKD lowers BCFA content, reduces membrane fluidity, and increases sensitivity to alkaline, oxidative, and solvent stress, with chemical rescue by an anteiso-BCFA precursor (2-methylbutyrate).[65] BCFAs are also required for activation of multiple two-component systems (TCSs), linking membrane composition to virulence signaling.[66] Concomitantly, *SAUSA300_0355,* annotated as a putative acetyl-CoA acyltransferase likely feeds the mevalonate pathway (MVA), MvaS (3-hydroxy-3-methylglutaryl-CoA synthase) and MvaA (3-hydroxy-3-methylglutaryl-CoA reductase) → IPP/DMAPP (isopentenyl/dimethylallyl diphosphate) **(Figure 4)** → FPP (farnesyl diphosphate), providing Und-PP (undecaprenyl pyrophosphate) for peptidoglycan/WTA (wall teichoic acid) export and the isoprenyl side chains of menaquinone for respiration; defects in MVA flux impair cell-wall biogenesis and are rescued by mevalonate/FPP.[67] Despite filtration thresholds, mutants in *bkdAB* remained significantly depleted in the kidney (Log_2FC –1.8), and competitive assays validated the essentiality of both *bkdAB* and *SAUSA300_0355* for *S. aureus* survival in the systemic infection model. The gene *bkdAB* encodes the beta subunit of the 2-oxoisovalerate dehydrogenase complex, a key enzyme in BCAA degradation, and has previously been linked to conditional essentiality in a pneumonia model and increased susceptibility to LL-37 and its synthetic analogs.[24,68] Its disruption results in increased membrane permeability, impaired biofilm formation, and reduced endothelial cytotoxicity, suggesting a role in membrane

integrity and virulence.[68,69] Additionally, the acetyl-CoA acyltransferase SAUSA300_0355 is implicated in the maintenance of membrane potential and aminoglycoside resistance.[70] Homologous loci in other *S. aureus* strains (e.g., *SAOUHSC_00336, Q2G124, SAPIG0434*) point to their involvement in lipid metabolism and the mevalonate pathway for isoprenoid biosynthesis. Disruption of *SAPIG0434* impairs bacterial fitness under stressors, including temperature fluctuations and vancomycin exposure.[71–73]

Taken together, these observations support a single, tissue-tuned metabolic network: amino-acid catabolism supplies TCA intermediates that are recycled via Fbp/PckA/GapB to regenerate hexose phosphates and may sustain PPP-dependent NADPH and anabolism.[7,59,74] BCAA-derived acyl-CoAs prime FabH-initiated FASII for membrane remodeling.[62,64,65] In parallel, SAUSA300_0355 supports the MVA pathway, channeling acetyl-CoA to isoprenoids and Und-PP for respiration and cell-wall/WTA export.[75,76]

In parallel, the catabolism of basic amino acids is also required during systemic infection. Mutants in *SAUSA300_0458* were specifically depleted in the kidney and spleen but not in the skin, suggesting a selective requirement for deep-tissue colonization. Annotated as the sole putative ornithine/lysine/arginine decarboxylase in *S. aureus* (EC 4.1.1.17, EC 4.1.1.18, EC 4.1.1.19), this gene likely encodes an enzyme involved in the decarboxylation of basic amino acids to produce the polyamines, consistent with the roles described for polyamine biosynthesis decarboxylases by Li *et al*.[77] These decarboxylation reactions produce biogenic polyamines; putrescine, cadaverine, and agmatine which may ultimately give rise to spermidine and spermine through subsequent biochemical steps, as shown in other microorganisms.[78,79] These biogenic polyamines play important roles in stabilizing nucleic acids and cellular membranes, and are implicated in gene regulation and biofilm formation.[79] While *S. aureus* was long considered incapable of synthesizing polyamines and was highly susceptible to their bactericidal effects, particularly spermine and spermidine, the acquisition of the Arginine Catabolic Mobile Element (ACME) in USA300 strains conferred resistance to polyamine toxicity.[78] Although early studies failed to detect endogenous polyamine production, recent reports have demonstrated the presence of putrescine and its derivative N-acetyl-putrescine in *S. aureus*, suggesting an unrecognized role for this pathway in systemic infection.[80,81] These observations raise the possibility that *SAUSA300_0458* contributes to a broader metabolic strategy that includes amino acid catabolism, membrane adaptation, and redox balance, potentially supporting the persistence of *S. aureus* in the nutrient-limited and immunologically hostile environments in systemic tissues.

In conclusion, these findings provide a comprehensive map of tissue-specific fitness genes required for *S. aureus* survival during infection and reveal the organism's remarkable metabolic flexibility. By combining high-resolution TraDIS screening with *in vivo* and *in vitro* validation, we identified key fitness genes involved in nucleotide biosynthesis, oxidative stress response, central carbon, and amino acid metabolism with clear organ level differences. Stress-response functions predominate in skin, consistent with an inflammatory milieu, whereas amino-acid catabolism is uniquely critical in systemic tissues, aligning with higher metabolic demand and constrained nutrients.[82] These results reveal distinct, tissue-tailored adaptations and expose vulnerabilities that could be leveraged for precision antimicrobial strategies.

Limitations of the study

While this study provides a comprehensive analysis of organ-specific fitness determinants in *S. aureus* using high-resolution TraDIS and *in vivo* murine infection models, several limitations should be noted. An inherent challenge of TraDIS is that it measures gene fitness effects within a pooled, competitive environment, making it difficult to draw definitive conclusions about individual gene fitness without follow-up validation. Using a high inoculum preserves library coverage but likely emphasizes acute, early fitness requirements, extrapolation to low-dose or chronic models should be done with cautious. Pooled TraDIS under-captures 'public-goods' genes because mutants benefit via trans-complementation, so these loci may not appear depleted. We did validate key hits using competitive index assays, but these analyses could not be extended to all genes of possible interest, nor were single-mutant infections performed, which could further support individual gene contributions to fitness. NTML mutants were used as supplied (JE2 background) without re-transduction; thus, potential unlinked secondary mutations cannot be fully excluded. *In vivo* competition assays were performed once per model (n = 5 mice) using mixed inoculum, without day or batch repeats. With a view to the importance of the results in relation to human health, it is important to note that essentiality was assessed under murine conditions, which may not fully represent the complexity of human infections. In addition, our stringent QC and statistics-based filtering, implemented to maximize specificity, can exclude borderline but biologically plausible signals, for example, *bkdAB* ($\log_2$FC −1.8) fell just short of our ≤ −2 threshold yet was independently validated as a potential requirement during systemic infection. Finally, our approach does not capture genes that are essential under all conditions and therefore lack transposon insertions, nor does it fully account for polar effects within operons and it was only performed with one strain, which is not representative of all lineages of this important pathogen. Cross-strain portability was not evaluated. This could be addressed

by transducing priority mutations into other *S. aureus* backgrounds and testing fitness versus wild type; unbiased confirmation would require multi-library screens across strains. Future studies incorporating single-mutant infections, other strains, complementary omics approaches, and human-relevant models will help to address these limitations.

Resource availability

Lead contact:

Further information and requests for resources and reagents should be directed to and will be fulfilled by the lead contact, Bianca Paglietti (biancap@uniss.it).

Materials availability:

This study did not generate new bacterial strains. All mutants used were obtained from the Nebraska Transposon Mutant Library (NTML) and are listed in **(Table 2)**. No new unique reagents were generated in this study.

Data and code availability:

- TraDIS sequencing data generated in this study have been deposited in the NCBI Sequence Read Archive (SRA) under BioProject accession number PRJNA1284342.
- Our previously published input library data used in this study are available under BioProject accession number PRJNA1137847, as reported by Yousief *et al.* (2024) in *Scientific Reports* (PMID: 39354068; DOI: 10.1038/s41598-024-73731-y). In addition, outgrowth control libraries, where the input library was grown under standard *in vitro* conditions, are available under BioProject accession number PRJNA1190087, as reported by Nader Abdelmalek *et al*. (2025) in *Antibiotics* (PMID: 40001356; DOI: 10.3390/antibiotics14020112)
- Sample-specific BioSample and SRA Run accession numbers for all output, input and outgrowth control libraries are provided in **(Table S6)**.
- Custom analysis code used in this study is available in a private GitHub repository and includes ***Data*** S1 (read-depth–aware QC and three-tier curation). QC thresholds (ΔUIS% ≤ 20; $UIS_{in/out} \geq 5$; $RPU_{FC} \leq 0.5$ or ≥ 2.0) were pre-specified and recorded in GitHub release v0.9.0, pre-analysis

prior to differential testing. The QC procedure described above is implemented in ***Data S1*** in supplementary section, and per-organ QC outputs are provided **(Table S2)**. The script requires only *readr* and *dplyr* and accepts generic three-column input files (locus_tag, gene_name, value) for both read counts and UIS.

- Any additional information required to reanalyze the data reported in this paper is available from the lead contact upon reasonable request.
- The codes used for TraDIS analysis is available through the Bio-Tradis GitHub repository: https://github.com/sanger-pathogens/Bio-Tradis.
- Additional data supporting the findings of this study are available from the corresponding author upon request.

Acknowledgments

This work was supported by the European Union's Horizon 2020 research and innovation program under the Marie Skłodowska-Curie grant agreement No. 956154, as part of the Innovative Training Network (Innovative approaches to identification of metabolic Targets for antimicrobials, INNOTARGETS) (https://cordis.europa.eu/project/id/956154). We thank BEI Resources, NIAID, NIH for providing *S. aureus* subsp. *aureus*, strain JE2 and NTML. We are grateful to Assistant Professor Mattia Pirolo, Section for Veterinary Clinical Microbiology, Department of Veterinary and Animal Sciences, University of Copenhagen, for providing materials used in DNA extraction from *S. aureus*. Special thanks are extended to Birgitte Regenberg's research group in the Department of Biology, University of Copenhagen, for kindly providing access to the Bioruptor device. We also thank the staff of the Department of Experimental Medicine (AEM) and the technicians at the Department of Veterinary and Animal Sciences, University of Copenhagen, for their support with murine infection models and media preparation and specialized laboratory services, respectively.

Author contributions

Conceptualization, S.W.Y and B.P.; methodology, S.W.Y., N.A., and P.R.G., ; software, S.W.Y; validation, S.W.Y; formal analysis, S.W.Y; investigation, S.W.Y; resources, B.P.; data curation, S.W.Y; writing, original draft preparation, S.W.Y; writing, review and editing, S.W.Y., N.A. M.S.B., Y.M., P.R.G,

S.N., J.E.O. and B.P.; visualization S.W.Y., N.A. M.S.B., Y.M., P.R.G, S.N., and J.E.O.; supervision, B.P.; project administration, J.E.O. and B.P.; funding acquisition, B.P. All authors have read and agreed to the published version of the manuscript.

Declaration of interests

The authors declare no competing interests.

STAR★Methods

Key resources table

Reagent or Resource	***Source***	***Identifier***
Bacterial Strains		
S. aureus subsp. *aureus* USA300 JE2	BEI Resources, NIAID, NIH	NR-46543
S. aureus USA300 JE2 *uvrC::Tn (NE1212)*	BEI Resources, NIAID, NIH	NR-47755
S. aureus USA300 JE2 *xseA::Tn (NE458)*	BEI Resources, NIAID, NIH	NR-47001
S. aureus USA300 JE2 *ahpC::Tn (NE911)*	BEI Resources, NIAID, NIH	NR-47454
S. aureus USA300 JE2 *ahpF::Tn (NE1571)*	BEI Resources, NIAID, NIH	NR-48113
S. aureus USA300 JE2 *dps::Tn (NE1929)*	BEI Resources, NIAID, NIH	NR-48471
S. aureus USA300 JE2 *pckA::Tn (NE1260)*	BEI Resources, NIAID, NIH	NR-47803
S. aureus USA300 JE2 *gapB::Tn (NE1343)*	BEI Resources, NIAID, NIH	NR-47885
S. aureus USA300 JE2 *fbp::Tn (NE542)*	BEI Resources, NIAID, NIH	NR-47085
S. aureus USA300 JE2 *SAUSA300_0355::Tn (NE1901)*	BEI Resources, NIAID, NIH	NR-48443
S. aureus USA300 JE2 *bkdAB::Tn (NE1829)*	BEI Resources, NIAID, NIH	NR-48371
S. aureus USA300 JE2 *SAUSA300_0458::Tn (NE895)*	BEI Resources, NIAID, NIH	NR-47438
Critical commercial assays		
DNeasy Blood & Tissue Kit (250)	Qiagen	Cat# 69506
Bioanalyzer High Sensitivity DNA kit	Agilent Technologies	Cat# 5067-4626
AMPure XP PCR Purification Beads	Beckman Coulter	Cat# A63881
NEBNext End Repair module	New England Biolab	Cat# E6050
NEBNext dA-Tailing Module	New England Biolab	Cat# E6053
NEBNext Quick Ligation Module	New England Biolab	Cat# E6056
KAPA HiFi HotStart ReadyMix	KAPA Biosystems (Roche)	Cat# KK2601
KAPA Library Quantification Kit (Illumina, SYBR)	KAPA Biosystems (Roche)	Cat# KK4824
MiSeq V2 Kit	Illumina	Cat# MS-102-2001
Chemicals		
Brain Heart Infusion (BHI) broth/agar	Microbiol, Italy	Cat# 70.031
Tryptic Soy Broth (TSB)	Microbiol, Italy	Cat# 70.196
M9 minimal medium (glucose-free, 0.2% glycerol)	Prepared in lab (see STAR★Methods)	
Erythromycin	Sigma-Aldrich, USA	Cat# E5389
DPBS	Sigma-Aldrich, USA	Cat# D8537-500ML
Saline NaCl 0.9%	B. Braun Melsungen AG, Germany	Cat# 36553
H_2O_2	Sigma-Aldrich, USA	Cat# H1009-100ML
Magnesium sulfate (anhydrous)	Sigma-Aldrich, USA	Cat# M7506-500G
Calcium chloride (anhydrous)	Sigma-Aldrich, USA	Cat# C5670-100G
Ammonium chloride	Sigma-Aldrich, USA	Cat# 1011430050
Sodium chloride	Sigma-Aldrich, USA	Cat# 1041631000
Sodium phosphate dibasic	Sigma-Aldrich, USA	Cat# 567550-500GM
Potassium phosphate monobasic	Sigma-Aldrich, USA	Cat# 529568-250GM
UltraPure™ Glycerol	Invitrogen™	Cat# 15514011
Deposited Data		

Raw sequencing data	NCBI SRA	PRJNA1284342
Previously published input data	NCBI SRA	PRJNA834801
Outgrowth control libraries	NCBI SRA	PRJNA928137
Experimental models: Organisms/strains		
BALB/c mice (6–8 weeks old, female)	Taconic Bioscience	BALB/cAnNTac
C57BL/6 mice (6–8 weeks old, female)	Taconic Bioscience	C57BL/6NTac
Oligonucleotides		
Table S7		
Instruments		
Qubit™ 4 Fluorometer	Thermo Fisher	Cat# Q33226
Bioruptor® Pico	Diagenode	Cat# B01060010
Agilent 2100 Bioanalyzer	Agilent Technologies	Cat# 228250
LightCycler® 96	Roche	Cat# 05815916001
MiSeq Sequencing Platform	Illumina	Cat# SY-410-1003
Sensititre™ Nephelometer	Thermo Fisher	Cat# V3011
Bioscreen C	Oy Growth Curves Ab Ltd., Finland	N/A
Software and algorithms		
Agilent 2100 Expert	Agilent Technologies	RRID: SCR_018043
LightCycler® 96 system	Roche	RRID: SCR_023415
Bio-TraDIS Toolkit	Wellcome Sanger Institute (GitHub)	RRID: SCR_015993
GraphPad Prism	GraphPad Software	RRID:SCR_002798
RStudio	Posit	RRID:SCR_000432

Experimental model and subject details

Mice

Female BALB/c (BALB/cAnNTac) and C57BL/6 (C57BL/6NTac) mice (6–8 weeks old) were purchased from Taconic Biosciences. All mice were housed in individually ventilated cages under specific pathogen–free (SPF) conditions, with a 12-hour light/dark cycle and ad libitum access to food and water.

Both mouse strains were used for skin and systemic infection models. All animal experiments were approved by the Danish Animal Experiments Inspectorate (https://dyreforsoegstilsynet.dk) under protocol number 2021-15-0201-0098, in accordance with Danish Law LBK 474 of 15/05/2014 (Animal Experimentation and Welfare Act).

Method details

Bacterial strains and growth conditions

S. aureus USA300 JE2 (WT) and selected transposon mutants were obtained from the NTML, originally described by Fey *et al*.[25] Strain details and infection model usage are provided in **Table 2**. All strains were routinely cultured in BHI broth or agar at 37°C under aerobic conditions. When appropriate, BHI was supplemented with 5 µg/mL erythromycin for transposon mutant selection.

Growth curves of the WT and selected mutant strains were monitored using the Bioscreen C instrument. Overnight cultures were diluted to a starting OD_{600} of 0.05 in BHI broth, and 300 µL was transferred to honeycomb plates. Optical density (OD_{600}) was recorded every 15 minutes for up to 24 h at 37°C with continuous shaking. Inoculum density for growth curves was standardized using a Sensititre™ Nephelometer according to the manufacturer's instructions.

All the competition assays done based on CFU-matched (1:1) (WT: mutant).

Table 2: Bacterial strains used in this study.

Strain	Infection mode used in	Description
USA300 JE2	Skin/ Systemic	Wild-type parent strain of NTML
NE1212 (uvrC::Tn)	Skin	Transposon insertion in *SAUSA300_1045*. Erm^r
NE458 (xseA::Tn)	Skin	Transposon Insertion in *SAUSA300_1472.* Erm^r
NE911 (ahpC::Tn)	Skin	Transposon Insertion in *SAUSA300_0380.* Erm^r
NE1571(ahpF::Tn)	Skin	Transposon Insertion in *SAUSA300_0379.* Erm^r
NE1929 (SAUSA300_2092::Tn)	Skin	Transposon insertion in *SAUSA300_2092*. Erm^r
NE1260 (SAUSA300_ pckA::Tn)	Skin / Systemic	Transposon insertion in *SAUSA300_1731*. Erm^r
NE1343 (SAUSA300_gabB::Tn)	Skin / Systemic	Transposon insertion in *SAUSA300_1633*. Erm^r
NE542 (SAUSA300_fbp::Tn)	Skin / Systemic	Transposon insertion in *SAUSA300_2455*. Erm^r
NE1901 (SAUSA300_0355::Tn)	Systemic	Transposon insertion in *SAUSA300_0355*. Erm^r
NE1829 (SAUSA300_ bkdAB::Tn)	Systemic	Transposon insertion in *SAUSA300_1465*. Erm^r
NE895 (SAUSA300_0458::Tn)	Systemic	Transposon insertion in *SAUSA300_0458*. Erm^r

Animal inoculum

TraDIS screening inoculum (pooled library), frozen glycerol stocks of the *S. aureus* USA300 JE2 transposon mutant library (stored at −80 °C) were thawed on ice. When multiple vials were used, they were pooled, pelleted (≈4,000 × g, 10 min, 4°C), washed 2x with DPBS, and resuspended in DPBS. The suspension was adjusted to deliver 3×10^9 CFU per mouse in a 0.1 mL injection volume within ~60 min of preparation.

In vivo competition assays (WT vs mutant), overnight cultures were pelleted (~4,000 × g, 10 min, 4 °C), washed 2× with DPBS, and diluted in DPBS to the target concentration. The mixed inoculum contained ~1 × 10^9 CFU per mouse, 1:1 WT: mutant (~5 × 10^8 CFU each)

***In vitro* competition assays**

In rich BHI medium, overnight cultures (12–14 h) of WT and the indicated mutants were grown in BHI at 37 °C, 180 rpm, diluted to OD_{600} = 0.05 in pre-warmed BHI, and mixed 1:1 (WT: mutant) to a starting density of ~10^8–10^9 CFU/mL (total volume 10 mL).

Short H_2O_2 exposure outgrowth variant, after mixing WT and the corresponding mutants 1:1, the inoculum was immediately diluted into 10 mL sterile saline (0.85–0.9% NaCl) and pulsed with H_2O_2 (final 5 mM,[83] stock 30% ≈ 9.8 M) for 15 min at 37 °C, 180 rpm. H_2O_2 was added last. At pulse end, 1.0 mL was transferred into 9.0 mL pre-warmed BHI (1:10) and outgrown 3.5 h at 37 °C, 180 rpm.

Glucose-free M9[84] (gluconeogenic) competition, overnight WT and the corresponding mutants were washed 2× in PBS, resuspended in M9 minimal salts (Na_2HPO_4 6.78 g, KH_2PO_4 3.0 g, NaCl 0.5 g, and NH_4Cl 1.0 g/ L) (post-autoclave supplemented with filtered $MgSO_4$ 1 mM, $CaCl_2$ 0.1 mM, and glycerol 0.2% v/v as the sole carbon source), adjusted to OD_{600} = 0.05, and mixed 1:1 to ~10^6 CFU/mL (10 mL total; 37 °C, 180 rpm).

Sampling and enumeration (all assays), an input (t_0) sample was taken immediately, serially diluted in DPBS, and plated in parallel on BHI agar (total CFU) and BHI + erythromycin (5 μg/mL) to enumerate the erythromycin-marked mutant fraction; WT CFU were calculated as (BHI CFU − BHI+ery CFU) and plates were incubated at 37 °C. For BHI and M9 competitions, endpoint samples were taken at 24 h, for the H_2O_2 outgrowth variant, the endpoint sample was taken at 3.5 h. All timepoints were plated using the same scheme.

For archiving, glycerol stocks were prepared by mixing cultures with 50% glycerol to a final concentration of 25% and stored at –80°C.

Mouse infection models

In vivo screening with BALB/c mice

A high-density transposon mutant library constructed in the USA300 JE2 background[12] was used to screen for fitness genes required for survival during skin and systemic infections. Female BALB/c mice were used as the *in vivo* model host for library infection. For each model, mice were divided into two groups: a control group of five mice injected with 0.1 mL sterile DPBS, and an experimental group of ten mice infected with 3×10^9 CFU/mouse of the transposon mutant library suspended in 0.1 mL DPBS, the same inoculum was used for both models. Infections were administered subcutaneously (SC) for the skin model and intraperitoneally (IP) for the systemic model. Mice were euthanized at 48 hours post-infection (skin) or 24 hours post-infection (systemic), and abscesses, kidneys, and spleens were aseptically harvested. For each condition, two mice were processed individually, and samples from the remaining eight mice were pooled, resulting in three biological replicates per group for downstream analysis. Each sample was homogenized in 0.1 mL DPBS. Ten-fold dilutions were prepared, and 100 µL was plated on BHI agar supplemented with 5 µg/mL erythromycin, followed by overnight incubation at 37°C to determine CFU counts. The remaining diluted suspensions were plated on 15 cm BHI + erythromycin plates (0.3 mL per plate) for mutant library recovery. Colonies were collected in 1 mL aliquots, re-expanded, and stored in 1 mL volumes (~1×10^{10} CFU) at −80°C for DNA extraction and sequencing.

In vivo validation with C57BL/6 mice

Selected NTML mutants were validated *in vivo* using competitive index (CI) assays in C57BL/6 mice (6–8 weeks old; Taconic Biosciences, C57BL/6NTac). For each mutant–WT comparison, a single mixed inoculum (WT: mutant) (1:1) was prepared once per model and administered to independent biological replicates (n=5 mice); organs were processed individually per mouse. For the skin infection model, nine groups (n = 5 mice/group) were infected subcutaneously with ~1×10^9 CFU in 0.1 mL DPBS. For the systemic model, seven groups (n = 5 mice/group) were infected intraperitoneally under the same conditions. One group per model received sterile DPBS as a negative control. Organs were harvested at 48 hours post-infection (skin) or 24 hours post-infection (systemic). In three systemic infection groups, early euthanasia at 12 hours was required due to humane endpoints. Samples were homogenized in DPBS and plated on BHI and BHI + erythromycin agar to enumerate CFUs of wild-type and mutant strains.

DNA extraction and TraDIS sequencing

Genomic DNA was isolated as previously described[85] using the DNeasy Blood & Tissue Kit. For each infection model, three biological replicates were processed per condition: two from individual mice and one pooled organ sample, each processed in duplicate. DNA was fragmented to an average size of 300–400 bp using the Bioruptor® Pico, and fragment size was verified using the Agilent 2100 Bioanalyzer with the High Sensitivity DNA Kit. Libraries were prepared following the protocol by Barquist *et al.*,[17] using pre-designed transposon-specific adapters and primers **(Table S7)**. Final library quality was assessed using the Bioanalyzer, and DNA concentrations were measured with the Qubit™ 4 Fluorometer. Libraries were quantified using the KAPA Library Quantification Kit for Illumina platforms on a LightCycler® 96 instrument. Sequencing was performed on an Illumina MiSeq platform using the MiSeq Reagent Kit v2 (50-cycle),[19] generating single end reads. The first 10 bp of each read (CAACCTGTTA) corresponded to the transposon junction and were used to map insertions. Read alignment and unique insertion site (UIS) mapping were performed using the Bio-Tradis pipeline, aligned to the *S. aureus* USA300 JE2 reference genome (GenBank accession: CP000255.1). Comparative analysis of output versus input libraries was conducted using the *tradis_comparison.R* script included in the Bio-Tradis Toolkit.

Quantification and statistical analysis

To assess bottleneck effects, unique insertion site (UIS) counts, and diversity metrics were calculated. Effective population size (Ne) was computed as: $N_e = \frac{(N_t)^2}{\sum N_i}$ where N_t is the number of UISs for a given sample and $\sum N_i$ is the total UISs in the respective infection group (Skin, Kidney, or Spleen).[27] Second, insertion reduction percentage was calculated relative to the input library (400,000 UISs)[12] using the formula, $Insertion\ Reduction\ (\%) = \frac{(UIS_S\ Input - UIS_S\ Output)}{UIS_S\ Input} \times 100.$

Bio-TraDIS (*tradis_comparison.R* /edgeR) tested Output vs Input and Output vs Outgrowth control. q-values are Benjamini–Hochberg FDR–adjusted p-values (edgeR 'FDR'); thresholds: $\log_2FC \leq -2$, $q < 0.01$.

Fitness genes for *S. aureus* survival during both infection models were defined by a three-step filtering strategy: (i) identify genes depleted in output versus input, (ii) intersect with those depleted versus the outgrowth control, and (iii) exclude genes also depleted in outgrowth versus input. To distinguish true

biological changes in mutant representation from coverage artifacts, we implemented a read-depth–aware post hoc QC on genes called differentially represented by Bio-TraDIS/edgeR. For each gene we summarized, per organ, (i) unique insertion sites (UIS) and (ii) total reads, separately for inputs and outputs (combined biological replicates per organ). We then computed $\Delta UIS\% = 100 \times \frac{UIS_S\ Outputs - UIS_S\ Inputs}{UIS_S Inputs}$ and $RPU = \frac{Reads}{UIS}$ with its fold change $RPU_{FC} = \frac{RPU_{Outputs}}{RPU_{Inputs}}$. We defined stable insertion diversity as ΔUIS% ≤20 and required minimum diversity ($UIS_{inputs} \geq 5$ and $UIS_{outputs} \geq 5$). We flagged as read-depth-only enriched those genes that were DE-enriched ($\log_2 FC \geq 2$, q value < 0.01) *and* had stable UIS with $RPU_{FC} \geq 2$. Conversely, we flagged false-depleted genes as DE-depleted ($\log_2 FC \leq -2$, q value < 0.01) with stable UIS and $RPU_{FC} \leq 0.5$. QC-flagged genes were excluded from organ-specific fitness lists and are provided in **(Table S2)** together with per-gene counts (reads, UIS, ΔUIS%, RPU metrics). This procedure complements standard TraDIS statistics. Statistical analyses were performed using GraphPad Prism (RRID: SCR_002798). The competitive index (CI) was defined as $CI = \frac{(\frac{Mutant_{CFU}}{WT_{CFU}})_{Recovered}}{(\frac{Mutant_{CFU}}{WT_{CFU}})_{Injected}}$. CI data were analyzed with one-sample, two-tailed t-tests, *in vitro* vs a theoretical mean of $\log_{10}(CI)=0$ (neutrality)[86,87] and *in vivo* vs $\log_{10}(CI)= -1$ (10-fold depletion). CFU time-course data were analyzed by two-way repeated-measures ANOVA with Sidak's post hoc test. P values are reported.

Supplemental information

Document S1. Figure S1 and S2 Download: Download Acrobat PDF file (374KB)

Data S1. Script implementing the read-depth–aware QC and three-tier curation workflow used to identify high-confidence fitness calls across infection models. Download: Download zip file (3KB)

Table S1. Gene-level TraDIS differential abundance analysis across all infection models (S1A–S1G) covering comparisons of organs vs input, organs vs outgrowth control, and outgrowth control vs input. Download: Download spreadsheet (1MB)

Table S2. QC-flagged genes with stable insertion-site diversity but altered read depth identified read depth only artifacts across all infection-model comparisons. Download: Download spreadsheet (66KB)

Table S3. Differential fitness genes from TraDIS screens across skin, kidney, and spleen, referenced to outgrowth controls and corresponding to **Figure 1B**. Download: Download spreadsheet (41KB)

Table S4. Provenance and curation of enriched (anti-fitness) genes across skin, kidney, and spleen infection models, following source comparisons, read depth quality assessment, contrast intersections, and final exclusion steps to produce the curated sets in **Figure 2A–B**. Download: Download spreadsheet (59KB)

Table S5. Cross-study concordance between fitness determinants identified in this study and those reported in previously published *in vivo* Tn-Seq screens of *S. aureus* USA300 JE2. Download: Download spreadsheet (15KB)

Table S6. Metadata for all samples submitted to the NCBI SRA and BioProject repositories. Download: Download spreadsheet (23KB)

Table S7. Oligonucleotides used in this study. Download: Download spreadsheet (13KB)

References

1. Murray, C.J., Ikuta, K.S., Sharara, F., Swetschinski, L., Robles Aguilar, G., Gray, A., Han, C., Bisignano, C., Rao, P., Wool, E., et al. (2022). Global burden of bacterial antimicrobial resistance in 2019: a systematic analysis. *Lancet* **399**, 629–655. https://doi.org/10.1016/S0140-6736(21)02724-0

2. Jenul, C., and Horswill, A.R. (2019). Regulation of *Staphylococcus aureus* virulence. *Microbiology Spectrum* **7**(2), GPP3-0031-2018. https://doi.org/10.1128/microbiolspec.GPP3-0031-2018.

3. Howden, B.P., Giulieri, S.G., Wong Fok Lung, T., Baines, S.L., Sharkey, L.K., Lee, J.Y.H., Hachani, A., Monk, I.R., and Stinear, T.P. (2023). *Staphylococcus aureus* host interactions and adaptation. *Nature Reviews Microbiology* **21**, 380–395. https://doi.org/10.1038/s41579-023-00852-y.

4. Horn, C.M., and Kielian, T. (2021). Crosstalk between *Staphylococcus aureus* and innate immunity: focus on immunometabolism. *Frontiers in Immunology* **11**, 621750. https://doi.org/10.3389/fimmu.2020.621750

5. Ledala, N., Zhang, B., Seravalli, J., Powers, R., and Somerville, G.A. (2014). Influence of iron and aeration on *Staphylococcus aureus* growth, metabolism, and transcription. *Journal of Bacteriology* **196**, 2178–2189. https://doi.org/10.1128/JB.01475-14.

6. Krismer, B., Liebeke, M., Janek, D., Nega, M., Rautenberg, M., Hornig, G., Unger, C., Weidenmaier, C., Lalk, M., and Peschel, A. (2014). Nutrient limitation governs *Staphylococcus*

aureus metabolism and niche adaptation in the human nose. *PLOS Pathogens* **10**, e1003862. https://doi.org/10.1371/journal.ppat.1003862.

7. Halsey, C.R., Lei, S., Wax, J.K., Lehman, M.K., Nuxoll, A.S., Steinke, L., Sadykov, M., Powers, R., and Fey, P.D. (2017). Amino acid catabolism in *Staphylococcus aureus* and the function of carbon catabolite repression. *mBio* **8**, e01434-16. https://doi.org/10.1128/mBio.01434-16.

8. Troitzsch, A., Van Loi, V., Methling, K., Zühlke, D., Lalk, M., Riedel, K., Bernhardt, J., Elsayed, E.M., Bange, G., Antelmann, H., et al. (2021). Carbon source-dependent reprogramming of anaerobic metabolism in *Staphylococcus aureus*. *Journal of Bacteriology* **203**, e00639-20. https://doi.org/10.1128/JB.00639-20..

9. Poudel, S., Hefner, Y., Szubin, R., Sastry, A., Gao, Y., Nizet, V., and Palsson, B.O. (2022). Coordination of CcpA and CodY regulators in *Staphylococcus aureus* USA300 strains. *mSystems* **7**, e00480-22. https://doi.org/10.1128/mSystems.00480-22.

10. Szafranska, A.K., Oxley, A.P.A., Chaves-Moreno, D., Horst, S.A., Roßlenbroich, S., Peters, G., Goldmann, O., Rohde, M., Sinha, B., Pieper, D.H., et al. (2014). High-resolution transcriptomic analysis of the adaptive response of *Staphylococcus aureus* during acute and chronic phases of osteomyelitis. *mBio* **5**, e01775-14. https://doi.org/10.1128/mBio.01775-14.

11. Chaffin, D.O., Taylor, D., Skerrett, S.J., and Rubens, C.E. (2012). Changes in the *Staphylococcus aureus* transcriptome during early adaptation to the lung. *PLOS ONE* **7**, e41329. https://doi.org/10.1371/journal.pone.0041329..

12. Yousief, S.W., Abdelmalek, N., and Paglietti, B. (2024). Optimizing phage-based mutant recovery and minimizing heat effect in the construction of transposon libraries in *Staphylococcus aureus*. *Scientific Reports* **14**, 22831. https://doi.org/10.1038/s41598-024-73731-y

13. Langridge, G.C., Phan, M.D., Turner, D.J., Perkins, T.T., Parts, L., Haase, J., Charles, I., Maskell, D.J., Peters, S.E., Dougan, G., et al. (2009). Simultaneous assay of every *Salmonella Typhi* gene using one million transposon mutants. *Genome Research* **19**, 2308–2316. https://doi.org/10.1101/gr.097097.109.

14. van Opijnen, T., and Levin, H.L. (2020). Transposon insertion sequencing, a global measure of gene function. *Annual Review of Genetics* **54**, 337–365. https://doi.org/10.1146/annurev-genet-112618-043838.

15. Ghosh, O.M., and Good, B.H. (2022). Emergent evolutionary forces in spatial models of luminal growth and their application to the human gut microbiota. *Proceedings of the National Academy of Sciences of the United States of America* **119**, e2114931119. https://doi.org/10.1073/pnas.2114931119.

16. Chao, M.C., Abel, S., Davis, B.M., and Waldor, M.K. (2016). The design and analysis of transposon insertion sequencing experiments. *Nature Reviews Microbiology* **14**, 119–128. https://doi.org/10.1038/nrmicro.2015.7.

17. Barquist, L., Mayho, M., Cummins, C., Cain, A.K., Boinett, C.J., Page, A.J., Langridge, G.C., Quail, M.A., Keane, J.A., and Parkhill, J. (2016). The TraDIS toolkit: sequencing and analysis for dense transposon mutant libraries. *Bioinformatics* **32**, 1109–1111. https://doi.org/10.1093/bioinformatics/btw022.

18. DeJesus, M.A., Ambadipudi, C., Baker, R., Sassetti, C., and Ioerger, T.R. (2015). TRANSIT: a software tool for Himar1 TnSeq analysis. *PLOS Computational Biology* **11**, e1004401. https://doi.org/10.1371/journal.pcbi.1004401

19. Abdelmalek, N., Yousief, S.W., Bojer, M.S., Alobaidallah, M.S.A., Olsen, J.E., and Paglietti, B. (2025). The secondary resistome of methicillin-resistant *Staphylococcus aureus* to β-lactam antibiotics. *Antibiotics* **14**, 112. https://doi.org/10.3390/antibiotics14020112.

20. Valentino, M.D., Foulston, L., Sadaka, A., Kos, V.N., Villet, R.A., Maria, J.S., Lazinski, D.W., Camilli, A., Walker, S., Hooper, D.C., et al. (2014). Genes contributing to *Staphylococcus aureus* fitness in abscess- and infection-related ecologies. *mBio* **5**, e01729-14. https://doi.org/10.1128/mBio.01729-14.

21. Grosser, M.R., Paluscio, E., Thurlow, L.R., Dillon, M.M., Cooper, V.S., Kawula, T.H., and Richardson, A.R. (2018). Genetic requirements for *Staphylococcus aureus* nitric oxide resistance and virulence. *PLOS Pathogens* **14**, e1006907. https://doi.org/10.1371/journal.ppat.1006907

22. Chang, J.O., Lee, C.Y., Kim, I., Kim, J., Kim, J.H., Yun, T., Hooper, D.C., Walker, S., and Lee, W. (2025). Environmental cues in different host niches shape the survival fitness of *Staphylococcus aureus*. *Nature Communications* **16**, 1–14. https://doi.org/10.1038/s41467-025-62292-x.

23. Li, G., Shen, W., Gong, Y., Li, M., Rao, X., Liu, Q., Yu, Y., Zhou, J., Zhu, K., and Yuan, M. (2022). Essential fitness repertoire of *Staphylococcus aureus* during co-infection with *Acinetobacter baumannii* in vivo. *mSystems* **7**, e00338-22. https://doi.org/10.1128/msystems.00338-22.

24. Kim, G.L., Hooven, T.A., Norambuena, J., Li, B., Boyd, J.M., Yang, J.H., and Parker, D. (2021). Growth and stress tolerance comprise independent metabolic strategies critical for *Staphylococcus aureus* infection. *mBio* **12**, e00814-21. https://doi.org/10.1128/mBio.00814-21.

25. Fey, P.D., Endres, J.L., Yajjala, V.K., Widhelm, T.J., Boissy, R.J., Bose, J.L., and Bayles, K.W. (2013). A genetic resource for rapid and comprehensive phenotype screening of nonessential *Staphylococcus aureus* genes. *mBio* **4**, e00537-12. https://doi.org/10.1128/mBio.00537-12.

26. Abel, S., Abel zur Wiesch, P., Chang, H.H., Davis, B.M., Lipsitch, M., and Waldor, M.K. (2015). Sequence tag–based analysis of microbial population dynamics. *Nature Methods* **12**, 223–226. https://doi.org/10.1038/nmeth.3253.

27. van Opijnen, T., and Camilli, A. (2013). Transposon insertion sequencing: a new tool for systems-level analysis of microorganisms. *Nature Reviews Microbiology* **11**, 435–442. https://doi.org/10.1038/nrmicro3033.

28. Warr, A.R., Hubbard, T.P., Munera, D., Blondel, C.J., Abel zur Wiesch, P., Abel, S., Wang, X., Davis, B.M., and Waldor, M.K. (2019). Transposon-insertion sequencing screens unveil requirements for EHEC growth and intestinal colonization. *PLOS Pathogens* **15**, e1007652. https://doi.org/10.1371/journal.ppat.1007652.

29. van Opijnen, T., Lazinski, D.W., and Camilli, A. (2014). Genome-wide fitness and genetic interactions determined by Tn-seq, a high-throughput massively parallel sequencing method for microorganisms. *Current Protocols in Molecular Biology* **106**, 7.16.1–7.16.24. https://doi.org/10.1002/0471142727.mb0716s106.

30. Goncheva, M.I., Chin, D., and Heinrichs, D.E. (2022). Nucleotide biosynthesis: the base of bacterial pathogenesis. *Trends in Microbiology* **30**, 793–804. https://doi.org/10.1016/j.tim.2021.12.007.

31. Goncheva, M.I., Flannagan, R.S., and Heinrichs, D.E. (2020). De novo purine biosynthesis is required for intracellular growth of *Staphylococcus aureus* and for the hypervirulence phenotype of a *purR* mutant. *Infection and Immunity* **88**, e00104-20. https://doi.org/10.1128/iai.00104-20.

32. Jatana, S., Homer, C.R., Madajka, M., Ponti, A.K., Kabi, A., Papay, F., and McDonald, C. (2018). Pyrimidine synthesis inhibition enhances cutaneous defenses against antibiotic-resistant bacteria through activation of NOD2 signaling. *Scientific Reports* **8**, 8708. https://doi.org/10.1038/s41598-018-27012-0.

33. Rigby, K.M., and DeLeo, F.R. (2012). Neutrophils in innate host defense against *Staphylococcus aureus* infections. *Seminars in Immunopathology* **34**, 237–259. https://doi.org/10.1007/s00281-011-0295-3.

34. Cho, J.S., Guo, Y., Ramos, R.I., Hebroni, F., Plaisier, S.B., Xuan, C., Granick, J.L., Matsushima, H., Takashima, A., Iwakura, Y., et al. (2012). Neutrophil-derived IL-1β is sufficient for abscess formation in immunity against *Staphylococcus aureus* in mice. *PLOS Pathogens* **8**, e1003047. https://doi.org/10.1371/journal.ppat.1003047.

35. Miller, L.S., and Cho, J.S. (2011). Immunity against *Staphylococcus aureus* cutaneous infections. *Nature Reviews Immunology* **11**, 505–518. https://doi.org/10.1038/nri3010.

36. Winstel, V., Missiakas, D., and Schneewind, O. (2018). *Staphylococcus aureus* targets the purine salvage pathway to kill phagocytes. *Proceedings of the National Academy of Sciences of the United States of America* **115**, 6846–6851. https://doi.org/10.1073/pnas.1805622115.

37. Winstel, V., Schneewind, O., and Missiakas, D. (2019). *Staphylococcus aureus* exploits the host apoptotic pathway to persist during infection. *mBio* **10**, e02270-19. https://doi.org/10.1128/mBio.02270-19.

38. Hofstee, M.I., Riool, M., Terjajevs, I., Thompson, K., Stoddart, M.J., Richards, R.G., Zaat, S.A.J., and Moriarty, T.F. (2020). Three-dimensional in vitro *Staphylococcus aureus* abscess communities display antibiotic tolerance and protection from neutrophil clearance. *Infection and Immunity* **88**,

e00293-20 https://doi.org/10.1128/iai.00293-20.

39. Cheng, A.G., Kim, H.K., Burts, M.L., Krausz, T., Schneewind, O., and Missiakas, D.M. (2009). Genetic requirements for *Staphylococcus aureus* abscess formation and persistence in host tissues. *FASEB Journal* **23**, 3393–3404. https://doi.org/10.1096/fj.09-135467.

40. Borges Da Silva, H., Fonseca, R., Pereira, R.M., Cassado, A.A., Álvarez, J.M., and D'Império Lima, M.R. (2015). Splenic macrophage subsets and their function during blood-borne infections. *Frontiers in Immunology* **6**, 480. https://doi.org/10.3389/fimmu.2015.00480.

41. Choueiry, F., Xu, R., and Zhu, J. (2022). Adaptive metabolism of *Staphylococcus aureus* revealed by untargeted metabolomics. *Journal of Proteome Research* **21**, 470–481. https://doi.org/10.1021/acs.jproteome.1c00797.

42. Li, L., Bayer, A.S., Cheung, A., Lu, L., Abdelhady, W., Donegan, N.P., Hong, J.I., Yeaman, M.R., and Xiong, Y.Q. (2020). The stringent response contributes to persistent methicillin-resistant *Staphylococcus aureus* endovascular infection through the purine biosynthetic pathway. *Journal of Infectious Diseases* **222**, 1188–1198. https://doi.org/10.1093/infdis/jiaa202.

43. Kofoed, E.M., Yan, D., Katakam, A.K., Reichelt, M., Lin, B., Kim, J., Park, S., Date, S.V., Monk, I.R., Xu, M., et al. (2016). De novo guanine biosynthesis but not the riboswitch-regulated purine salvage pathway is required for *Staphylococcus aureus* infection in vivo. *Journal of Bacteriology* **198**, 2001–2015. https://doi.org/10.1128/jb.00051-16.

44. Goncheva, M.I., Flannagan, R.S., Sterling, B.E., Laakso, H.A., Friedrich, N.C., Kaiser, J.C., Watson, D.W., Wilson, C.H., Sheldon, J.R., McGavin, M.J., et al. (2019). Stress-induced inactivation of the *Staphylococcus aureus* purine biosynthesis repressor leads to hypervirulence. *Nature Communications* **10**, 1–14. https://doi.org/10.1038/s41467-019-08724-x.

45. Sause, W.E., Balasubramanian, D., Irnov, I., Copin, R., Sullivan, M.J., Sommerfield, A., Chan, R., Dhabaria, A., Askenazi, M., Ueberheide, B., et al. (2019). The purine biosynthesis regulator PurR moonlights as a virulence regulator in *Staphylococcus aureus*. *Proceedings of the National Academy of Sciences of the United States of America* **116**, 13563–13572. https://doi.org/10.1073/pnas.1904280116.

46. Savin, A., Anderson, E.E., Dyzenhaus, S., Podkowik, M., Shopsin, B., Pironti, A., and Torres, V.J. (2024). *Staphylococcus aureus* senses human neutrophils via PerR to coordinate the expression of the toxin LukAB. *Infection and Immunity* **92**, e00526-23. https://doi.org/10.1128/iai.00526-23.

47. Ji, C.-J., Kim, J.-H., Won, Y.-B., Lee, Y.-E., Choi, T.-W., Ju, S.-Y., Youn, H., Helmann, J.D., and Lee, J.-W. (2015). *Staphylococcus aureus* PerR is a hypersensitive hydrogen peroxide sensor using iron-mediated histidine oxidation. *Journal of Biological Chemistry*. https://doi.org/10.1074/jbc.M115.664961.

48. Horsburgh, M.J., Clements, M.O., Crossley, H., Ingham, E., and Foster, S.J. (2001). PerR controls oxidative stress resistance and iron storage proteins and is required for virulence in *Staphylococcus*

aureus. *Infection and Immunity* **69**, 3744–3754. https://doi.org/10.1128/IAI.69.6.3744-3754.2001.

49. Haber, F., and Weiss, J. (1932). On the catalysis of hydroperoxide. *Naturwissenschaften* **20**, 948–950. https://doi.org/10.1007/BF01504715.

50. Aruoma, O.I., Halliwell, B., Gajewski, E., and Dizdaroglu, M. (1989). Damage to the bases in DNA induced by hydrogen peroxide and ferric ion chelates. *Journal of Biological Chemistry* **264**, 20509–20512. https://doi.org/10.1016/S0021-9258(19)47091-9.

51. Imlay, J.A., Chin, S.M., and Linn, S. (1988). Toxic DNA damage by hydrogen peroxide through the Fenton reaction **in vivo** and **in vitro**. *Science* **240**, 640–642. https://doi.org/10.1126/science.2834821.

52. Schlacher, K., Pham, P., Cox, M.M., and Goodman, M.F. (2006). Roles of DNA polymerase V and RecA protein in SOS damage-induced mutation. *Chemical Reviews* **106**, 406–419. https://doi.org/10.1021/cr0404951.

53. Podlesek, Z., and Žgur Bertok, D. (2020). The DNA damage-inducible SOS response is a key player in the generation of bacterial persister cells and population-wide tolerance. *Frontiers in Microbiology* **11**, 1785. https://doi.org/10.3389/fmicb.2020.01785.

54. Ledger, E.V.K., Lau, K., Tate, E.W., and Edwards, A.M. (2023). XerC is required for the repair of antibiotic- and immune-mediated DNA damage in *Staphylococcus aureus*. *Antimicrobial Agents and Chemotherapy* **67**, e01206-22. https://doi.org/10.1128/aac.01206-22.

55. Somerville, G.A., and Proctor, R.A. (2009). At the crossroads of bacterial metabolism and virulence factor synthesis in staphylococci. *Microbiology and Molecular Biology Reviews* **73**, 233–248. https://doi.org/10.1128/mmbr.00005-09.

56. Lehman, M.K., Nuxoll, A.S., Yamada, K.J., Kielian, T., Carson, S.D., and Fey, P.D. (2019). Protease-mediated growth of *Staphylococcus aureus* on host proteins is Opp3 dependent. *mBio* **10**, e02553-18. https://doi.org/10.1128/mBio.02553-18.

57. Tan, X., Ramond, E., Jamet, A., Barnier, J.-P., Decaux-Tramoni, B., Dupuis, M., Euphrasie, D., Tros, F., Nemazanyy, I., Ziveri, J., et al. (2019). Transketolase of *Staphylococcus aureus* in the control of master regulators of stress response during infection. *Journal of Infectious Diseases* **220**, 1967–1976. https://doi.org/10.1093/infdis/jiz404.

58. Kim, J., Kim, G.L., Norambuena, J., Boyd, J.M., and Parker, D. (2023). Impact of the pentose phosphate pathway on metabolism and pathogenesis of *Staphylococcus aureus*. *PLOS Pathogens* **19**, e1011531. https://doi.org/10.1371/journal.ppat.1011531.

59. Vitko, N.P., Spahich, N.A., and Richardson, A.R. (2015). Glycolytic dependency of high-level nitric oxide resistance and virulence in *Staphylococcus aureus*. *mBio* **6**, e00045-15. https://doi.org/10.1128/mBio.00045-15.

60. Purves, J., Cockayne, A., Moody, P.C.E., and Morrissey, J.A. (2010). Comparison of the

regulation, metabolic functions, and roles in virulence of the glyceraldehyde-3-phosphate dehydrogenase homologues gapA and gapB in *Staphylococcus aureus*. *Infection and Immunity* **78**, 5223–5232. https://doi.org/10.1128/IAI.00762-10.

61. Ye, S., von Delft, F., Brooun, A., Knuth, M.W., Swanson, R.V., and McRee, D.E. (2003). The crystal structure of shikimate dehydrogenase (AroE) reveals a unique NADPH binding mode. *Journal of Bacteriology* **185**, 4144–4151. https://doi.org/10.1128/JB.185.14.4144-4151.2003.

62. Frank, M.W., Whaley, S.G., and Rock, C.O. (2021). Branched-chain amino acid metabolism controls membrane phospholipid structure in *Staphylococcus aureus*. *Journal of Biological Chemistry* **297**, 101255. https://doi.org/10.1016/j.jbc.2021.101255.

63. Kaneda, T. (1991). Iso- and anteiso-fatty acids in bacteria: biosynthesis, function, and taxonomic significance. *Microbiological Reviews* **55**, 288–302. https://doi.org/10.1128/mr.55.2.288-302.1991.

64. Whaley, S.G., Frank, M.W., and Rock, C.O. (2023). A short-chain acyl-CoA synthetase that supports branched-chain fatty acid synthesis in *Staphylococcus aureus*. *Journal of Biological Chemistry* **299**, 103036. https://doi.org/10.1016/j.jbc.2023.103036.

65. Singh, V.K., Hattangady, D.S., Giotis, E.S., Singh, A.K., Chamberlain, N.R., Stuart, M.K., and Wilkinson, B.J. (2008). Insertional inactivation of branched-chain α-keto acid dehydrogenase in *Staphylococcus aureus* leads to decreased branched-chain membrane fatty acid content and increased susceptibility to certain stresses. *Applied and Environmental Microbiology* **74**(19), 5882–5890. https://doi.org/10.1128/AEM.00882-08.

66. Pendleton, A., Yeo, W.S., Alqahtani, S., DiMaggio, D.A., Stone, C.J., Li, Z., Singh, V.K., Montgomery, C.P., Bae, T., and Brinsmade, S.R. (2022). Regulation of the Sae two-component system by branched-chain fatty acids in *Staphylococcus aureus*. *mBio* **13**, e01472-22. https://doi.org/10.1128/mbio.01472-22.

67. Matsumoto, Y., Yasukawa, J., Ishii, M., Hayashi, Y., Miyazaki, S., and Sekimizu, K. (2016). A critical role of mevalonate for peptidoglycan synthesis in *Staphylococcus aureus*. *Scientific Reports* **6**, 22894. https://doi.org/10.1038/srep22894.

68. Golla, R.M., Mishra, B., Dang, X., Narayana, L., Li, A., Xu, L., and Wang, G. (2020). Resistome of *Staphylococcus aureus* in response to human cathelicidin LL-37 and its engineered antimicrobial peptides. *ACS Infectious Diseases* **6**, 1866–1881. https://doi.org/10.1021/acsinfecdis.0c00112.

69. Xiao, X., Li, Y., Li, L., and Xiong, Y.Q. (2022). Identification of methicillin-resistant *Staphylococcus aureus* (MRSA) genetic factors involved in human endothelial cell damage, an important phenotype correlated with persistent endovascular infection. *Antibiotics* **11**, 316. https://doi.org/10.3390/antibiotics11030316.

70. Vestergaard, M., Nøhr-Meldgaard, K., and Ingmer, H. (2018). Multiple pathways towards reduced

membrane potential and concomitant reduction in aminoglycoside susceptibility in *Staphylococcus aureus*. *International Journal of Antimicrobial Agents* **51**, 132–135. https://doi.org/10.1016/j.ijantimicag.2017.08.024.

71. Canè, C., Gallucci, N., Amoresano, A., Fontanarosa, C., Paduano, L., De Gregorio, E., Duilio, A., and Di Somma, A. (2024). The antimicrobial peptide temporin-L induces vesicle formation and reduces the virulence in *Staphylococcus aureus*. *Biochemistry and Biophysics Reports* **39**, 101808. https://doi.org/10.1016/j.bbrep.2024.101808.

72. Liu, S., Huang, Y., Jensen, S., Laman, P., Kramer, G., Zaat, S.A.J., and Brul, S. (2024). Molecular physiological characterization of the dynamics of persister formation in *Staphylococcus aureus*. *Antimicrobial Agents and Chemotherapy* **68**, e00850-23. https://doi.org/10.1128/aac.00850-23.

73. Christiansen, M.T., Kaas, R.S., Chaudhuri, R.R., Holmes, M.A., Hasman, H., and Aarestrup, F.M. (2014). Genome-wide high-throughput screening to investigate essential genes involved in methicillin-resistant *Staphylococcus aureus* sequence type 398 survival. *PLOS ONE* **9**, e89018. https://doi.org/10.1371/journal.pone.0089018.

74. Rios-Delgado, G., McReynolds, A.K.G., Pagella, E.A., Norambuena, J., Briaud, P., Zheng, V., Munneke, M.J., Kim, J., Racine, H., Carroll, R.K., et al. (2025). The *Staphylococcus aureus* non-coding RNA IsrR regulates TCA cycle activity and virulence. *Nucleic Acids Research* **53**, gkae1243. https://doi.org/10.1093/nar/gkae1243.

75. Balibar, C.J., Shen, X., and Tao, J. (2009). The mevalonate pathway of *Staphylococcus aureus*. *Journal of Bacteriology* **191**, 851–861. https://doi.org/10.1128/JB.01357-08.

76. Reichert, S., Ebner, P., Bonetti, E.J., Luqman, A., Nega, M., Schrenzel, J., Spröer, C., Bunk, B., Overmann, J., Sass, P., et al. (2018). Genetic adaptation of a mevalonate pathway-deficient mutant in *Staphylococcus aureus*. *Frontiers in Microbiology* **9**, 1539. https://doi.org/10.3389/fmicb.2018.01539.

77. Li, B., Liang, J., Hanfrey, C.C., Phillips, M.A., and Michael, A.J. (2021). Discovery of ancestral L-ornithine and L-lysine decarboxylases reveals parallel, pseudoconvergent evolution of polyamine biosynthesis. *Journal of Biological Chemistry* **297**, 101219. https://doi.org/10.1016/j.jbc.2021.101219.

78. Joshi, G.S., Spontak, J.S., Klapper, D.G., and Richardson, A.R. (2011). Arginine catabolic mobile element–encoded *speG* abrogates the unique hypersensitivity of *Staphylococcus aureus* to exogenous polyamines. *Molecular Microbiology* **82**, 9–20. https://doi.org/10.1111/j.1365-2958.2011.07809.x.

79. Michael, A.J. (2016). Polyamines in eukaryotes, bacteria, and archaea. *Journal of Biological Chemistry* **291**, 14896–14903. https://doi.org/10.1074/jbc.R116.734780.

80. Seravalli, J., and Portugal, F. (2023). Putrescine detected in strains of *Staphylococcus aureus*. *Pathogens* **12**, 881. https://doi.org/10.3390/pathogens12070881.

81. Lillie, I.M., Booth, C.E., Horvath, A.E., Mondragon, M., Engevik, M.A., and Horvath, T.D. (2024). Characterizing arginine, ornithine, and putrescine pathways in enteric pathobionts. *MicrobiologyOpen* **13**(2), e1408. https://doi.org/10.1002/mbo3.1408.

82. Potter, A.D., Butrico, C.E., Ford, C.A., Curry, J.M., Trenary, I.A., Tummarakota, S.S., Hendrix, A.S., Young, J.D., and Cassat, J.E. (2020). Host nutrient milieu drives an essential role for aspartate biosynthesis during invasive *Staphylococcus aureus* infection. *Proceedings of the National Academy of Sciences of the United States of America* **117**, 12394–12401. https://doi.org/10.1073/pnas.1922211117.

83. Corrigan, R.M., Bowman, L., Willis, A.R., Kaever, V., and Gründling, A. (2015). Cross-talk between two nucleotide-signaling pathways in *Staphylococcus aureus*. *Journal of Biological Chemistry* **290**, 5826–5839. https://doi.org/10.1074/jbc.M114.598300.

84. Kelliher, J.L., Macek, A.J.L., Grudzinski, K.M., Radin, J.N., and Kehl-Fie, T.E. (2020). *Staphylococcus aureus* preferentially liberates inorganic phosphate from organophosphates in environments where this nutrient is limiting. *Journal of Bacteriology* **202**(22), e00264-20. https://doi.org/10.1128/JB.00264-20.

85. Pirolo, M., Sieber, R.N., Moodley, A., Visaggio, D., Artuso, I., Gioffrè, A., Casalinuovo, F., Spatari, G., Guardabassi, L., Stegger, M., et al. (2020). Local and transboundary transmissions of methicillin-resistant *Staphylococcus aureus* sequence type 398 through pig trading. *Applied and Environmental Microbiology* **86**, e00430-20. https://doi.org/10.1128/AEM.00430-20.

86. Frick-Cheng, A.E., Sintsova, A., Smith, S.N., Pirani, A., Snitkin, E.S., and Mobley, H.L.T. (2022). Ferric citrate uptake is a virulence factor in uropathogenic *Escherichia coli*. *mBio* **13**, e01035-22. https://doi.org/10.1128/mbio.01035-22.

87. Lyon, L.M., Marroquin, S.M., Thorstenson, J.C., Joyce, L.R., Fuentes, E.J., Doran, K.S., and Horswill, A.R. (2025). Genome-wide mutagenesis identifies factors involved in MRSA vaginal colonization. *Cell Reports* **44**, 115421. https://doi.org/10.1016/j.celrep.2025.115421.

Profiling of Genetic Determinants for Required Fitness of Community-Associated Methicillin-Resistant *Staphylococcus aureus* During Growth in Human Blood

Nader Abdelmalek [1,2] †, Sally W. Yousief [1] †, Martin S. Bojer [3], John E. Olsen [3], Salvatore Rubino [1], Bianca Paglietti [1]#

[1] Department of Biomedical Sciences, University of Sassari, Sassari, 07100, Italy

[2] Unit of Microbiology and Virology, University Hospital of Sassari, Sassari, 07100, Italy

[3] Department of Veterinary and Animal Sciences, Faculty of Health and Medical Sciences, University of Copenhagen, Frederiksberg C, 1870, Denmark.

Correspondence: biancap@uniss.it

† Nader Abdelmalek and Sally W. Yousief contributed equally to this work. Author order was determined by mutual agreement.

This manuscript is accepted for publication in Microbiology Spectrum, 10.1128/spectrum.03585-25

Abstract

Community-associated methicillin-resistant *Staphylococcus aureus* (CA-MRSA) is a leading cause of bacteremia, yet the genetic basis for its success in this hostile environment remains poorly defined. In this study, we employed transposon-directed insertion site sequencing (TraDIS) to map the fitness landscape of CA-MRSA strain USA300 JE2 through a genome-wide screening in fresh, immunocompetent human blood. We identified 76 genes required for fitness, including genes involved in respiratory and central carbon metabolisms, heme detoxification, and *de novo* purine biosynthesis. As validation of fitness genes, competition assays confirmed that individual disruption of *purA*, *purB*, *fbp*, *hssR*, or *aroA2* significantly reduced bacterial fitness in blood. Conversely, inactivation of specific regulators, such as the *saeRS* two-component system, the alternative sigma factor σ^B, and adhesins including *fnbA* and *clfA*, conferred a competitive advantage. These findings provide a genome-scale map of *S. aureus* fitness requirements in a physiologically relevant blood model, offering a platform for further investigation of bacterial adaptation to the intravascular environment.

Importance

Understanding how *Staphylococcus aureus* maintains fitness in the human bloodstream is essential for explaining its success as an invasive pathogen. This study provides a comprehensive, genome-wide

definition of the genes that enable *S. aureus* to remain competitive in blood, revealing the key physiological requirements for adaptation to this challenging environment. By identifying genetic functions whose disruption impairs fitness, our findings highlight the specific pathways that sustain adaptation and competitiveness under host-imposed stress. Extending previous genome-scale investigations conducted in other infection niches, this study emphasizes the importance of physiological context in shaping bacterial fitness and identifies conserved cross-fitness determinants shared among *S. aureus* lineages. These insights advance our current understanding of how *S. aureus* adapts to the bloodstream and strengthen the foundation for future functional and comparative studies on staphylococcal pathophysiology.

Keywords: *Staphylococcus aureus*, TraDIS, Bloodstream infection, Fitness, Metabolism

Introduction

Staphylococcus aureus is an opportunistic pathogen capable of causing a wide range of infections, from superficial skin abscesses to life-threatening systemic conditions such as bacteremia and endocarditis (1). Among these, bloodstream infections pose a particularly severe clinical challenge to healthcare system. *S. aureus* is the leading cause of invasive infection-related mortality worldwide, with case fatality rates ranging from 15% to 30% and an estimated 300,000 deaths annually (2). A substantial proportion of these fatalities are attributed to methicillin-resistant *S. aureus* (MRSA), which exhibits elevated resistance to conventional antibiotics and offers limited therapeutic options, resulting in poorer patient outcomes (3).

A major contributor to the pathogenicity of *S. aureus* is its ability to survive and proliferate within the human bloodstream, an environment characterized by robust immune defenses and limited nutrient availability (4). Upon entering the bloodstream, *S. aureus* encounters multiple host defense mechanisms, including neutrophil-mediated immune surveillance, complement activation, and nutritional immunity which restrict microbial fitness (5). In response to these barriers, *S. aureus* has evolved a diverse array of strategies to evade immune clearance and establish invasive infections (4, 5). However, the full repertoire of genetic determinants required for fitness in the bloodstream remains incompletely defined.

Recent advances in functional genomics have facilitated comprehensive investigations into the fitness of *S. aureus* and other bacteria across diverse host environments (6–9). Approaches such as transcriptomics, genome-wide association studies, and high-throughput transposon mutant library screens have shed light on *S. aureus* adaptation within the bloodstream (10–13). Among these, Transposon-Directed Insertion Site Sequencing (TraDIS) has emerged as a particularly powerful method for genome-wide fitness

profiling (14). While TraDIS has been applied to livestock-associated MRSA (LA-MRSA) in fresh human blood (12), and Tn-seq recently to CA-MRSA in commercially sourced, immune-depleted blood (15), a genome-wide investigation has not yet been applied to CA-MRSA in fresh, immune-competent human blood.

In this study, we employed TraDIS to comprehensively investigate both fitness-enhancing and fitness-reducing genetic determinants involved in CA-MRSA fitness and metabolic adaptation in human blood. These findings provide novel insights into the molecular mechanisms underlying MRSA persistence in the bloodstream and establish a foundation for the development of targeted therapeutic strategies.

Results

Assessment of bottleneck effects during TraDIS screening in human blood

To investigate the genetic determinants of *S. aureus* fitness in human blood, a high-density USA300 JE2 transposon mutant library, containing approximately 2×10^9 CFU/mL (16), were seeded into fresh blood from three independent human volunteers. Following the blood challenge, the recovered populations (approximately 10^9 CFU/mL from each replicate) were processed for genomic DNA extraction and sequencing (Table S1). Principal Component Analysis (PCA) of insertion counts revealed clear separation among blood replicates, input (16), and outgrowth control samples (17), with high consistency across blood replicates (Fig. S1). TraDIS analysis of libraries recovered after growth showed preserved insertional richness, with approximately 400,000 unique insertion sites comparable to the input library (Table S1). To quantitatively assess population bottlenecks, we calculated Shannon, Simpson, and Pielou's evenness indices from normalized gene-level read counts. All three indices confirmed that neither diversity nor evenness were significantly reduced in the output libraries, indicating that the overall complexity was largely maintained (Fig. 1A, 1B, 1C). The rank-abundance curve further showed nearly overlapping input and output distributions (Fig. 1D), confirming that the relative abundance of most mutants was conserved. The effective population size (N_e) estimated from the inverse Simpson index remained at 70–84 % of the input, averaging 77 %, consistent with a moderate bottleneck.

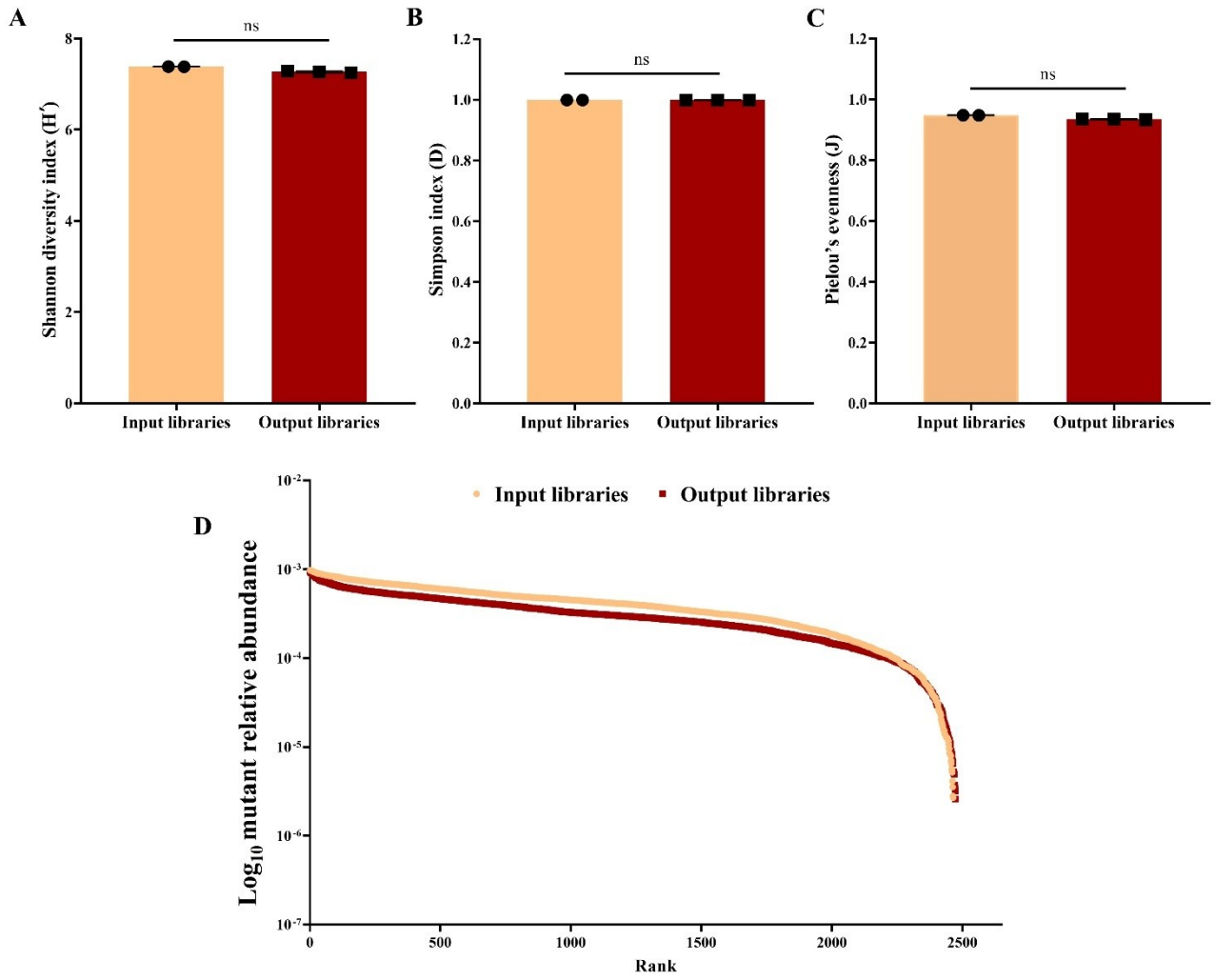

Fig 1. Diversity and rank–abundance of transposon mutant libraries. (A) Shannon index, (B) Simpson index, and (C) Pielou's evenness for input (orange) and output (red) libraries. Points represent biological replicates and bars indicate means. P values were determined by Mann–Whitney U test; asterisks indicate adjusted significance levels (ns = not significant). (D) Rank-abundance curve showing the relative abundance of each mutant ranked from most to least abundant in input (orange) and output (red) libraries; curves largely overlap, indicating conservation of mutant representation.

Identification of genes of *S. aureus* with decreased fitness during growth in human blood

To identify genes required for bacterial fitness in human blood, we first compared the transposon insertion profiles after 24 hours of exposure to human blood with the input transposon library, revealing 146 genes significantly depleted during growth in blood ($\log_2$ fold change (Log_2FC) ≤ -2, q-value < 0.01, log count per million (logCPM) >2, mean control reads > 150) (Table S2A). To distinguish genes specifically required for fitness in blood from those broadly essential for growth under laboratory

conditions, we next compared the blood dataset with two previously generated outgrowth controls in Brain Heart Infusion (BHI) broth (Table S2B) (17). TraDIS analysis identified 76 genes significantly depleted during growth in blood (log_2 fold change ($Log_2FC \leq -2$, q-value < 0.01, logCPM >2, mean control reads > 150) but not during growth in BHI, indicating that disruption of these genes specifically impaired fitness in blood. These genes included many involved in menaquinone-dependent respiration, nucleotide metabolism, and metal regulation (Table 1, Fig. S2).

Table 1. Predicted genes required for *S. aureus* USA300 JE2 fitness during growth in human blood.

Locus tag	Gene Name	Description	Log_2FC	q-Value
Menaquinone biosynthesis				
SAUSA300_1737	*menE*	O-succinylbenzoate-CoA ligase	-5.31	8.04×10^{-29}
SAUSA300_0948	*menB*	naphthoate synthase	-4.22	4.04×10^{-18}
SAUSA300_1360	*ubiE*	menaquinone biosynthesis methyltransferase ubiE	-4.05	3.89×10^{-24}
SAUSA300_0946	*menD*	2-succinyl-6-hydroxy-2, 4-cyclohexadiene-1-carboxylic acid synthase/2-oxoglutarate decarboxylase	-3.65	4.18×10^{-19}
SAUSA300_0945	*menF*	isochorismate synthase family protein	-3.61	4.90×10^{-17}
SAUSA300_1735	*menC*	O-succinylbenzoic acid synthetase	-3.31	4.85×10^{-08}
Chorismate biosynthesis				
SAUSA300_1357	*aroC*	chorismate synthase	-4.60	3.40×10^{-17}
SAUSA300_1355	*aroA*	3-phosphoshikimate 1-carboxyvinyltransferase	-4.56	1.28×10^{-24}
SAUSA300_0787	*aroD*	3-dehydroquinate dehydratase, type I	-4.25	1.49×10^{-13}
SAUSA300_1356	*aroB*	3-dehydroquinate synthase	-3.79	6.58×10^{-08}
SAUSA300_1683	***aroA2***	chorismate mutase/phospho-2-dehydro-3-deoxyheptonate aldolase	-3.65	8.52×10^{-06}
SAUSA300_1499	*aroK*	shikimate kinase	-3.55	1.09×10^{-18}
SAUSA300_1555	*aroE*	shikimate 5-dehydrogenase	-2.67	2.48×10^{-15}
Isoprenoid biosynthesis				
SAUSA300_0355	***SAUSA300_0355***	acetyl-CoA acetyltransferase	-8.15	1.26×10^{-61}
SAUSA300_2484	*mvaS*	hydroxymethylglutaryl-CoA synthase	-7.37	1.01×10^{-54}
SAUSA300_2483	*mvaA*	hydroxymethylglutaryl-CoA reductase	-7.16	4.96×10^{-67}
Central carbon metabolism				
SAUSA300_1193	***glpD***	glycerol-3-phosphate dehydrogenase	-10.35	4.97×10^{-47}
SAUSA300_2455	***fbp***	putative fructose-1,6-bisphosphatase	-7.40	1.27×10^{-40}
SAUSA300_1916	*aspB*	Aminotransferase	-5.88	1.68×10^{-125}
SAUSA300_1246	*acnA*	aconitate hydratase	-3.36	1.12×10^{-10}
SAUSA300_1640	*icd*	isocitrate dehydrogenase, NADP-dependent	-2.65	3.44×10^{-08}
SAUSA300_2362	*gpmA*	2,3-bisphosphoglycerate-dependent phosphoglycerate mutase	-2.39	3.06×10^{-21}
SAUSA300_1014	*pyc*	pyruvate carboxylase	-2.08	5.08×10^{-19}
SAUSA300_1190	*glpP*	glycerol uptake operon antiterminator regulatory protein	-2.19	1.17×10^{-16}
Nucleotide biosynthesis				
SAUSA300_1889	***purB***	adenylosuccinate lyase	-6.16	1.62×10^{-85}
SAUSA300_0017	***purA***	adenylosuccinate synthetase	-5.58	4.28×10^{-43}

SAUSA300_0965	*folD*	methylenetetrahydrofolate dehydrogenase/methenyltetrahydrofolate cyclohydrolase	-4.46	6.25×10^{-36}
SAUSA300_0473	*purR*	pur operon repressor	-4.26	7.38×10^{-06}
SAUSA300_2526	*pyrD*	dihydroorotate dehydrogenase	-2.28	1.15×10^{-13}
Transport and nutrient uptake systems				
SAUSA300_2406	*cntE*	putative transporter	-9.72	0
SAUSA300_0620	*mntA*	ABC transporter ATP-binding protein	-7.60	6.93×10^{-39}
SAUSA300_0619	*mntB*	ABC transporter, permease protein	-7.19	2.24×10^{-26}
SAUSA300_0618	*mntC*	ABC transporter, substrate-binding protein	-6.60	3.90×10^{-28}
SAUSA300_0633	*fhuA*	ferrichrome transport ATP-binding protein fhuA	-6.05	1.60×10^{-59}
SAUSA300_2306	*hrtA*	ABC transporter, ATP-binding protein	-3.67	3.92×10^{-25}
SAUSA300_2307	*hrtB*	ABC transporter, permease protein	-3.55	7.51×10^{-29}
SAUSA300_2308	***hssR***	response regulator protein	-3.53	1.04×10^{-44}
SAUSA300_1785	*ecsB*	putative ABC transporter protein EcsB	-3.13	1.16×10^{-30}
SAUSA300_2309	*hssS*	sensor histidine kinase	-2.91	2.13×10^{-26}
SAUSA300_1786	*ecsA*	ABC transporter, ATP-binding protein EcsA	-2.80	6.54×10^{-14}
SAUSA300_1516	*znuC*	ABC transporter, ATP-binding protein	-2.30	3.73×10^{-11}
SAUSA300_1515	*znuB*	ABC transporter, permease protein	-2.26	4.77×10^{-15}
SAUSA300_0687	*mpfA*	putative hemolysin	-2.06	4.21×10^{-27}
Chromosome maintenance and cell division				
SAUSA300_1127	*smc*	chromosome segregation protein SMC	-4.72	2.46×10^{-27}
SAUSA300_1120	*recG*	ATP-dependent DNA helicase RecG	-3.54	1.54×10^{-21}
SAUSA300_1086	*divIVA*	putative cell-division initiation protein	-2.51	1.40×10^{-12}
SAUSA300_1793	*SAUSA300_1793*	conserved hypothetical protein	-2.35	5.25×10^{-07}
SAUSA300_1792	*SAUSA300_1792*	conserved hypothetical protein	-2.28	5.92 x 10-07
Cell envelope biogenesis and lipoprotein processing				
SAUSA300_0744	*lgt*	prolipoprotein diacylglyceryl transferase	-3.44	5.68×10^{-15}
SAUSA300_0980	*auxA*	putative membrane protein	-3.36	1.52×10^{-28}
SAUSA300_0918	*ugtP*	diacylglycerol glucosyltransferase	-3.22	2.51×10^{-11}
SAUSA300_2439	*galU*	UTP-glucose-1-phosphate uridylyltransferase	-2.96	6.65×10^{-07}
SAUSA300_1089	*lspA*	lipoprotein signal peptidase	-2.26	1.03×10^{-09}
Virulence- and stress-related genes				
SAUSA300_2100	*SAUSA300_2100*	lytic regulatory protein	-4.71	3.25×10^{-60}
SAUSA300_2467	*srtA*	Sortase	-4.49	1.03×10^{-16}
SAUSA300_2245	*sarR*	staphylococcal accessory regulator R	-4.43	3.76×10^{-22}
SAUSA300_2506	*isaA*	immunodominant staphylococcal antigen A precursor	-4.40	9.25×10^{-30}
SAUSA300_1842	*perR*	transcriptional regulator, Fur family	-2.61	7.79×10^{-10}
SAUSA300_1257	*msrR*	peptide methionine sulfoxide reductase regulator MsrR	-2.34	1.75×10^{-11}
SAUSA300_0310	*pfoR*	perfringolysin O regulator protein	-2.33	1.79×10^{-54}
SAUSA300_2249	*ssaA*	secretory antigen precursor SsaA	-2.11	1.49×10^{-13}
Two-component system				
SAUSA300_0022	*walH*	YycH protein	-3.03	5.05×10^{-42}
SAUSA300_0023	*walI*	YycI protein	-2.78	7.33×10^{-21}
Others				
SAUSA300_1899	***pncA***	conserved hypothetical protein	-4.86	6.67×10^{-43}
SAUSA300_0443	*SAUSA300_0443*	YibE/F-like protein	-4.64	1.33×10^{-34}
SAUSA300_0442	*SAUSA300_0442*	YibE/F-like protein	-4.40	3.51×10^{-27}

SAUSA300_1231	*SAUSA300_1231*	gamma-aminobutyrate permease	-3.02	1.88×10^{-31}
SAUSA300_1155	*rasP*	putative membrane-associated zinc metalloprotease	-3.02	9.88×10^{-19}
SAUSA300_2075	*rho*	transcription termination factor Rho	-2.73	2.86×10^{-08}
SAUSA300_1289	*dapB*	dihydrodipicolinate reductase	-2.67	2.49×10^{-14}
SAUSA300_1583	*cymR*	conserved hypothetical protein	-2.60	1.69×10^{-14}
SAUSA300_1017	*ctaM*	conserved hypothetical protein	-2.56	1.47×10^{-09}
SAUSA300_1112	*stp1*	protein phosphatase 2C domain protein	-2.48	1.74×10^{-15}
SAUSA300_0957	*SAUSA300_0957*	conserved hypothetical protein	-2.42	5.99×10^{-15}
SAUSA300_2156	*lacR*	lactose phosphotransferase system repressor	-2.40	2.94×10^{-06}
SAUSA300_2037	*cshA*	ATP-dependent RNA helicase	-2.24	4.09×10^{-07}

Genes shown in bold were selected for further validation.

Respiratory and carbon metabolic pathways support *S. aureus* fitness in human blood

TraDIS analysis revealed that *S. aureus* fitness in human blood depends on intact electron transport chain (ETC) and energy metabolism pathways. Mutants disrupted in chorismate biosynthesis (*aroA, aroE*, *aroB*, *aroD*, *aroK*, *aroC*, *aroA2*) and isoprenoid biosynthesis (*SAUSA300_0355*, *mvaA*, *mvaS*) were significantly underrepresented following blood exposure. These pathways intersect with menaquinone biosynthesis (*menF, menD, menC, menH, menE, menB, menG, ubiE*), which also showed marked depletion in mutant representation (Table 1, Table S2a, Table S2B, Fig 2A).

In addition to the menaquinone biosynthesis, *glpD* (glycerol-3-phosphate dehydrogenase) and its regulator *glpP* emerged as critical for *S. aureus* blood fitness. *glpD* links glycerol catabolism to respiratory electron transfer and gluconeogenesis (Fig 2A). Transposon insertions in genes encoding for gluconeogenic enzymes (*fbp, gpmA*) directing carbon flux from glycerone-P to glucose were underrepresented. Similarly, mutants in tricarboxylic acid (TCA) cycle genes (*acnA, icd*) and NAD^+ biosynthesis gene *pncA* showed significantly reduced representation compared to outgrowth controls (Table 1, Table S2B).

To validate these findings, transposon mutants of *aroA2*, *SAUSA300_0355*, *glpD*, *pncA*, and *fbp* were subjected to fitness competition assays against the wild type (WT) strain in BHI and human blood. Mutants lacking *aroA2*, *pncA*, or *fbp* exhibited pronounced fitness defects in blood relative to BHI (Fig. 2B). The *glpD* mutant was modestly reduced in human blood relative to BHI but stayed above the defect threshold ($\log_{10}$ competitive index ($\log_{10}$CI) < -1), while *SAUSA300_0355* mutants showed no significant competitive fitness defect in blood (Fig 2B, Table S3A, Table S3B).

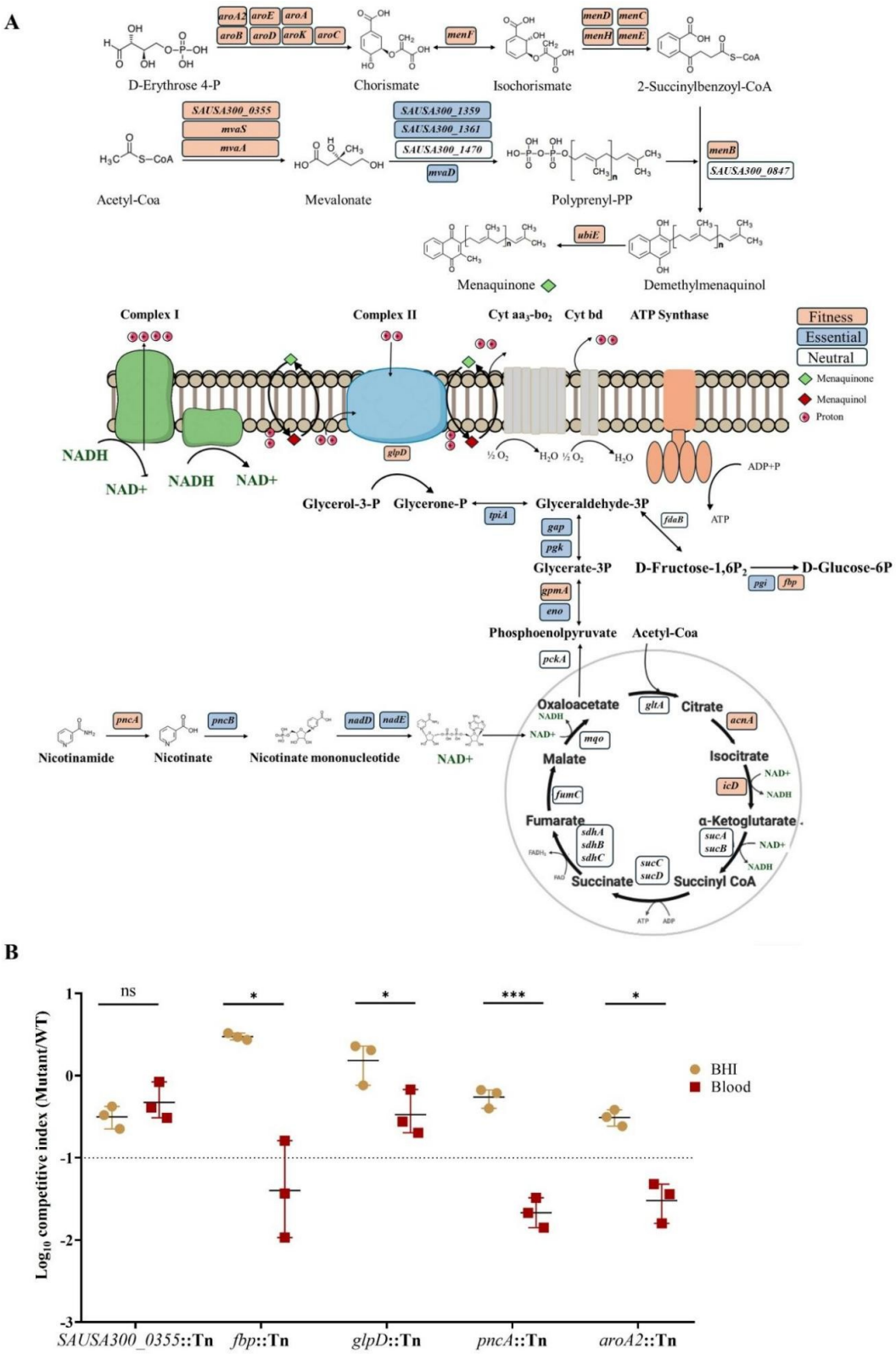

Fig 2. Schematic overview of fitness-associated gene depletion in the menaquinone pathway and central carbon metabolism of *S. aureus*. (A) The diagram illustrates the menaquinone biosynthesis pathway, gluconeogenesis, and the NAD^+ salvage pathway, highlighting genes that contribute to bacterial fitness

in human blood. Gene fitness was assessed using TraDIS analysis. Genes are color-coded based on fitness classification: orange indicates genes whose disruption significantly reduced fitness in blood ($Log_2FC \leq -2$, q-value < 0.01, logCPM >2, mean control reads > 150), blue denotes genes essential for growth under standard laboratory conditions, and white represents genes with no significant fitness impact or lacking statistical significance. (B) Competitive assays in which *SAUSA300_0355, fbp, glpD, pncA*, and *aroA2* mutants were each co-cultured with WT during growth in BHI and human blood. Data represent mean ± SD of biological replicates. The dashed line represents the cut-off ($log_{10}CI = -1$). Statistical significance was assessed using a two-tailed unpaired Welch's t-test. Asterisks indicate adjusted *P* values: * p < 0.05, ** p < 0.01, *** p < 0.001, ns = not significant.

Purine auxotrophy impairs *S. aureus* fitness during bloodstream infection

The *de novo* purine biosynthesis pathway was identified as required for *S. aureus* fitness in human blood. Among the most significantly depleted mutants were *purA* ($Log_2FC = -5.58$) and *purB* ($Log_2FC = -6.16$) (Table 1, Table S2A, Table S2B, Fig 3A). Additionally, *folD*, which encodes a bifunctional enzyme involved in one-carbon metabolism and purine precursor synthesis, also showed substantial depletion. To validate these findings, *ex vivo* competition assays demons trated that *purA* and *purB* mutants were significantly outcompeted by the WT strain in blood (Fig 3B, Table S3A, Table S3B).

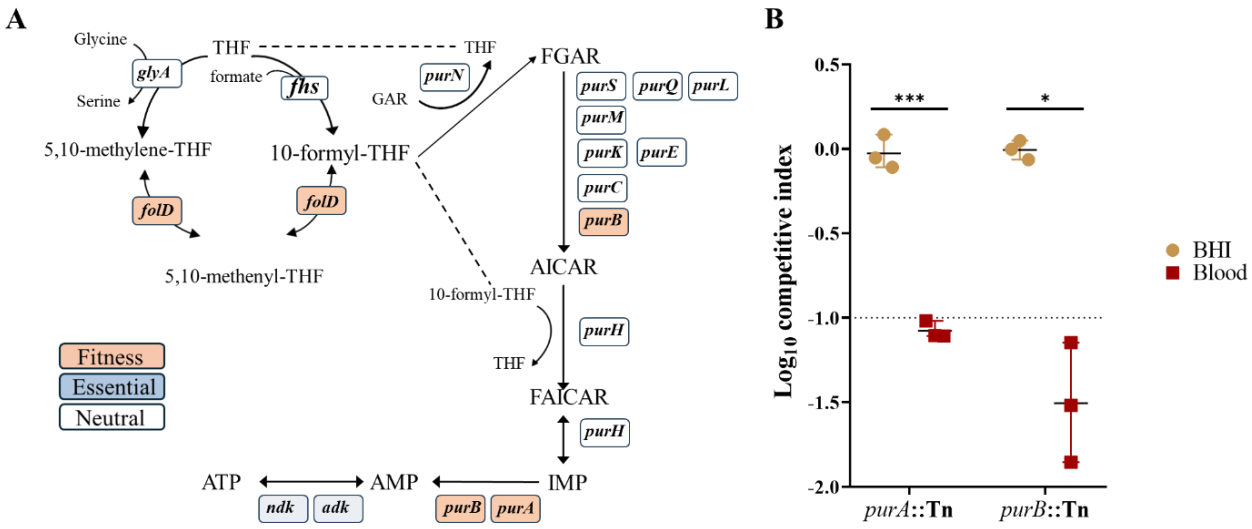

Fig. 3. *De novo* purine biosynthesis is essential for *S. aureus* fitness in human blood. (A) Schematic representation of the de novo purine biosynthesis pathway. Genes are color-coded to indicate fitness, with orange for reduced fitness in blood, blue for essential genes under standard conditions, and white for genes without significant effect. (B) Competitive assay of *purA* and *purB* transposon mutants relative to the WT strain during *ex vivo* growth in human blood. Individual data values correspond to biological replicates, shown as mean ± SD. The dashed line marks the cut-off $log_{10}CI$ equal to –1. Statistical significance was assessed using a two-tailed unpaired Welch's t-test. Adjusted *P* values: * p < 0.05, *** p < 0.001.

Maintenance of metal acquisition and heme detoxification systems enhances *S. aureus* fitness in blood

We also identified several genes involved in metal ion acquisition and heme detoxification that contribute to *S. aureus* fitness in human blood. Among iron uptake systems, only *fhuA*, encoding a ferrichrome-specific ATP-binding cassette (ABC) transporter, showed significant depletion following blood exposure. Similarly, transposon insertions in manganese transport genes (*mntA, mntB, mntC*) and zinc transport components (*znuB, znuC*) were markedly underrepresented (Fig 4A).

Disruption of the heme detoxification machinery, comprising the *hssRS* heme-sensing two-component system and the associated *hrtAB* efflux transporter, also resulted in a significant loss of fitness in blood (Fig 4A). To experimentally assess this effect, an *hssR* transposon mutant was tested in competition assays, exhibiting reduced competitiveness in human blood relative to BHI (Fig. 4B, Table S3A, Table S3B).

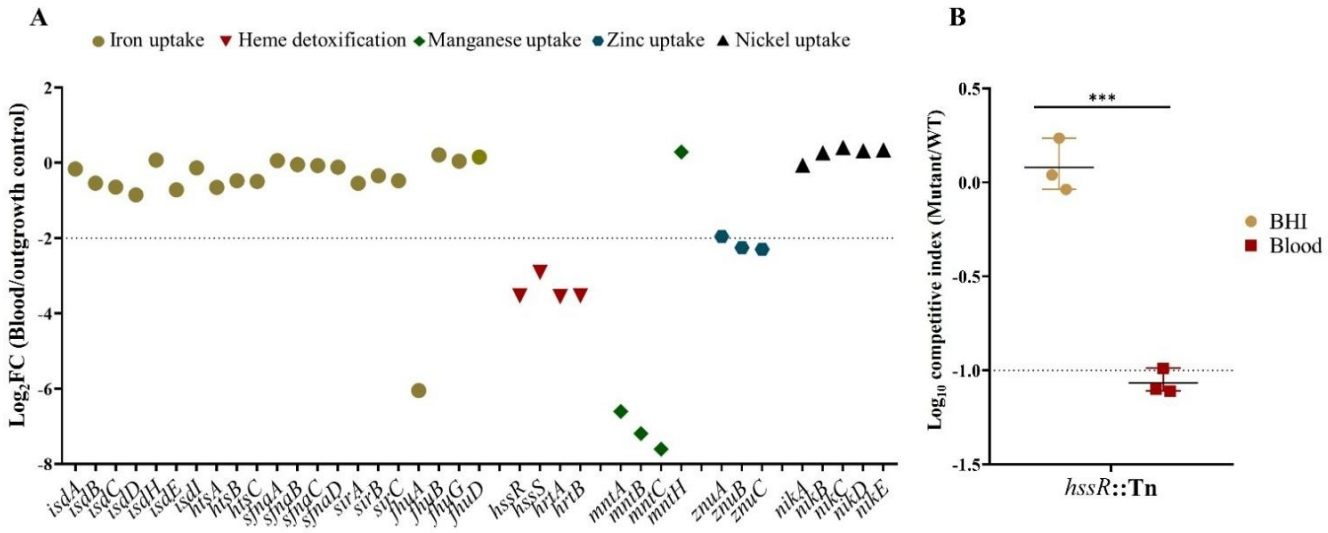

Fig. 4. Heme detoxification and metal ion uptake systems are essential for *S. aureus* fitness in human blood. (A) Log_2FC values from TraDIS analysis of *S. aureus* transposon mutants exposed to human blood. Genes included those involved in the heme detoxification system, manganese transporter, zinc transporter, nickel transporter and iron uptake. Genes with $Log_2FC < -2$ (q-value < 0.01, logCPM >2, mean control reads > 150) are considered as conditionally essential in human blood (B) Competitive assay of the *hssR* mutant and WT strain during co-incubation in human blood. Biological replicates are shown as mean ± SD. The dashed line indicates the cut-off $log_{10}CI$ equal to –1. Statistical significance was assessed using a two-tailed unpaired Welch's t-test. Significance levels are indicated as *** ($p < 0.001$).

Loss of the Sae and σ^B regulatory systems confers a selective advantage for *S. aureus* bloodstream fitness

TraDIS analysis revealed six mutants significantly enriched following exposure to human blood (Table S2A, Table S2B). These included disruptions of the *saeRS* two-component system and genes of the alternative sigma factor σ^B operon (*sigB*, *rsbV*, and *rsbU),* which were among the most strongly enriched (Fig. 5A). Notably, mutants in *fnbA*, co-regulated by both the Sae and σ^B systems, were also highly enriched. Although *clfA* did not reach the statistical enrichment threshold, it displayed a modest increase in transposon read abundance and was retained for validation due to its known σ^B regulation alongside *fnbA* and *saeR* mutants (Fig. 5B). All selected enriched mutants showed a significant fitness advantage over WT in competitive assays within the human blood environment (Fig. 5C, Table S3A, Table S3B). To ensure that the enrichment represented a biologically meaningful advantage, we applied a cutoff of $\log_{10}$ CI > 0.17 (CI ≥ 1.5), corresponding to a ≥50% increase in fitness, which is more stringent than the $\log_{10}$ CI > 0 (CI ≥ 1) used in previous studies (18, 19).

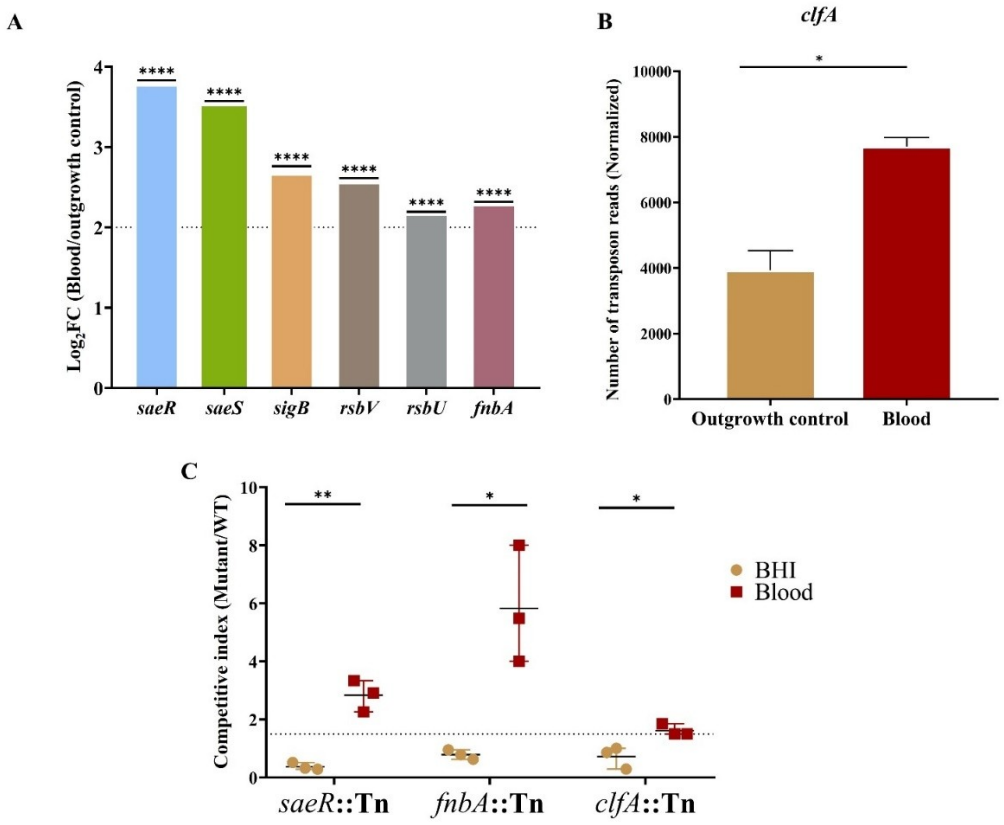

Fig 5. Inactivation of regulatory and adhesion genes enhances *S. aureus* fitness in human blood. (A) Log_2FC values from TraDIS analysis for genes whose inactivation conferred a selective advantage during survival in human blood ($Log_2FC > 2$, q-value < 0.01, logCPM > 2, mean control reads > 150). Statistical

significance is indicated by asterisks, with **** corresponding to q-value < 0.0001. All q-values are reported in Table S1B. (B) Normalized transposon read counts for *clfA* shown as mean ± SD of sequencing replicates. Statistical significance was determined by BioTraDIS analysis (Table S2B), with * indicating q-value = 0.016. (C) Fitness competition assays of mutants relative to WT during 1:1 co-culture in human blood. Data are shown as mean ± SD of three independent biological replicates. Statistical significance was assessed using a two-tailed unpaired Welch's t-test. Adjusted *P* values: * $p < 0.05$, ** $p < 0.01$.

Fitness landscape between community and livestock-associated MRSA

To identify conserved and lineage-specific fitness determinants in human blood, we compared our TraDIS dataset from the CA-MRSA strain USA300 JE2 with two publicly available datasets from livestock-associated MRSA (LA-MRSA) strains SO385 and 09V grown in human blood (12). Both strains belong to Sequence Type 398 (ST398) within Clonal Complex 398 (CC398), allowing for a direct comparison of fitness requirements between divergent lineages in the blood environment. We identified 21 genes consistently required for blood fitness across all three strains ($Log_2FC \leq -2$, q-value < 0.01, logCPM >2, mean control reads > 150), primarily involved in menaquinone biosynthesis and purine metabolism (Fig. 6A, 6B). In addition, we observed consistent enrichment of transposon reads the *saeRS* and *fnbA* genes in all three strains, where components of σ^B operon were selectively enriched in USA300 JE2 (Fig. 6B).

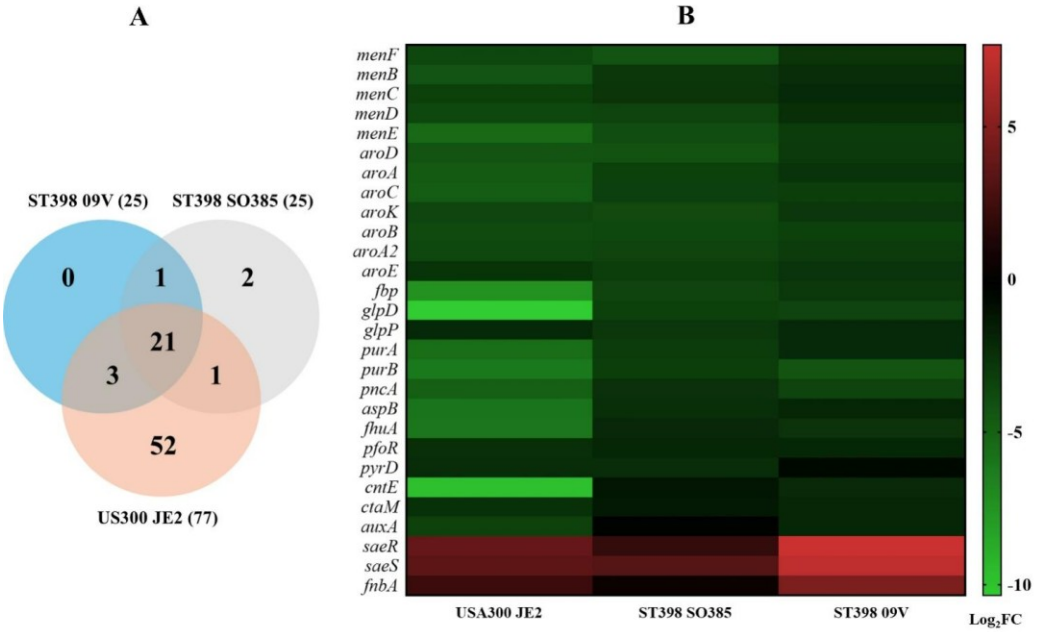

Fig 6. Comparative TraDIS analysis identifies conserved fitness determinants in *S. aureus*. (A)Venn diagram showing the overlap of fitness-associated genes identified via TraDIS in *S. aureus* USA300 JE2,

ST398 SO385 and ST398 09V strains during growth in human blood. (B) Heatmap showing log_2FC values of transposon mutant abundance conserved between USA300 JE2 and at least one ST398 strain, highlighting both fitness-enhancing (green) and fitness-reducing (red) loci.

Discussion

To establish infection in the bloodstream, *S. aureus* must adapt to multiple host-imposed stresses, including nutrient limitation, oxidative burst, and immune recognition (20). These challenges drive extensive metabolic reprogramming and coordinated expression of virulence factors that enable persistence across diverse host environments (20, 21). Several high-throughput genetic approaches have been applied to investigate fitness requirements during bloodstream infection. For example, phenotypic screens utilizing the Nebraska transposon mutant library (NTML) have identified mutants with impaired growth on blood agar plates (22). Additionally, genome-wide TraDIS analyses of livestock-associated MRSA lineages, including ST398, have revealed genes that contribute to fitness in human blood (12). Chang et al. recently performed a Tn-seq screen of USA300 in commercially processed, leukocyte-depleted blood (15). While these studies offered important insights, a genome-wide analysis of CA-MRSA fitness in fresh, immune-competent human blood has been lacking.

To address this gap, we conducted a genome wide TraDIS screen using a highly saturated transposon mutant library constructed in the USA300 JE2 strain to systematically identify the genetic determinants essential for fitness in human blood (16). A major drawback of transposon mutant sequencing studies is the bottleneck effect, in which only a fraction of the initial mutant pool contributes to the surviving population, reducing diversity and compromising statistical power (23). To mitigate this limitation, a high inoculum was used to preserve library representation, consistent with strategies validated in infection models (24,25). Despite the enrichment of mutants with specific fitness advantages under blood-specific pressures, overall library richness and gene representation were found to be preserved. Thus, the bottleneck observed in our TraDIS screen using fresh human blood was selective rather than restrictive and did not compromise downstream analyses. Preservation of the transposon library diversity is fundamental, as fresh blood represents a complex milieu of viable immune cells, active complement, antimicrobial peptides and nutritional immunity absent in processed preparations (4, 26). The high biological relevance of this environment, coupled with preserved library complexity, enabled robust identification of clinically important genetic traits involved in fitness in human blood. Despite its recent decline in prevalence, USA300 remains a clinically significant CA-MRSA lineage, and its well-annotated genome provides a robust platform for functional genomics (27). Our screen identified 76 fitness-

associated genes, and six genes whose disruption enhanced fitness in human blood. Although bacterial fitness in blood does not capture the full complexity of *in vivo* pathogenesis, it represents a crucial early step in invasive disease (28). Several genes identified in our screen, including *pyc*, *SAUSA300_1231*, *lgt*, *lspA*, *msrR*, *srtA*, *gpmA*, *mntABC*, *cntE*, *stp1, cymR* and *isaA*, have previously been validated in animal models of systemic infection or proposed as immunotherapeutic targets, highlighting the biological relevance of our findings (15, 29–36).

Our TraDIS screen highlighted *de novo* purine biosynthesis pathway as a critical determinant of *S. aureus* fitness during bloodstream infection, evidenced by the significant depletion of *purA* and *purB*. This pathway is essential for sustaining intracellular pools of purine nucleotides necessary for DNA replication, RNA transcription, and energy metabolism (37). While *S. aureus* can salvage exogenous purines under nutrient-rich conditions, the human bloodstream represents a nutrient-restricted environment, where purine availability is constrained by host-mediated sequestration mechanisms and rapid turnover of circulating nucleotides (38). While previous studies have reported inconsistent validation outcomes in blood (12, 15, 22), our competitive assays confirmed that the *purA* and *purB* mutants are significantly impaired in blood, affirming the necessity of metabolic autonomy in nucleotide biosynthesis for bloodstream fitness (15, 22). Given their essentiality in multiple infection models, including murine pneumonia and osteomyelitis, purine biosynthetic enzymes have been proposed as attractive antimicrobial targets (7, 29). However, their considerable structural homology to mammalian counterparts poses a major challenge in developing selective inhibitors.

Respiratory metabolism is a cornerstone of *S. aureus* physiology, supporting ATP generation, redox homeostasis, and metabolic flexibility (39). In line with its central role in bacterial fitness, our genome-wide TraDIS screen in blood revealed a pronounced depletion of transposon mutants in genes encoding key components of ETC, including those required for the biosynthesis of chorismate (*aroA, aroE*, *aroB*, *aroD*, *aroK*, *aroC*, *aroA2*), mevalonate (*SAUSA300_0355*, *mvaA*, *mvaS*), and menaquinone (*menF, menD, menC, menH, menE, menB, menG, ubiE*). Menaquinone serves as the predominant quinone electron carrier in *S. aureus*, and its biosynthetic disruption impairs aerobic respiration, resulting in profound metabolic consequences (39, 40). Such defects often lead to small colony variants (SCVs), a subpopulation with reduced growth, diminished virulence, and enhanced intracellular persistence, traits that confer a short-term survival advantage after exposure to blood (39, 41). However, our competitive fitness assays revealed that mutants such as *aroA2* showed reduced long-term fitness in blood, suggesting that transient stress tolerance does not substitute for the robust metabolic capacity required to sustain

adaptation and persistence in this nutrient limited environment. In accordance with these findings, our previous genome-wide TraDIS screens in murine infection models revealed that genes in the mevalonate, menaquinone, and chorismate pathways were differentially required depending on the host niche (24). In a systemic infection model, mutants disrupted in *SAUSA300_0355*, *mvaA*, *mvaS*, *menE*, *aroB*, and *aroC* were depleted in transposon libraries recovered from the kidney, whereas in a skin infection model, mutants disrupted in *menF* and *ubiE* were enriched (24). These data demonstrate how host niche-specific conditions shape metabolic fitness requirements and highlight the importance of interpreting genome-wide fitness screens within their environmental context.

S. aureus reprograms its carbon metabolism in human blood in response to the available nutrients rather than following the hierarchical substrate preferences observed in rich laboratory media (15). Human blood provides only modest glucose together with lactate and free amino acids, and *S. aureus* can assimilate these substrates concurrently rather than sequentially (15). Consistent with this metabolic flexibility, our genome-wide TraDIS screen identified a set of genes that channel diverse carbon sources into central metabolism and biosynthesis, including *fbp* and *gpmA*, anaplerotic enzymes such as *pyc* and *aspA*, and glycerol catabolic functions *glpD* and *glpP*, as key determinants of fitness. *fbp*, which encodes fructose-1,6-bisphosphatase that produces hexose phosphates to feed the pentose phosphate pathway and support anabolic processes, was selected for competition assays and exhibited a pronounced fitness defect, confirming its broad requirement in blood consistent with tissue-specific studies (15, 24). In contrast, other gluconeogenic nodes, including *pckA* and *gapB*, did not emerge as fitness determinants, consistent with previous reports suggesting context-dependence (24). Although staphylococcal infections have often been described as glycolysis dependent, *pyk*, encoding pyruvate kinase and previously identified as essential in osteomyelitis, was not required for fitness in our human blood screen (42,43). This observation aligns with prior studies in which *pyk* similarly did not contribute to fitness across diverse infection models (15,24).

Mutants in TCA cycle enzymes, including *acnA* and *icd*, were also depleted, highlighting the central role of the TCA cycle in generating reducing equivalents for the ETC and supporting oxidative-stress defense (44). These results demonstrate the metabolic plasticity of *S. aureus*, which allows the pathogen to dynamically recalibrate its central pathways in response to the diverse host environments encountered during infection.

Importantly, this integration of central carbon metabolism and TCA cycle activity depends on NAD^+ availability. PncA sustains NAD^+ pools by converting nicotinamide to nicotinic acid, fueling NAD^+

regeneration and allowing continuous TCA flux (45). This, in turn, ensures a steady supply of NADH to the electron transport chain, supporting ATP production and maintaining redox homeostasis (46). In blood, transposon insertions in *pncA* were significantly depleted, a finding that was further confirmed by phenotypic assays. Notably, PncA was recently identified as a novel regulator of the agr system, and its loss was shown to reduce virulence in both *Galleria mellonella* and murine infection models (47). Together, these findings support a model in which *S. aureus* fitness in blood relies on an integrated energy hub that couple glycerol and amino acid catabolism, gluconeogenesis, TCA-cycle flux, and NAD^+ regeneration to sustain respiratory ATP production, redox balance, and resistance to oxidative-stress.

The bloodstream imposes additional constraints on pathogens via nutritional immunity, limiting access to essential metals such as iron, manganese, and zinc (48). Consistent with this, TraDIS results showed that mutants in manganese (*mntA, mntB, mntC*) and zinc (*znuB, znuC*) acquisition systems were found to contribute to bacterial fitness in blood. While iron acquisition pathways are known to be upregulated during infection, our screen revealed only *fhuA*, encoding an ATPase essential for siderophore-mediated iron uptake, as a fitness determinant in blood (10). FhuA supports the import of staphyloferrin A and B, as well as hydroxamate-type siderophores, likely explaining its non-redundant function in iron acquisition under iron-restricted conditions (49).

During bloodstream infection, hemoglobin-derived heme serves as a primary iron source for *S. aureus*. However, while heme is a rich reservoir of iron, its intracellular accumulation poses a significant risk for bacterial fitness due to its pro-oxidant potential. Free heme can drive the production of reactive oxygen species (ROS) that inflict oxidative damage on cellular macromolecules, including lipids, proteins, and nucleic acids (50). Our TraDIS screen identified the *hssRS* two-component regulatory system and its associated efflux transporter *hrtAB* as key contributors to bacterial fitness in blood. *hssRS* functions as a heme-responsive sensor that activates *hrtAB*-mediated efflux in response to toxic intracellular heme levels. This was validated by the reduced competitiveness of *hssR* transposon mutant. Previous *in vivo* studies further demonstrated that disruption of *hssRS* or *hrtAB* impairs USA300 fitness in the spleen but not in the kidney, lung and liver (15,24). This tissue-specific requirement likely reflects the spleen's function as a primary site of erythrocyte turnover and hemoglobin catabolism, which creates a locally concentrated, heme-rich environment (51). However, disruption of *hssRS* or *hrtAB* in the ST398 lineage did not affect fitness in either human or porcine blood, suggesting lineage-specific differences in heme handling or compensatory detoxification mechanisms, pointing to a broader diversity in metal homeostasis strategies across *S. aureus* strains (12).

To assess conservation of fitness determinants, we reanalyzed TraDIS data from two MRSA ST398 strains (12). We found that 21 fitness genes overlapped, including genes involved in menaquinone and purine biosynthesis. For some genes we observed differences between lineages. These differences may reflect lineage-specific gene regulation or host adaptation, beyond technical variability.

Interestingly, we also identified several genes whose inactivation enhanced fitness in human blood. Insertions in *saeRS* and the σ^B operon (*sigB*, *rsbU*, *rsbV*).

These regulators control a broad array of surface-associated proteins, secreted factors, and stress response pathways (52, 53). SaeRS is essential for cytotoxicity and intracellular survival in mammalian host cells and has been reported to contribute to virulence in systemic infection models (15, 54). Paradoxically, loss of *saeRS* has been reported to increase survival in both human and murine blood (53,54). Consistently, *saeRS* and *fnbA* were enriched when analyzing fitness-disadvantageous genes in livestock-associated MRSA strains exposed to human blood and in a USA300 transposon library challenged in immune-depleted blood, highlighting a context-dependent effect (12,15). In this environment, where adhesive substrates are limited, expression of SaeRS- and σ^B -regulated surface proteins such as FnbA and ClfA may impose a fitness cost. These data must be interpreted with nuance, as reduced expression of these genes may confer a fitness advantage in blood while they remain essential for tissue colonization, abscess formation, and systemic dissemination in *vivo* (55,56).

To assess the influence of experimental context, we compared our results with a recent Tn-seq study in USA300 performed in commercially processed, leukocyte-depleted blood (15). Only 13 genes overlapped between the two datasets (*fhuA, purA, purB, srtA, glpD, fbp, mntA, mntB, mntC, cntE, pncA, ubiE, perR*) (15). These loci encode core metabolic and nutrient-acquisition functions that appear essential in blood irrespective of the presence of immune effectors. The limited overlap likely reflects both technical and biological factors. Technical differences may arise from variations in transposon library saturation and size, experimental design, and statistical thresholds. Biologically, our study employed fresh whole blood, which retains active immune components including leukocytes, complement, antimicrobial peptides, and nutrient sequestration mechanisms (5). In contrast, Chang et al. used processed blood, in which immune cells are removed and complement activity is largely inactivated (15). This physiological distinction likely underlies the divergent signatures observed, particularly within stress response and energy metabolism pathways. In processed blood, mutants lacking oxidative stress protection (*ahpC, ahpF*) and mutants in several DNA repair genes (*uvrA, uvrB, uvrC, recA, recG, recN, xseA, xseB, nfo, nth, polA*) were strongly enriched (15). This pattern reflects the reduced requirement for

these defensive systems in the absence of leukocyte derived reactive oxygen species and genotoxic pressure (57). Pathways that support oxidative stress-defenses displayed an opposing fitness profile between whole blood and processed blood. Mutants in genes of the mevalonate pathway (*mvaA, mvaS*), which produce isoprenoid intermediates serving as precursors for menaquinone and the antioxidant carotenoid staphyloxanthin, were enriched in processed blood but depleted in whole blood (58). The same trend was observed for *acnA*, which encodes aconitase and links the tricarboxylic acid cycle to NADPH production (44). A recent study has shown that loss of *acnA* markedly reduces NADPH generation and staphyloxanthin levels, compromising the cell's ability to detoxify reactive oxygen species (44). In the absence of immune cells and oxidative stress, these pathways become dispensable and disrupting them appears to confer a growth advantage. These observations illustrate that bacterial fitness is context dependent and that the physiological environment can reshape the definition of fitness requirements.

Despite the successful identification and validation of several fitness determinants, we observed that some mutants depleted in TraDIS did not show fitness defects when tested individually. Such discrepancies are common in pooled mutant screens and may result from stochastic loss, sampling noise, or trans-complementation effects within complex transposon libraries (12, 23, 59, 60). Furthermore, the use of stringent thresholds in both TraDIS analysis and competitive index assays may exclude genes with moderate but biologically relevant effects. For example, *rpoE* ($Log_2FC = –1.8$), has been previously shown to support fitness in blood (61). In competition assays, the choice of cut-off can affect classification. Previous studies considered mutants with $\log_{10}CI < 0$ as having reduced fitness relative to the WT, whereas we applied a more stringent threshold of $\log_{10}CI < -1$ (18, 19). This approach may explain why some mutants, such as *glpD*, were not identified as defective according to our criteria. In addition, although the high density of independent transposon insertions and concordant competitive assays provide internal validation, individual genetic complementation was not performed. While the NTML is a well-characterized resource, the potential for secondary mutations cannot be fully excluded. Finally, our *ex vivo* model relies on blood from healthy donors. Although this system is invaluable for controlled experimentation, it may not fully capture the complex immunometabolic landscape present during clinical bacteremia (62).

In summary, we identified and validated a set of genes that either promote or impair *S. aureus* fitness in human blood. These findings expand our understanding of CA-MRSA pathophysiology and demonstrate the utility of genome-wide fitness profiling in clinically relevant conditions. Future studies integrating *in*

vivo validation and cross-lineage comparisons will enhance our knowledge of *S. aureus* pathogenesis and support the development of more effective targeted therapies.

Materials and methods

Bacterial strains and antibiotics

The strains used in this study are listed in Table S4. Transposon mutants were obtained from the NTML (63). Strains were cultured in Brain Heart Infusion (BHI) broth or on Brain Heart Infusion Agar (BHIA) (Microbiol, Cagliari, Italy). When required, erythromycin (5 mg/L) (Sigma-Aldrich, St. Louis, MO, USA) was added to the medium to select for transposon mutants.

Screening of transposon mutant library in whole blood

Aliquots of the JE2 transposon mutant library were pooled, washed, and inoculated at approximately 4 × 10^9 colony-forming units (CFU) into 10 mL of whole human blood obtained from three healthy volunteers. Blood was collected in lithium heparin vacutainer tubes (Hebei Xinle Sci&Tech Co., Ltd, Hebei, China) and used immediately upon collection. The inoculated blood cultures were processed independently and incubated at 37°C with aeration for 24 hours. After the first incubation, CFU counts were determined on BHIA supplemented with erythromycin (5 mg/L). To enhance selection sensitivity and increase the bacteria-to-blood ratio, 100 µL from each blood culture was transferred into 9.9 mL of BHI broth and incubated at 37°C with aeration for an additional 24 hours (12). Following the second growth round, genomic DNA was extracted from approximately 10^9 mutants using the DNeasy Blood & Tissue Kit (Qiagen, Hilden, Germany) with the addition of 0.5 mg/mL (250 units/mL) of lysostaphin (Sigma Aldrich). The extracted DNA was considered as output and stored at -80°C for subsequent analysis. A preliminary survival assay in whole human blood was conducted to determine the optimal inoculum size. This step ensured that sufficient copies of each mutant were present to account for the expected initial decline in bacterial cell counts upon exposure to whole blood.

TraDIS sequencing

Two micrograms of extracted DNA from the output libraries were resuspended in 100 µL of nuclease-free water and mechanically sheared to approximately 300 bp using the Bioruptor® Pico sonicator (Diagenode, Liège, Belgium). The efficacy of the mechanical fragmentation process was assessed by evaluating the size distribution of the DNA fragments with a High-Sensitivity DNA Kit via the Agilent 2100 Bioanalyzer System (Agilent Technologies, Santa Clara, CA, USA). The fragmented DNA was

subsequently processed to generate blunt-ended fragments using the NEBNext End Repair Module (New England Biolabs, Ipswich, MA, USA), followed by dA-tailing with the NEBNext dA-Tailing Module (New England Biolabs). Subsequently, the dA-tailed DNA was ligated to SpIA5 adapters using the NEBNext Quick Ligation Module. To enrich for transposon-inserted fragments, PCR amplification was performed using transposon-specific primers and adapter primers (Table S5) (13, 64). After each step of library preparation, DNA fragments were purified and size-selected using Agencourt AMPure XP beads (Beckman Coulter, Brea, CA, USA). The prepared libraries were sequenced on an Illumina MiSeq platform with the MiSeq V2 50-cycle reagent kit (Illumina), as previously described (60).

TraDIS data analysis

Sequence reads obtained from both the input and output libraries were filtered, mapped, and analyzed using the BioTraDIS pipeline as modified by Garcia et. al (59, 64). Sequencing quality control of raw data was verified by FastQC and then processed using the *fq2bam.pl* script, which adds the transposon tag (TAAGAGACAG) at the end of the read name and converts the FASTQ files to SAM format. To add tags to the read strings, SAM files were converted to BAM files using Samtools 1.6, and then back to FASTQ files for further analysis. Using the Bacteria_tradis script, tags were filtered and removed from the resulting reads. These reads were then aligned to the reference genome (GenBank accession number: CP000255.1) using SMALT 0.7.6, with no mismatches permitted. As a result, unique transposon insertion sites and the corresponding read counts were identified for each gene. The *tradis_comparisons.R* script was used to assess the statistical significance of insertion differences between input and output data and to calculate Log_2FC, after normalizing read counts with the trimmed mean of M (TMM) method in R. Significant genes (q-value < 0.01 and log_2 counts per million > 3) were categorized based on their transposon insertion profiles following exposure to human blood. Genes with Log_2FC of < -2 were classified as fitness genes, indicating depletion of transposon insertions under these conditions. Conversely, genes with a Log_2FC > 2 were considered enriched, reflecting an increased representation of transposon insertions. To minimize false identification of fitness genes, we excluded genes with a mean read count below 150 in the outgrowth control (65). The selected genes were re-annotated using the AureoWiki database (http://aureowiki.med.uni-greifswald.de) and functionally characterized using the eggNOG-mapper 2.1.9.

Diversity and bottleneck assessment

Insertional richness and diversity of the transposon mutant library during the *ex vivo* human blood assay were quantified at the gene level using read counts from input and output samples. Read counts were adjusted to account for differences in library size, and for each gene, proportional abundance (p_i) was calculated as the gene's count divided by the total counts across all genes. Shannon's diversity index, Simpson's diversity index, and Pielou's evenness were computed from these proportional abundances using the vegan R package (v4.3.2). Rank abundance curves were generated by plotting the logarithm of proportional abundances against the ranked mutant lineages, allowing a visual comparison between input and output libraries. To further quantify potential bottlenecks, the effective population size (N_e) was computed from proportional abundance data using the inverse Simpson diversity index:

$$Ne = \frac{1}{\sum p_i^2}$$

This metric reflects the number of equally abundant contributors effectively represented in the population (66). A decrease in the output relative to input indicates a reduction in library complexity in response to the selective pressures of the blood assay and is interpreted as evidence of a genetic bottleneck (67). PCA was performed on normalized insertion counts for all genes using *factoextra* package to assess replicate similarity across input, outgrowth control, and blood conditions.

***In vitro* competition assays**

Overnight cultures of WT and mutant strains were washed and mixed at a 1:1 ratio, then inoculated into 5 mL of human blood in triplicate to achieve an initial inoculum of approximately 10^7 CFU/mL. Cultures were incubated at 37 °C for 24 h. After incubation, mutant counts were determined on erythromycin-supplemented plates. WT counts were calculated by subtracting mutant CFUs from the total CFUs obtained on plates without erythromycin. For assays conducted in BHI, the initial inoculum (T0) was used as the reference for CI calculations. However, preliminary experiments in blood revealed early population bottlenecks and rapid fluctuations in the mutant-to-WT ratio, which could bias measurements. Therefore, the bacterial population after 2 h of incubation (T1) was used as the reference inoculum. CI was calculated as the ratio of the mutant-to-WT population at the end of the assay divided by the mutant-to-WT ratio in the initial inoculum.

Ethical approval and consent to participate

Informed consent was obtained from all the volunteer participants to collect blood for screening of transposon mutant library. The study was approved by the Ethics Committee of Sardinia, Italy (authorization no. 19, approved on 11 March 2025; All. 2.10).

Acknowledgments

This work was supported by the European Union's Horizon 2020 Research and Innovation Programme under the Marie Skłodowska-Curie Grant Agreement No. 956154. We thank Dr. Pietro Carmelo Manca, Director of S.C. Servizio Immunotrasfusionale e Terapia delle Emoglobinopatie e delle Coagulopatie dell'AOU Sassari, for his invaluable assistance with blood collection and for facilitating the ethical approval procedures. We also thank Dr. Yibing Ma for technical support with the TraDIS experiments. Finally, we are grateful to the volunteers who generously donated their blood, making this study possible.

Competing interests

The authors declare no competing interests.

Data availability

Raw sequencing data and metadata are available in the NCBI Sequence Read Archive (SRA), under BioProject accession no. PRJNA1345259.

Supplemental information

Supplementary_files_Table S1-S3_S4_Fig.S1-S2.

https://drive.google.com/drive/folders/1uR8TFh4EV8K5Jrt2NUY04bYuKEKbA9rG

Supplementary_file_Table S2 and Table S3.

https://drive.google.com/drive/folders/1uR8TFh4EV8K5Jrt2NUY04bYuKEKbA9rG

References

1. O'Gara JP. 2017. *Into the storm* : Chasing the opportunistic pathogen *Staphylococcus aureus* from skin colonisation to life-threatening infections. Environ Microbiol 19:3823–3833. https://doi.org/10.1111/1462-2920.13833.

2. Tong SYC, Fowler VG, Skalla L, Holland TL. 2025. Management of *Staphylococcus aureus* Bacteremia: A Review. JAMA https://doi.org/10.1001/jama.2025.4288.

3. Ippolito G, Leone S, Lauria FN, Nicastri E, Wenzel RP. 2010. Methicillin-resistant Staphylococcus aureus: the superbug. Int J Infect Dis 14:S7–S11. https://doi.org/10.1016/j.ijid.2010.05.003.

4. Kwiecinski JM, Horswill AR. 2020. Staphylococcus aureus bloodstream infections: pathogenesis and regulatory mechanisms. Curr Opin Microbiol 53:51–60. https://doi.org/10.1016/j.mib.2020.02.005.

5. Cheung GYC, Bae JS, Otto M. 2021. Pathogenicity and virulence of *Staphylococcus aureus*. Virulence 12:547–569. https://doi.org/10.1080/21505594.2021.1878688.

6. Valentino MD, Foulston L, Sadaka A, Kos VN, Villet RA, Santa Maria J, Lazinski DW, Camilli A, Walker S, Hooper DC, Gilmore MS. 2014. Genes Contributing to Staphylococcus aureus Fitness in Abscess- and Infection-Related Ecologies. mBio 5:e01729-14. https://doi.org/10.1128/mBio.01729-14.

7. Wilde AD, Snyder DJ, Putnam NE, Valentino MD, Hammer ND, Lonergan ZR, Hinger SA, Aysanoa EE, Blanchard C, Dunman PM, Wasserman GA, Chen J, Shopsin B, Gilmore MS, Skaar EP, Cassat JE. 2015. Bacterial Hypoxic Responses Revealed as Critical Determinants of the Host-Pathogen Outcome by TnSeq Analysis of Staphylococcus aureus Invasive Infection. PLOS Pathog 11:e1005341. https://doi.org/10.1371/journal.ppat.1005341.

8. Lo H-Y, Long DR, Holmes EA, Penewit K, Hodgson T, Lewis JD, Waalkes A, Salipante SJ. 2023. Transposon sequencing identifies genes impacting *Staphylococcus aureus* invasion in a human macrophage model. Infect Immun 91:e00228-23. https://doi.org/10.1128/iai.00228-23.

9. Li G, Shen W, Gong Y, Li M, Rao X, Liu Q, Yu Y, Zhou J, Zhu K, Yuan M, Shang W, Yang Y, Lu S, Wang J, Zhao Y. 2022. Essential Fitness Repertoire of Staphylococcus aureus during Co-infection with Acinetobacter baumannii *In Vivo*. mSystems 7:e00338-22. https://doi.org/10.1128/msystems.00338-22.

10. Malachowa N, Whitney AR, Kobayashi SD, Sturdevant DE, Kennedy AD, Braughton KR, Shabb DW, Diep BA, Chambers HF, Otto M, DeLeo FR. 2011. Global Changes in Staphylococcus aureus Gene Expression in Human Blood. PLoS ONE 6:e18617. https://doi.org/10.1371/journal.pone.0018617.

11. Young BC, Wu C-H, Charlesworth J, Earle S, Price JR, Gordon NC, Cole K, Dunn L, Liu E, Oakley S, Godwin H, Fung R, Miller R, Knox K, Votintseva A, Quan TP, Tilley R, Scarborough M, Crook DW, Peto TE, Walker AS, Llewelyn MJ, Wilson DJ. 2021. Antimicrobial resistance determinants are associated with Staphylococcus aureus bacteraemia and adaptation to the healthcare environment: a bacterial genome-wide association study. Microb Genomics 7. https://doi.org/10.1099/mgen.0.000700.

12. Ba X, Matuszewska M, Kalmar L, Fan J, Zou G, Corander D, Raisen CL, Li S, Li L, Weinert LA, Tucker AW, Grant AJ, Zhou R, Holmes MA. 2023. High-Throughput Mutagenesis Reveals a Role for Antimicrobial Resistance- and Virulence-Associated Mobile Genetic Elements in

Staphylococcus aureus Host Adaptation. Microbiol Spectr 11:e04213-22. https://doi.org/10.1128/spectrum.04213-22.

13. Christiansen MT, Kaas RS, Chaudhuri RR, Holmes MA, Hasman H, Aarestrup FM. 2014. Genome-Wide High-Throughput Screening to Investigate Essential Genes Involved in Methicillin-Resistant Staphylococcus aureus Sequence Type 398 Survival. PLoS ONE 9:e89018. https://doi.org/10.1371/journal.pone.0089018.

14. Nolan LM, Webber MA, Filloux A. 2025. Throwing a spotlight on genomic dark matter: the power and potential of transposon-insertion sequencing. J Biol Chem 110231. https://doi.org/10.1016/j.jbc.2025.110231.

15. Chang J, Lee C, Kim I, Kim J, Kim J-H, Yun T, Hooper DC, Walker S, Lee W. 2025. Environmental cues in different host niches shape the survival fitness of Staphylococcus aureus. Nat Commun 16:6928. https://doi.org/10.1038/s41467-025-62292-x.

16. Yousief SW, Abdelmalek N, Paglietti B. 2024. Optimizing phage-based mutant recovery and minimizing heat effect in the construction of transposon libraries in Staphylococcus aureus. Sci Rep 14:22831. https://doi.org/10.1038/s41598-024-73731-y.

17. Abdelmalek N, Yousief SW, Bojer MS, Alobaidallah MSA, Olsen JE, Paglietti B. 2025. The Secondary Resistome of Methicillin-Resistant Staphylococcus aureus to β-Lactam Antibiotics. Antibiotics 14:112. https://doi.org/10.3390/antibiotics14020112.

18. Linkevicius M, Anderssen JM, Sandegren L, Andersson DI. 2016. Fitness of *Escherichia coli* mutants with reduced susceptibility to tigecycline. J Antimicrob Chemother 71:1307–1313. https://doi.org/10.1093/jac/dkv486.

19. Tan YH, Chen Y, Chu WHW, Sham L, Gan Y. 2020. Cell envelope defects of different capsule-null mutants in K1 hypervirulent *Klebsiella pneumoniae* can affect bacterial pathogenesis. Mol Microbiol 113:889–905. https://doi.org/10.1111/mmi.14447.

20. Thomsen IP, Liu GY. 2018. Targeting fundamental pathways to disrupt Staphylococcus aureus survival: clinical implications of recent discoveries. JCI Insight 3:e98216. https://doi.org/10.1172/jci.insight.98216.

21. Wong Fok Lung T, Prince A. 2020. Consequences of Metabolic Interactions during Staphylococcus aureus Infection. Toxins 12:581. https://doi.org/10.3390/toxins12090581.

22. Connolly J, Boldock E, Prince LR, Renshaw SA, Whyte MK, Foster SJ. 2017. Identification of Staphylococcus aureus Factors Required for Pathogenicity and Growth in Human Blood. Infect Immun 85:e00337-17. https://doi.org/10.1128/IAI.00337-17.

23. Mahmutovic A, Abel Zur Wiesch P, Abel S. 2020. Selection or drift: The population biology underlying transposon insertion sequencing experiments. Comput Struct Biotechnol J 18:791–804. https://doi.org/10.1016/j.csbj.2020.03.021.

24. Yousief SW, Abdelmalek N, Bojer MS, Ma Y, Guerra PR, Nisar S, Olsen JE, Paglietti B. 2026. Genome-wide identification of tissue-specific fitness genes in murine models of *Staphylococcus aureus* infection. iScience 29:114261. https://doi.org/10.1016/j.isci.2025.114261

25. Chao MC, Abel S, Davis BM, Waldor MK. 2016. The design and analysis of transposon insertion sequencing experiments. Nat Rev Microbiol 14:119–128. https://doi.org/10.1038/nrmicro.2015.726. Murdoch CC, Skaar EP. 2022. Nutritional immunity: the battle for nutrient metals at the host–pathogen interface. Nat Rev Microbiol 20:657–670. https://doi.org/10.1038/s41579-022-00745-6.

27. Planet PJ. 2017. Life After USA300: The Rise and Fall of a Superbug. J Infect Dis 215:S71–S77. https://doi.org/10.1093/infdis/jiw444.

28. Thomer L, Schneewind O, Missiakas D. 2016. Pathogenesis of *Staphylococcus aureus* Bloodstream Infections. Annu Rev Pathol Mech Dis 11:343–364. https://doi.org/10.1146/annurev-pathol-012615-044351.

29. Kim G-L, Hooven TA, Norambuena J, Li B, Boyd JM, Yang JH, Parker D. 2021. Growth and Stress Tolerance Comprise Independent Metabolic Strategies Critical for Staphylococcus aureus Infection. mBio 12:e00814-21. https://doi.org/10.1128/mBio.00814-21.

30 Bubeck Wardenburg J, Williams WA, Missiakas D. 2006. Host defenses against *Staphylococcus aureus* infection require recognition of bacterial lipoproteins. Proc Natl Acad Sci 103:13831–13836. https://doi.org/10.1073/pnas.0603072103.

31. Hübscher J, McCallum N, Sifri CD, Majcherczyk PA, Entenza JM, Heusser R, Berger-Bächi B, Stutzmann Meier P. 2009. MsrR contributes to cell surface characteristics and virulence in *Staphylococcus aureus*. FEMS Microbiol Lett 295:251–260. https://doi.org/10.1111/j.1574-6968.2009.01603.x.

32. Kehl-Fie TE, Zhang Y, Moore JL, Farrand AJ, Hood MI, Rathi S, Chazin WJ, Caprioli RM, Skaar EP. 2013. MntABC and MntH Contribute to Systemic Staphylococcus aureus Infection by Competing with Calprotectin for Nutrient Manganese. Infect Immun 81:3395–3405. https://doi.org/10.1128/IAI.00420-13.

33. Chen C, Hooper DC. 2019. Intracellular accumulation of staphylopine impairs the fitness of *Staphylococcus aureus cntE* mutant. FEBS Lett 593:1213–1222. https://doi.org/10.1002/1873-3468.13396.

34. Cameron DR, Ward DV, Kostoulias X, Howden BP, Moellering RC, Eliopoulos GM, Peleg AY. 2012. Serine/Threonine Phosphatase Stp1 Contributes to Reduced Susceptibility to Vancomycin and Virulence in Staphylococcus aureus. J Infect Dis 205:1677–1687. https://doi.org/10.1093/infdis/jis252.

35. Koedijk DGAM, Pastrana FR, Hoekstra H, Berg SVD, Back JW, Kerstholt C, Prins RC, Bakker-Woudenberg IAJM, Van Dijl JM, Buist G. 2017. Differential epitope recognition in the immunodominant staphylococcal antigen A of Staphylococcus aureus by mouse versus human IgG antibodies. Sci Rep 7:8141. https://doi.org/10.1038/s41598-017-08182-9.

36. Soutourina O, Dubrac S, Poupel O, Msadek T, Martin-Verstraete I. 2010. The Pleiotropic CymR Regulator of Staphylococcus aureus Plays an Important Role in Virulence and Stress Response. PLoS Pathog 6:e1000894. https://doi.org/10.1371/journal.ppat.1000894.

37. Kim J, Kim G-L, Norambuena J, Boyd JM, Parker D. 2023. Impact of the pentose phosphate pathway on metabolism and pathogenesis of Staphylococcus aureus. PLOS Pathog 19:e1011531. https://doi.org/10.1371/journal.ppat.1011531.

38. Goncheva MI, Flannagan RS, Heinrichs DE. 2020. *De Novo* Purine Biosynthesis Is Required for Intracellular Growth of Staphylococcus aureus and for the Hypervirulence Phenotype of a *purR* Mutant. Infect Immun 88:e00104-20. https://doi.org/10.1128/IAI.00104-20.

39. Proctor R. 2019. Respiration and Small Colony Variants of *Staphylococcus aureus*. Microbiol Spectr 7:7.3.22. https://doi.org/10.1128/microbiolspec.GPP3-0069-2019.

40. Wakeman CA, Hammer ND, Stauff DL, Attia AS, Anzaldi LL, Dikalov SI, Calcutt MW, Skaar EP. 2012. Menaquinone biosynthesis potentiates haem toxicity in *S taphylococcus aureus* . Mol Microbiol 86:1376–1392. https://doi.org/10.1111/mmi.12063.

41. Painter KL, Hall A, Ha KP, Edwards AM. 2017. The Electron Transport Chain Sensitizes Staphylococcus aureus and Enterococcus faecalis to the Oxidative Burst. Infect Immun 85:e00659-17. https://doi.org/10.1128/IAI.00659-17.

42. Vitko NP, Spahich NA, Richardson AR. 2015. Glycolytic Dependency of High-Level Nitric Oxide Resistance and Virulence in *Staphylococcus aureus*. mBio 6:e00045-15. https://doi.org/10.1128/mBio.00045-15

43. Potter AD, Butrico CE, Ford CA, Curry JM, Trenary IA, Tummarakota SS, Hendrix AS, Young JD, Cassat JE. 2020. Host nutrient milieu drives an essential role for aspartate biosynthesis during invasive *Staphylococcus aureus* infection. Proc Natl Acad Sci USA 117:12394–12401. https://doi.org/10.1073/pnas.1922211117

44. Li J, Hou W, Chang J, Tian X, He M, Zhang Z, Shi C. 2025. The pivotal role of *acnA* in linking carbon metabolism to virulence and antimicrobial resistance in methicillin-resistant *Staphylococcus aureus*. J Antimicrob Chemother dkaf317. https://doi.org/10.1093/jac/dkaf317.

45. Singh JK, Singh J, Jha I, Rajput T, Srivastava S, Srivastava SK. 2024. In silico studies on nicotinamide analogs as competitive inhibitors of nicotinamidase in methicillin-resistant Staphylococcus aureus. Mol Divers https://doi.org/10.1007/s11030-024-11036-y46. Sena FV, Sousa FM, Pereira AR, Catarino T, Cabrita EJ, Pinho MG, Pinto FR, Pereira MM. 2024. The two alternative NADH:quinone oxidoreductases from *Staphylococcus aureus* : two players with different molecular and cellular roles. Microbiol Spectr 12:e04152-23. https://doi.org/10.1128/spectrum.04152-23

47. Rodrigues Lopes I, Alcantara LM, Lopez-Bravo M, Liu Y, Larrouy-Maumus G, Lopez D, Mano M, Eulalio A. 2025. Systematic identification of bacterial factors driving *Staphylococcus aureus* intracellular lifestyle in non-professional phagocytes. Nat Commun 16:10907. https://doi.org/10.1038/s41467-025-66373-9

48. Hennigar SR, McClung JP. 2016. Nutritional Immunity: Starving Pathogens of Trace Minerals. Am J Lifestyle Med 10:170–173. https://doi.org/10.1177/1559827616629117.

49. Hammer ND, Skaar EP. 2011. Molecular Mechanisms of *Staphylococcus aureus* Iron Acquisition. Annu Rev Microbiol 65:129–147. https://doi.org/10.1146/annurev-micro-090110-102851.

50. Saillant V, Morey L, Lipuma D, Boëton P, Siponen M, Arnoux P, Lechardeur D. 2024. HssS activation by membrane heme defines a paradigm for two-component system signaling in *Staphylococcus aureus*. mBio 15:e00230-24. https://doi.org/10.1128/mbio.00230-24.

51. Mebius RE, Kraal G. 2005. Structure and function of the spleen. Nat Rev Immunol 5:606–616. https://doi.org/10.1038/nri1669

52. Pané-Farré J, Jonas B, Förstner K, Engelmann S, Hecker M. 2006. The σB regulon in Staphylococcus aureus and its regulation. Int J Med Microbiol 296:237–258. https://doi.org/10.1016/j.ijmm.2005.11.011.

53. Guo H, Hall JW, Yang J, Ji Y. 2017. The SaeRS Two-Component System Controls Survival of Staphylococcus aureus in Human Blood through Regulation of Coagulase. Front Cell Infect Microbiol 7:204. https://doi.org/10.3389/fcimb.2017.00204.

54. Liu Y, Gao W, Yang J, Guo H, Zhang J, Ji Y. 2021. Contribution of Coagulase and Its Regulator SaeRS to Lethality of CA-MRSA 923 Bacteremia. Pathogens 10:1396. https://doi.org/10.3390/pathogens10111396

55. Speziale P, Foster TJ, Arciola CR. 2025. The endothelium at the interface between tissues and *Staphylococcus aureus* in the bloodstream. Clin Microbiol Rev 38:e00098-24. https://doi.org/10.1128/cmr.00098-24

56. Li M, Wang B, Chen J, Jiang L, Zhou Y, Guo G, Jiang F, Hu Y, Wang C, Yang Y, Tang J, Han P, Yu J, Shen H. 2024. Staphylococcus aureus SaeRS impairs macrophage immune functions through bacterial clumps formation in the early stage of infection. Npj Biofilms Microbiomes 10:102. https://doi.org/10.1038/s41522-024-00576-8.

57. Gaupp R, Ledala N, Somerville GA. 2012. Staphylococcal response to oxidative stress. Front Cell Infect Microbiol 2. https://doi.org/10.3389/fcimb.2012.00033.

58. Reichert S, Ebner P, Bonetti E-J, Luqman A, Nega M, Schrenzel J, Spröer C, Bunk B, Overmann J, Sass P, François P, Götz F. 2018. Genetic Adaptation of a Mevalonate Pathway Deficient Mutant in Staphylococcus aureus. Front Microbiol 9:1539. https://doi.org/10.3389/fmicb.2018.01539.

59. García V, Grønnemose RB, Torres-Puig S, Kudirkiene E, Piantelli M, Ahmed S, Andersen TE, Møller-Jensen J, Olsen JE, Herrero-Fresno A. 2021. Genome-wide analysis of fitness-factors in uropathogenic Escherichia coli during growth in laboratory media and during urinary tract infections. Microb Genomics 7. https://doi.org/10.1099/mgen.0.000719.

60. Canals R, Chaudhuri RR, Steiner RE, Owen SV, Quinones-Olvera N, Gordon MA, Baym M, Ibba M, Hinton JCD. 2019. The fitness landscape of the African Salmonella Typhimurium ST313 strain

D23580 reveals unique properties of the pBT1 plasmid. PLOS Pathog 15:e1007948. https://doi.org/10.1371/journal.ppat.1007948.

61. Weiss A, Ibarra JA, Paoletti J, Carroll RK, Shaw LN. 2014. The δ Subunit of RNA Polymerase Guides Promoter Selectivity and Virulence in Staphylococcus aureus. Infect Immun 82:1424–1435. https://doi.org/10.1128/iai.01508-14.

62. Van Der Poll T, Shankar-Hari M, Wiersinga WJ. 2021. The immunology of sepsis. Immunity 54:2450–2464. https://doi.org/10.1016/j.immuni.2021.10.012

63. Fey PD, Endres JL, Yajjala VK, Widhelm TJ, Boissy RJ, Bose JL, Bayles KW. 2013. A Genetic Resource for Rapid and Comprehensive Phenotype Screening of Nonessential Staphylococcus aureus Genes. mBio 4:e00537-12. https://doi.org/10.1128/mbio.00537-12.

64. Barquist L, Mayho M, Cummins C, Cain AK, Boinett CJ, Page AJ, Langridge GC, Quail MA, Keane JA, Parkhill J. 2016. The TraDIS toolkit: sequencing and analysis for dense transposon mutant libraries. Bioinformatics 32:1109–1111. https://doi.org/10.1093/bioinformatics/btw022

65. Coe KA, Lee W, Stone MC, Komazin-Meredith G, Meredith TC, Grad YH, Walker S. 2019. Multi-strain Tn-Seq reveals common daptomycin resistance determinants in Staphylococcus aureus. PLOS Pathog 15:e1007862. https://doi.org/10.1371/journal.ppat.1007862.

66. Jost L. 2006. *Entropy and diversity*. Oikos 113:363–375. https://doi.org/10.1111/j.2006.0030-1299.14714.x.

67. Abel S, Abel Zur Wiesch P, Chang H-H, Davis BM, Lipsitch M, Waldor MK. 2015. Sequence tag–based analysis of microbial population dynamics. Nat Methods 12:223–226. https://doi.org/10.1038/nmeth.3253.

CHAPTER IV
GENERAL DISCUSSION

4. Discussion

S. aureus is an exceptionally adaptable pathogen whose capacity to transition from commensal carriage to invasive disease depends on coordinated metabolic, regulatory, and stress response networks.[8,65,66] This thesis used genome-wide functional genomics to interrogate how methicillin-resistant *S. aureus* (MRSA) survives across three distinct but complementary environments: (i) the laboratory setting of transposon library construction and optimization (Paper I), (ii) tissue-specific niches in murine skin, kidney, and spleen (Paper II), and (iii) fresh immune-competent human blood *ex vivo* (Paper III). Across these studies, we employed TraDIS, a specific implementation of Transposon Insertion Sequencing (TIS), and developed an explicit quality control (QC) and filtration framework to address the unique vulnerabilities of TIS to bottlenecks, insertion-site bias, and read-depth artifacts.[55,59,67,68] Together, these data provide a unified view of the metabolic and physiological architectures that support *S. aureus* fitness and highlight how niche specific pressures shape the deployment of shared pathways.

4.1 Strategic Use of TraDIS and the Foundation Laid by Library Optimization (Paper I)

TIS has transformed bacterial genetics by enabling simultaneous measurement of the fitness contribution of thousands of genes across environmental conditions.[56,59,67,69] However, the quality and interpretability of TIS results are entirely dependent on the properties of the underlying mutant library, its saturation, evenness of insertion distribution, and absence of strong pre-selection events during construction.[70,71] In *S. aureus*, genetic manipulation is particularly challenging due to its thick cell wall, robust restriction modification systems, and limited options for conjugative transfer.[49,72] These barriers have historically limited library density and introduced strain specific biases that complicate cross study comparisons.

Paper I addressed these issues by systematically optimizing phage-based transposon delivery and plasmid curing using *Himar1* mariner transposon and ϕ11-based transduction. *Himar1* insertions are restricted to TA sites, but *S. aureus* has a relatively high AT content, making this system well suited for high saturation mutagenesis in this organism.[73,74] We selected TraDIS as our TIS platform because it directly sequences the transposon–genome junctions, enabling both accurate read count quantification and explicit tracking of unique insertion sites (UIS) at nucleotide resolution.[55,59,68]

A first methodological pillar of Paper I was enhancing transduction efficiency. Phage adsorption to *S. aureus* depends critically on wall teichoic acids (WTA), which act as primary receptors for many siphoviruses, including ϕ11.[75,76] We showed that sub-inhibitory chloramphenicol treatment increased the

number of transductants, consistent with reports that certain antibiotics trigger cell wall and WTA remodeling that can increase phage receptor density on the cell surface.[77,78] In parallel, we developed an in-house "SN" transduction medium supplemented with β-glycerophosphate and divalent cations (Ca^{2+}, Mg^{2+}), which likely modulate surface charge and cell wall architecture to favor phage adsorption and early steps of infection.[78] These optimizations significantly increased transduction efficiency across multiple *S. aureus* lineages (JE2, Newman, COL, MW2, ST398), allowing construction of dense libraries in both MRSA and MSSA backgrounds.

The second and arguably more conceptually important pillar of Paper I was the demonstration that temperature-sensitive plasmid curing can itself act as a strong selection bottleneck. Conventional protocols employ a rapid temperature shift to 43 °C to eliminate the transposon delivery plasmid.[58,72] By comparing two libraries in JE2, one cured using an abrupt 43 °C shift and one cured using a gradual, multi-step temperature increase, we showed that the rapid protocol caused dramatic depletion of mutants in heat stress, cell wall, and DNA stability pathways, including genes in cell wall biosynthesis (*pbp3, pbp4, lcpA, auxA, auxB*), chaperon e systems (*dnaJ, dnaK, grpE*), and menaquinone and pyrimidine metabolism previously linked to small colony variants and temperature sensitivity.[72,79,80] These changes occurred before any *in vitro* or *in vivo* fitness experiment and would have been misinterpreted as "essentiality" or conditional essentiality if library construction were not examined explicitly.

By implementing a gradual curing regimen with shorter exposure at 43 °C and additional passages, we reduced this curing-associated selection and preserved mutants in pathways that are known to be important for virulence and stress adaptation.[72,79] Both libraries nonetheless reached ~76% TA-site coverage, substantially higher than prior USA300 TIS studies that reported ~28–55% coverage.[58,61] Thus, Paper I established that high-density, relatively unbiased transposon libraries can be constructed in MRSA when curing is carefully controlled, and that library construction steps must be considered an integral part of experimental design and interpretation rather than a neutral prelude.

This optimized library and the accompanying methodological insight set the stage for Papers II and III, where we applied TraDIS in murine infection models and fresh human blood to dissect tissue-specific fitness signatures.

4.2 Design and QC of *In Vivo* TraDIS Screens: Bottlenecks, Filtration, and Read Depth Aware Analysis (Paper II)

In vivo TraDIS experiments are uniquely vulnerable to population bottlenecks and PCR "jackpots" that can distort apparent fitness signatures independently of true biological effects.[55,61] To address this, Paper II combined (i) experimental strategies to minimize bottlenecks, (ii) explicit quantification of library complexity using UIS, and (iii) a multi-layer filtration pipeline including a bespoke read depth aware QC step.[50,56,68,70]

First, we used high dose inocula in all murine models, following theoretical and empirical recommendations that each insertion mutant should be represented by at least 10–100 cells in the inoculum to maintain diversity.[50] This resulted in high colony-forming unit (CFU) burdens and strong retention of UIS across skin, kidney, and spleen samples. By quantifying effective population size and UIS retention per sample, we found that most organs preserved sufficient diversity to support robust TraDIS inference, with one outlier mouse in the skin model mouse B (MB) showing a pronounced bottleneck. MB still displayed a depletion profile that was biologically concordant with other skin samples, so it was retained for initial differential analysis to preserve statistical power but excluded from downstream read depth aware QC and curation steps, which assume relatively stable UIS diversity and are highly sensitive to bottlenecks.

Second, we implemented a three-tier filtration pipeline to define fitness and anti-fitness genes during infection:

1. Dual-contrast requirement (Input→Output ∩ Outgrowth Control→Output)

We required genes to be significantly depleted (or enriched) in both Input-Output (IO) and Outgrowth Control-Output (CO) contrasts. This design was crucial, because the outgrowth control helps to distinguish genuine *in vivo* fitness effects from changes arising during standardized *in vitro* handling and early outgrowth in the absence of host pressures.[68] Genes that appeared significant in only one contrast (e.g., only IO or only CO) were treated as potential artifacts and removed. This step already eliminated many candidates that could have been misclassified as "hits" by a simpler IO-only pipeline.

2. *In vitro* exclusion

We next excluded genes that were also significantly depleted or enriched under purely *in vitro* conditions, such as medium-specific growth effects. This ensured that our final set of hits reflected *in vivo* specific fitness requirements, removing genes whose altered representation was driven by general growth defects or medium composition rather than by host factors.

3. Post-hoc, read depth aware QC using UIS and reads per UIS (RPU)

Classical TIS analysis treats read counts as proxies for mutant abundance, but read depth alone is vulnerable to amplification bias and stochastic fluctuations. To address this, we developed a custom "read depth aware" QC script that jointly evaluated changes in UIS and reads per UIS (RPU) between conditions.[54,70,71] If a locus showed large changes in read counts but stable UIS numbers, with ≥2-fold shifts in average RPU, it was flagged as a "read depth only" artifact, for example, PCR jackpots or mapping bias, not a genuine change in mutant abundance. Conversely, loci with reduced UIS and concordant declines in read depth were considered true depletions, reflecting actual loss of mutant diversity under selective pressure. This read depth aware QC step is conceptually aligned with guidance from Chao, DeJesus, Barquist, and others[55,59,67,68,70,71] It allowed us to classify genes into curated categories such as "true depleted," "true enriched," and "flagged (read depth only)", improving specificity without sacrificing genuine signal.

A clear illustration of this issue comes from the behavior of *purB* and *purR* in the skin abscess model. In the initial read count only analysis, both loci appeared enriched, which without further scrutiny could have been misinterpreted as a true increase in mutant abundance. However, when examined through the read depth aware QC framework, their UIS counts remained stable, and the apparent "enrichment" was instead driven by a disproportionate rise in RPU, a hallmark of PCR jackpotting or mapping bias rather than biological selection.[55,56,59,67,70,71] Consequently, *purB* and *purR* were reclassified as "flagged enriched", technical artifacts rather than genuine anti-fitness signals, and were excluded from the final tissue-specific hit list. This example underscores the necessity of applying a rigorous QC pipeline: without UIS-based verification, raw read count distortions would have been mistakenly interpreted as meaningful biological outcomes.[55,56,59,68,70,71] Together, the high-dose inoculum strategy, UIS-based bottleneck measurement, dual-contrast design, *in vitro* exclusion, and read depth aware QC produced a conservative but stable set of tissue-specific fitness and anti-fitness genes. This design explicitly addresses concerns raised in earlier *S. aureus* Tn-Seq studies, where replicate pooling, lack of input

output pairing, or unquantified bottlenecks hindered direct comparison and may have contributed to conflicting results in the literature.[58,60,61,81–83]

4.3 Tissue-Specific Fitness Architectures in Murine Skin, Kidney, and Spleen (Paper II)

With this rigorous framework in place, Paper II mapped the genetic requirements for *S. aureus* fitness in three distinct niches: skin abscess, kidney, and spleen. These environments differ in immune composition, oxygen tension, nutrient availability, and the balance of acute vs. chronic host responses, and our results highlight both a conserved metabolic core and strong niche specific specializations.

Across all three tissues, we observed a common dependence on *de novo* nucleotide biosynthesis, central carbon metabolism, and respiratory chain function, in agreement with recent reviews emphasizing nucleotide and carbon metabolism as central to *S. aureus* pathogenesis.[66,84–86] Pyrimidine biosynthesis mutants were consistently depleted in skin, kidney, and spleen, reinforcing the view that this pathway is broadly essential *in vivo*.[86–88] Purine biosynthesis genes were likewise required in systemic tissues, consistent with studies showing that *de novo* purine synthesis is crucial for intracellular growth and hypervirulence of *purR* mutants.[85,89,90] The concordance of our curated hits with independent data strengthens confidence in the biological signal after QC.

Gluconeogenesis emerged as a core requirement across sites, with fructose-1,6-bisphosphatase (*fbp*) consistently classified as a fitness gene. This is compatible with models in which glucose is scarce during infection and *S. aureus* must use gluconeogenic substrates -glycerol, amino acids, TCA intermediates- to sustain hexose phosphate pools and pentose phosphate pathway PPP flux, thereby generating NADPH for oxidative stress defense and supporting nucleotide and cell wall biosynthesis.[91–94] Although TraDIS alone could not fully resolve flux directionality, competitive assays in gluconeogenic medium (M9) confirmed that *fbp*, *pckA*, and *gapB* mutants are at a disadvantage, and tissue-specific competitive index results revealed that the relative importance of these nodes differs between kidney and spleen. In kidney, *pckA* and *fbp* were critical, suggesting reliance on canonical gluconeogenesis from oxaloacetate, whereas in spleen, *gapB* and *fbp* were more important, compatible with gluconeogenic input downstream of oxaloacetate via glycerol or certain amino acids. In skin, only *fbp* was essential, reflecting a more restricted but still crucial gluconeogenic role.

In the skin abscess model, strong depletion of *ahpC, ahpF, dps, uvrABC, recD, xseA*, and related loci highlighted the dominance of oxidative and genotoxic stress at the host–pathogen interface.[60,80,95,96] *In*

vivo and *in vitro* competition assays, including H_2O_2 exposure mimicking neutrophil-derived ROS, confirmed that disruption of *ahpC, ahpF*, and *dps* compromises bacterial fitness, and similarly for *uvrC* and *xseA*, underscoring the importance of DNA repair. Enrichment of *perR* mutants further supports a model in which constitutive derepression of antioxidant defenses is advantageous in this niche.[95–97] These findings are consistent with prior studies of neutrophil responses and ROS driven killing in *S. aureus* infection.[97]

In systemic tissues (kidney and spleen), fitness signatures shifted toward amino-acid catabolism, membrane remodeling, and energy coupled envelope biogenesis. Mutants in the branched-chain amino acid (BCAA) degradation pathway, *bkdAA, bkdAB, bkdB, ilvE, lpdA*, and in the uncharacterized *SAUSA300_0355* were strongly depleted in kidney and spleen but not in skin, pointing to a specific requirement for these pathways under systemic conditions.[91,98–100] BCAA catabolism supplies branched-chain acyl-CoAs that initiate branched-chain fatty acid (BCFA) synthesis via FabH, which in turn tunes membrane fluidity, resistance to environmental stress, and activation of two-component systems.[98,100–103] The link between membrane composition, envelope stress, and virulence regulation is well established, and our data position the BCFA pathway as a central hub in systemic infection.

SAUSA300_0355, annotated as a putative acetyl-CoA acyltransferase, likely connects BCAA- and acetyl-CoA–derived units to the mevalonate (MVA) pathway, which produces isoprenoid precursors used for menaquinone and undecaprenyl pyrophosphate (Und-PP) synthesis (30,57,58). These intermediates are required for respiration and for exporting peptidoglycan precursors and wall teichoic acid, so defects in MVA flux impair cell-wall integrity and respiratory capacity.[104–106] Competitive assays confirmed that mutants in *bkdAB* and *SAUSA300_0355* are severely compromised in systemic infection, supporting a model in which amino-acid catabolism and MVA-dependent isoprenoid synthesis create an integrated membrane respiration cell wall axis that is particularly important in kidney and spleen.

Parallel depletion of *SAUSA300_0458*, a putative ornithine/lysine/arginine decarboxylase, in systemic but not skin niches suggests that basic amino-acid catabolism and polyamine production may also contribute to deep-tissue fitness.[107–110] Polyamines are known to stabilize nucleic acids and membranes and to modulate stress responses in other bacteria, and recent evidence of endogenous putrescine and N-acetyl-putrescine in *S. aureus* indicates that this pathway may be more active than previously thought.[109,110] While our cautious interpretation avoids over-claiming functions not yet experimentally

validated, the systemic-specific depletion of *SAUSA300_0458* is consistent with a broader theme: amino-acid catabolism feeding global metabolic and envelope adaptations in deep tissues.

Taken together, Paper II delineates a tissue-tuned metabolic network wherein skin infection is dominated by oxidative stress and DNA damage control, whereas systemic infection is dominated by amino-acid catabolism, membrane remodeling, and energy-coupled envelope biosynthesis. Both regimes are layered on top of a shared backbone of nucleotide, carbon, and respiratory metabolism.

4.4 Fitness Determinants in Fresh Human Blood and Context-Dependent Definitions of "Fitness" (Paper III)

Paper III extended the TraDIS analysis to fresh human blood, an *ex vivo* system that captures key elements of bloodstream infection including viable neutrophils, monocytes, complement, antimicrobial peptides, and nutritional immunity factors.[35,80,97,99,111,112] Despite a detectable bottleneck during the blood exposure, UIS counts and effective population size indicated that the library remained sufficiently diverse for meaningful TraDIS inference. This is crucial, because blood imposes simultaneous nutrient, oxidative, and immune pressures that can rapidly collapse diversity if inoculum design and incubation conditions are not carefully controlled.[35,97,111,112]

The blood screen revealed a strong dependence on *de novo* purine biosynthesis (*purA, purB*), consistent with the view that the bloodstream offers limited salvageable purines due to host sequestration and rapid nucleotide turnover.[85,89,113] Competitive assays confirmed that *purA* and *purB* mutants are significantly impaired in human blood, underscoring the need for metabolic autonomy in nucleotide supply. Combined with prior data from pneumonia and osteomyelitis models, these findings reinforce purine biosynthetic enzymes as attractive but challenging antimicrobial targets due to homology with host enzymes.[84,89,90,114]

In line with the murine work, blood fitness also depended on central carbon metabolism and respiration. Mutants in *glpD, glpP, fbp, gpmA* and TCA-cycle genes (*acnA, icd*) were depleted, indicating a requirement for glycerol catabolism, gluconeogenesis, and TCA-derived reducing equivalents to power the electron transport chain.[86,91,93,94,115] The depletion of *pncA*, encoding nicotinamidase, further highlighted the importance of NAD^+ regeneration for sustaining respiratory flux and redox balance.[93,114,115] These patterns are consistent with the idea that energy generation and NADH/NADPH homeostasis form a central metabolic node that integrates inputs from glycerol, amino acids, and TCA intermediates to support survival in a nutrient-limited, oxidatively stressful environment.

Blood also sharpened the role of metal acquisition and heme homeostasis. Nutritional immunity restricts the availability of manganese, zinc, and iron through host proteins such as calprotectin, transferrin, and lactoferrin.[35,111,116,117] Mutants in manganese transport (*mntA, mntB, mntC*) and zinc uptake (*znuB, znuC*) were depleted, consistent with their established roles in systemic infection and oxidative-stress defense.[35,116,117] Surprisingly, only *fhuA* from the iron acquisition systems emerged as a robust fitness determinant, suggesting that siderophore-mediated iron import is particularly important under the specific conditions of our *ex vivo* blood model.[111,113,116]

The heme response regulator system hssRS and its efflux transporter hrtAB were also required for optimal blood fitness, in line with the dual role of heme as both nutrient iron source and pro-oxidant toxin.[94,118] Disruption of these systems impairs ability to detoxify excess heme and sensitizes bacteria to oxidative damage.[94,118] Interestingly, prior work in livestock-associated MRSA ST398 showed lineage-specific differences in the contribution of hssRS/hrtAB to blood fitness,[119] suggesting that heme toxicity management is an area where clonal background and ecological history strongly influence adaptation.

Perhaps the most conceptually intriguing findings in blood were the genes whose inactivation enhanced fitness. Insertions in *saeRS, sigB*, and downstream surface adhesins such as *fnbA* and *clfA* were enriched after blood exposure, indicating that full expression of these virulence and stress regulons imposes a cost in the bloodstream.[96,112,120] These loci are essential for tissue colonization, abscess formation, and immune evasion *in vivo*,[60,88,100,115] but in blood where adherence substrates are limited, and immune surveillance is intense high level expression of immunogenic surface proteins and toxins can accelerate opsonophagocytic killing. Thus, reduced expression of certain classical virulence factors can paradoxically increase short term fitness in blood, illustrating the context-dependent nature of "virulence" and "fitness."

Cross lineage and cross-experiment comparisons further emphasized context dependence. When we reanalyzed TraDIS data from ST398 strains and compared our fresh-blood results with a Tn-Seq study of USA300 in processed, leukocyte-depleted blood, we found relatively limited overlap outside of core metabolic and acquisition functions (e.g., *purA, purB, fhuA, glpD, fbp, mntABC, cntE, ubiE, pncA*).[69,112,119] Processed blood lacks active leukocytes and has reduced complement activity, which explains why mutants in DNA repair and oxidative-stress pathways that are disadvantaged in whole blood may appear neutral or even enriched in cell-depleted preparations (24,49).[97,111] These differences

illustrate a central point of this thesis: bacterial fitness is not an intrinsic property of a gene but an emergent property of the gene–environment interaction.

4.5 A Unified Model: Metabolic Backbone with Niche-Specific Specialization

Taken together, Papers I–III support a unified model in which *S. aureus* survival across host niches is built upon a conserved metabolic backbone overlaid with tissue-specific adaptations and context-dependent trade-offs.

5. Conserved Backbone
    a. *De novo* nucleotide biosynthesis, gluconeogenesis, TCA-cycle activity, and respiration (menaquinone/MVA pathways) are broadly required in skin, systemic tissues, and blood.
    b. Metal acquisition (Mn, Zn, Fe) and heme homeostasis are critical across host niches, with heme stress being most prominent in systemic tissues and blood where nutritional immunity is active.
    c. These pathways intersect with stress defenses (e.g., PPP-derived NADPH and ETC/quinone-mediated redox control) and are essential for supporting DNA repair, envelope biosynthesis, and energy intensive virulence programs.
6. Skin Abscess
    - Fitness dominated by oxidative stress defense (AhpCF, Dps) and DNA repair/SOS response (UvrABC, RecD, XseA).
    - Immune-driven ROS and RNS exposures create a landscape where maintaining genome integrity and detoxifying peroxides are paramount.
7. Kidney and Spleen (Systemic Infection)
    - Fitness dominated by amino-acid catabolism (BCAA, basic amino acids), BCFA-mediated membrane remodeling, and MVA-dependent isoprenoid synthesis.
    - These tissues demand robust energy generation, membrane integrity, and envelope biogenesis under conditions of fluctuating nutrients and strong but more distributed immune pressures.
8. Fresh Human Blood
    - Fitness dominated by nucleotide and energy metabolism, metal acquisition, and heme detoxification, alongside context-dependent costs of virulence expression.

- Genes that are essential for tissue colonization may be disadvantageous for transient survival in the bloodstream, highlighting a trade-off between "stealth" and "aggression."

This model helps reconcile some of the variability across previous Tn-Seq/TraDIS studies in *S. aureus*, by showing how differences in inoculum design, bottleneck severity, host compartment, and immune status can reshuffle the apparent hierarchy of essential genes.

4.6 Methodological Limitations and Future Directions

Despite the advances made, several limitations remain. TraDIS measures fitness in pooled mutant populations, so it underestimates the importance of secreted "public goods" and cooperative traits and cannot assess genes that are essential under all conditions because they lack insertions. Polar effects in operons complicate gene-level interpretation. Single-mutant infections were validated only for a subset of hits; broader validation and complementation would strengthen causal inference. The murine models, although physiologically relevant, cannot fully recapitulate the complexity of human infection, and the human blood experiments used *ex vivo* conditions without repeated day/batch experiments.

Nevertheless, the combination of optimized library construction, explicit bottleneck measurement, dual-contrast differential analysis, *in vitro* exclusion, read depth aware QC, and targeted competitive assays provides a rigorous framework that can be extended to other strains and infection models. Future work should integrate transcriptomics, metabolomics, and fluxomics with TraDIS to connect fitness phenotypes to pathway activity and metabolic flux and explore cross-strain portability by transducing key mutations into divergent lineages. Human-relevant models, such as 3D abscess systems, organoids, and chronic infection models, will help translate these findings into clinically meaningful insights.

Ultimately, this thesis demonstrates that *S. aureus* pathogenesis is best understood as the behavior of a tissue-tuned, metabolically wired, stress-responsive system, and that genome-wide fitness profiling, when paired with robust QC and deep biological interpretation, can uncover vulnerabilities that might be obscured in reductionist models.

CHAPTER V
CONCLUSION

5. Conclusion

This thesis provides a comprehensive functional genomic analysis of how *S. aureus* USA300 adapts to distinct host environments, integrating methodological refinement, rigorous TraDIS analytics, and targeted validation. Together, the three papers demonstrate that MRSA survival is governed not by a single universal set of essential genes but by the interaction between a conserved metabolic foundation and niche-specific pressures.

Paper I established that transposon library construction is not a neutral process: conventional temperature-sensitive curing can create strong, unrecognized selection on mutants involved in heat stress, cell wall stability, and DNA maintenance. By optimizing phage-based delivery and implementing a gradual curing protocol, we minimized these biases and produced a highly saturated, relatively unbiased library suitable for *in vivo* experimentation. This work highlights the need to treat library construction as a critical experimental variable when interpreting TIS data.

Using this optimized library, Papers II and III applied a stringent analytical framework -including high inoculum design, UIS-based bottleneck quantification, dual-contrast (IO and CO) comparisons, *in vitro* exclusion, and a bespoke read-depth–aware QC pipeline- to identify true fitness determinants while filtering out technical artifacts. This framework directly addressed limitations that have complicated earlier *S. aureus* Tn-seq studies, such as bottleneck distortion, PCR jackpotting, and misclassification of read-depth–only changes as biological signal. Validation using NTML mutants confirmed the accuracy of key findings.

Across infection models, a conserved metabolic backbone emerged: *de novo* nucleotide biosynthesis, gluconeogenesis, and TCA cycle activity supported MRSA survival across multiple host environments. However, each niche imposed distinct selective pressures that shaped specialized fitness signatures. In skin, oxidative, and genotoxic stresses dominated, leading to strong depletion of antioxidant systems (AhpCF, Dps) and DNA repair pathways (UvrABC, RecD, xseA), with enrichment of *perR* mutants reflecting the advantage of derepressed oxidative stress responses.

In systemic tissues (kidney and spleen), the fitness landscape shifted toward amino acid catabolism, branched chain fatty acid dependent membrane remodeling, and mevalonate/isoprenoid pathways feeding cell-wall and respiration-linked processes. The strong depletion of BCAA degradation genes and the uncharacterized *SAUSA300_0355* underscored the importance of metabolic inputs that sustain

envelope biogenesis and energy production under deep-tissue conditions. SAUSA300_0458, a putative basic amino-acid decarboxylase, showed similar systemic specificity, reinforcing the role of amino-acid catabolism in tissue adaptation.

In fresh human blood, fitness reflected the combined action of nutritional immunity, oxidative pressure, and energy limitation. Purine biosynthesis, central carbon metabolism, TCA-linked energy generation, and metal uptake systems (Mn^{++}, Zn^{++}) were critical, alongside heme detoxification through *hssRS/hrtAB*. Interestingly, several classical virulence regulators and adhesins (*saeRS*, *sigB*, *fnbA*, *clfA*) were disadvantageous, illustrating that high expression of immunogenic factors carries a cost in immune competent blood and emphasizing that "fitness" is context dependent.

Overall, these findings converge on a unified model: MRSA relies on a stable metabolic core but deploys highly tailored adaptations depending on the host niche. Skin infection is dominated by oxidative damage control; systemic infection depends on amino acid catabolism and membrane remodeling; and blood survival requires metabolic autonomy, metal acquisition, and heme stress management. This work clarifies inconsistencies in previous TIS datasets, provides methodological improvements to reduce false discoveries, and defines physiologically relevant adaptations that underlie MRSA survival during infection.

CHAPTER VI
REFERENCES
(GENERAL INTRODUCTION & DISCUSSION)

References

1. Parsons JB, Mourad A, Conlon BP, Kielian T, Fowler VG (2025). Methicillin-resistant and susceptible *Staphylococcus aureus*: tolerance, immune evasion and treatment. *Nat Rev Microbiol* 23, 1–19. https://doi.org/10.1038/s41579-025-01226-2.

2. Lowy FD (1998). *Staphylococcus aureus* infections. *N Engl J Med* 339, 520–532. https://doi.org/10.1056/NEJM199808203390806.

3. Tong SY C, Fowler VG, Skalla L, Holland TL (2025). Management of *Staphylococcus aureus* bacteremia: a review. *JAMA* 334, 798–808. https://doi.org/10.1001/jama.2025.4288.

4. Wertheim HFL, Melles DC, Vos MC, van Leeuwen W, van Belkum A, Verbrugh HA, Nouwen JL (2005). The role of nasal carriage in *Staphylococcus aureus* infections. *Lancet Infect Dis* 5, 751–762. https://doi.org/10.1016/S1473-3099(05)70295-4.

5. van Belkum A, Verkaik NJ, de Vogel CP, Boelens HA, Verveer J, Nouwen JL, Verbrugh HA, Wertheim HFL (2009). Reclassification of *Staphylococcus aureus* nasal carriage types. *J Infect Dis* 199, 1820–1826. https://doi.org/10.1086/599119.

6. Foster TJ (2019). Surface proteins of *Staphylococcus aureus*. *Microbiol Spectr* 7, 599–617. https://doi.org/10.1128/9781683670131.ch38.

7. Spaan AN, van Strijp JAG, Torres VJ (2017). Leukocidins: staphylococcal bi-component pore-forming toxins find their receptors. *Nat Rev Microbiol* 15, 435–447. https://doi.org/10.1038/nrmicro.2017.27.

8. Jenul C, Horswill AR (2019). Regulation of *Staphylococcus aureus* virulence. *Microbiol Spectr* 7, GPP3-0031-2018. https://doi.org/10.1128/microbiolspec.GPP3-0031-2018.

9. Heim CE, Vidlak D, Scherr TD, Kozel JA, Holzapfel M, Muirhead DE, et al. (2014). Myeloid-derived suppressor cells contribute to *Staphylococcus aureus* orthopedic biofilm infection. *J Immunol* 192, 3778–3792. https://doi.org/10.4049/jimmunol.1303408.

10. Heim CE, Vidlak D, Scherr TD, Hartman CW, Garvin KL, Kielian T (2015). IL-12 promotes myeloid-derived suppressor cell recruitment and bacterial persistence during *Staphylococcus aureus* orthopedic implant infection. *J Immunol* 194, 3861–3872. https://doi.org/10.4049/jimmunol.1402689.

11. Heim CE, Vidlak D, Kielian T (2015). Interleukin-10 production by myeloid-derived suppressor cells contributes to bacterial persistence during *Staphylococcus aureus* orthopedic biofilm infection. *J Leukoc Biol* 98, 1003–1013. https://doi.org/10.1189/jlb.4VMA0315-125RR.

12. Barber M (1961). Methicillin-resistant staphylococci. *J Clin Pathol* 14, 385–393. https://doi.org/10.1136/jcp.14.4.385.

13. Hartman BJ, Tomasz A (1984). Low-affinity penicillin-binding protein associated with beta-lactam resistance in *Staphylococcus aureus*. *J Bacteriol* 158, 513–516. https://doi.org/10.1128/jb.158.2.513-516.1984.

14. Boucher HW, Corey GR (2008). Epidemiology of methicillin-resistant *Staphylococcus aureus*. *Clin Infect Dis* 46, S344–S349. https://doi.org/10.1086/533590.

15. Moran GJ, Krishnadasan A, Gorwitz RJ, Fosheim GE, McDougal LK, Carey RB, Talan DA (2006). Methicillin-resistant *S. aureus* infections among patients in the emergency department. *N*

Engl J Med 355, 666–674. https://doi.org/10.1056/NEJMoa055356.

16. Otto M (2013). Community-associated MRSA: what makes them special? *Int J Med Microbiol* 303, 324–330. https://doi.org/10.1016/j.ijmm.2013.02.007.

17. Diep BA, Gill SR, Chang RF, Phan THV, Chen JH, Davidson MG, et al. (2006). Complete genome sequence of USA300, an epidemic clone of community-acquired meticillin-resistant *Staphylococcus aureus*. *Lancet* 367, 731–739. https://doi.org/10.1016/S0140-6736(06)68231-7.

18. Murray CJ, Ikuta KS, Sharara F, Swetschinski L, Robles Aguilar G, Gray A, et al. (2022). Global burden of bacterial antimicrobial resistance in 2019: a systematic analysis. *Lancet* 399, 629–655. https://doi.org/10.1016/S0140-6736(21)02724-0.

19. Long SW, Olsen RJ, Mehta SC, Palzkill T, Cernoch PL, Perez KK, et al. (2014). PBP2a mutations causing high-level ceftaroline resistance in clinical methicillin-resistant *Staphylococcus aureus* isolates. *Antimicrob Agents Chemother* 58, 6668–6674. https://doi.org/10.1128/AAC.03622-14.

20. Harrison EM, Ba X, Blane B, Ellington MJ, Loeffler A, Hill RLR, et al. (2016). PBP2a substitutions linked to ceftaroline resistance in MRSA isolates from the UK. *J Antimicrob Chemother* 71, 268–269. https://doi.org/10.1093/jac/dkv317.

21. Fischer A, Yang SJ, Bayer AS, Vaezzadeh AR, Herzig S, Stenz L, Girard M, Sakoulas G, Scherl A, Yeaman MR, et al. (2011). Daptomycin resistance mechanisms in clinically derived *Staphylococcus aureus* strains assessed by a combined transcriptomics and proteomics approach. *J Antimicrob Chemother* **66**, 1696–1711. https://doi.org/10.1093/jac/dkr195.

22. Ruffier D'Epenoux, L., Barbier, P., Fayoux, E., Guillouzouic, A., Lecomte, R., Deschanvres, C., Nich, C., Bemer, P., Gregoire, M., and Corvec, S. (2024). Dalbavancin-resistant Staphylococcus epidermidis in vivo selection following a prosthetic joint infection: phenotypic and genomic characterization. *JAC-Antimicrob. Resist.* 6. https://doi.org/10.1093/JACAMR/DLAE163.

23. Kussmann, M., Karer, M., Obermueller, M., Schmidt, K., Barousch, W., Moser, D., Nehr, M., Ramharter, M., Poeppl, W., Makristathis, A., et al. (2018). Emergence of a dalbavancin induced glycopeptide/lipoglycopeptide non-susceptible Staphylococcus aureus during treatment of a cardiac device-related endocarditis. *Emerg. Microbes Infect.* 7. https://doi.org/10.1038/S41426-018-0205-Z.

24. Fey PD, Endres JL, Yajjala VK, Widhelm TJ, Boissy RJ, Bose JL, Bayles KW (2013). A genetic resource for rapid and comprehensive phenotype screening of nonessential *Staphylococcus aureus* genes. *mBio* 4, e00537–12. https://doi.org/10.1128/mBio.00537-12.

25. Coll AG, Brown AF, Gaillard ME, Wheeler R, Molina-Santiago C, Pei XY, et al. (2025). Adaptive trajectories of *Staphylococcus aureus* during human nasal colonization. *Nat Commun* **16**, 112. https://doi.org/10.1038/s41467-024-55186-x.

26. Balasubramanian D, Harper L, Shopsin B, Torres VJ (2017). *Staphylococcus aureus* pathogenesis in diverse host environments. *Pathog Dis* **75**, ftx005. https://doi.org/10.1093/femspd/ftx005.

27. Dastgheyb, S.S., and Otto, M. (2015). Staphylococcal adaptation to diverse physiologic niches: an overview of transcriptomic and phenotypic changes in different biological environments. Future Microbiol. 10, 1981–1995. https://doi.org/10.2217/FMB.15.116.

28. Laux, C., Peschel, A., and Krismer, B. (2019). *Staphylococcus aureus* colonization of the human nose and interaction with other microbiome members. Microbiol. Spectr. 7, 723–730.

https://doi.org/10.1128/9781683670131.ch45.

29. Wang, S., Peng, G., Abudouwanli, A., Yang, M., Sun, Q., Zhao, W., et al. (2025). The interaction between the skin microbiome and antimicrobial peptides within the epidermal immune microenvironment: bridging insights into atopic dermatitis. Allergol. Int. (in press). https://doi.org/10.1016/J.ALIT.2025.08.002.

30. Boff, D., Chandrasekaran, R., Putzel, G., Kratofil, R.M., Zheng, X., Castellaw, A., et al. (2025). *Staphylococcus aureus* LukMF′ targets neutrophils to promote skin and soft tissue infection. Sci. Adv. 11, eadr5240. https://doi.org/10.1126/SCIADV.ADR5240.

31. Guiberson, E.R., Weiss, A., Ryan, D.J., Monteith, A.J., Sharman, K., Gutierrez, D.B., et al. (2020). Spatially targeted proteomics of the host–pathogen interface during staphylococcal abscess formation. ACS Infect. Dis. 7, 101–113. https://doi.org/10.1021/ACSINFECDIS.0C00647.

32. Potter, A.D., Butrico, C.E., Ford, C.A., Curry, J.M., Trenary, I.A., Tummarakota, S.S., et al. (2020). Host nutrient milieu drives an essential role for aspartate biosynthesis during invasive *Staphylococcus aureus* infection. Proc. Natl. Acad. Sci. U. S. A. 117, 12394–12401. https://doi.org/10.1073/pnas.1922211117.

33. Chen, Y., Liu, Z, Lin, Z., Lu, M., Fu, Y., Liu, G., and Yu, B. (2023). The effect of *Staphylococcus aureus* on innate and adaptive immunity and potential immunotherapy for *S. aureus*-induced osteomyelitis. Front. Immunol. 14, 1219895. https://doi.org/10.3389/FIMMU.2023.1219895.

34. Juttukonda, L.J., Berends, E.T.M., Zackular, J.P., Moore, J.L., Stier, M.T., Zhang, Y., et al. (2017). Dietary manganese promotes staphylococcal infection of the heart. Cell Host Microbe 22, 531–542.e8. https://doi.org/10.1016/j.chom.2017.08.009.

35. Murdoch, C.C., and Skaar, E.P. (2022). Nutritional immunity: the battle for nutrient metals at the host–pathogen interface. Nat. Rev. Microbiol. 20, 657–670. https://doi.org/10.1038/s41579-022-00745-6.

36. Marchetti, M., De Bei, O., Bettati, S., Campanini, B., Kovachka, S., Gianquinto, E., et al. (2020). Iron metabolism at the interface between host and pathogen: from nutritional immunity to antibacterial development. Int. J. Mol. Sci. 21, 2145. https://doi.org/10.3390/IJMS21062145.

37. Lu, K.-Y., Yang, X., Eldridge, M.J.G., Sun, R., Giorgio, R.T., Morris, B.I., et al. (2025). A host-directed adjuvant sensitizes intracellular bacterial persisters to antibiotics. Nat. Microbiol. 10, 3013–3025. https://doi.org/10.1038/s41564-025-02124-2.

38. Pidwill, G.R., Gibson, J.F., Cole, J., Renshaw, S.A., and Foster, S.J. (2021). The role of macrophages in *Staphylococcus aureus* infection. Front. Immunol. 11, 620339. https://doi.org/10.3389/FIMMU.2020.620339.

39. Flannagan, R.S., Heit, B., and Heinrichs, D.E. (2015). Antimicrobial mechanisms of macrophages and the immune evasion strategies of *Staphylococcus aureus*. Pathogens 4, 826–868. https://doi.org/10.3390/PATHOGENS4040826.

40. Xu, H., Wang, S., Liu, X., Li, M., Wang, X., Chen, H., et al. (2025). Strategies for survival of *Staphylococcus aureus* in host cells. Int. J. Mol. Sci. 26, 720. https://doi.org/10.3390/IJMS26020720.

41. Rowe, S.E., Wagner, N.J., Li, L., Beam, J.E., Wilkinson, A.D., Radlinski, L.C., et al. (2020). Reactive oxygen species induce antibiotic tolerance during systemic *Staphylococcus aureus*

infection. Nat. Microbiol. 5, 282–290. https://doi.org/10.1038/s41564-019-0627-y.

42. Garcia-Maset, R., Chu, V., Yuen, N., Blumgart, D., Yoon, J., Murray, B.O., et al. (2025). Effect of host microenvironment and bacterial lifestyles on antimicrobial sensitivity and implications for susceptibility testing. npj Antimicrob. Resist. 3, 42. https://doi.org/10.1038/s44259-025-00113-3.

43. Zhao, R., Xu, L., Chen, J., Yang, Y., Guo, X., Dai, M., et al. (2024). Itaconate induces tolerance of *Staphylococcus aureus* to aminoglycoside antibiotics. Front. Microbiol. 15, 1450085. https://doi.org/10.3389/FMICB.2024.1450085.

44. Zhou, Y., Liao, H., Pei, L., and Pu, Y. (2023). Combatting persister cells: the daunting task in post-antibiotics era. Cell Insight 2, 100104. https://doi.org/10.1016/J.CELLIN.2023.100104.

45. Heim, C.E., West, S.C., Ali, H., and Kielian, T. (2018). Heterogeneity of Ly6G+ Ly6C+ myeloid-derived suppressor cell infiltrates during *Staphylococcus aureus* biofilm infection. Infect. Immun. 86, e00684–18. https://doi.org/10.1128/IAI.00684-18.

46. Heim, C.E., Bosch, M.E., Yamada, K.J., Aldrich, A.L., Chaudhari, S.S., Klinkebiel, D., et al. (2020). Lactate production by *Staphylococcus aureus* biofilm inhibits HDAC11 to reprogramme the host immune response during persistent infection. Nat. Microbiol. 5, 1271–1284. https://doi.org/10.1038/S41564-020-0756-3.

47. Bosch, M.E., Bertrand, B.P., Heim, C.E., Alqarzaee, A.A., Chaudhari, S.S., Aldrich, A.L., et al. (2020). *Staphylococcus aureus* ATP synthase promotes biofilm persistence by influencing innate immunity. mBio 11, e01581–20. https://doi.org/10.1128/MBIO.01581-20.

48. Bertrand, B.P., Heim, C.E., West, S.C., Chaudhari, S.S., Ali, H., Thomas, V.C., and Kielian, T. (2022). Role of *Staphylococcus aureus* formate metabolism during prosthetic joint infection. Infect. Immun. 90, e00428–22. https://doi.org/10.1128/IAI.00428-22.

49. Monk, I.R., and Foster, T.J. (2012). Genetic manipulation of staphylococci – breaking through the barrier. Front. Cell. Infect. Microbiol. 2, 49. https://doi.org/10.3389/FCIMB.2012.00049.

50. van Opijnen, T., and Camilli, A. (2013). Transposon insertion sequencing: a new tool for systems-level analysis of microorganisms. Nat. Rev. Microbiol. 11, 435–442. https://doi.org/10.1038/NRMICRO3033.

51. van Opijnen, T., Bodi, K.L., and Camilli, A. (2009). Tn-seq: high-throughput parallel sequencing for fitness and genetic interaction studies in microorganisms. Nat. Methods 6, 767–772. https://doi.org/10.1038/nmeth.1377.

52. Gawronski, J.D., Wong, S.M.S., Giannoukos, G., Ward, D.V., and Akerley, B.J. (2009). Tracking insertion mutants within libraries by deep sequencing and a genome-wide screen for *Haemophilus* genes required in the lung. Proc. Natl. Acad. Sci. U. S. A. 106, 16422–16427. https://doi.org/10.1073/PNAS.0906627106.

53. Goodman, A.L., McNulty, N.P., Zhao, Y., Leip, D., Mitra, R.D., Lozupone, C.A., et al. (2009). Identifying genetic determinants needed to establish a human gut symbiont in its habitat. Cell Host Microbe 6, 279–289. https://doi.org/10.1016/J.CHOM.2009.08.003.

54. Langridge, G.C., Phan, M.D., Turner, D.J., Perkins, T.T., Parts, L., Haase, J., et al. (2009). Simultaneous assay of every *Salmonella Typhi* gene using one million transposon mutants. Genome Res. 19, 2308–2316. https://doi.org/10.1101/GR.097097.109.

55. Chao, M.C., Abel, S., Davis, B.M., and Waldor, M.K. (2016). The design and analysis of

transposon insertion sequencing experiments. Nat. Rev. Microbiol. 14, 119–128. https://doi.org/10.1038/nrmicro.2015.7.

56. Barquist, L., Mayho, M., Cummins, C., Cain, A.K., Boinett, C.J., Page, A.J., et al. (2016). The TraDIS toolkit: sequencing and analysis for dense transposon mutant libraries. Bioinformatics 32, 1109–1111. https://doi.org/10.1093/BIOINFORMATICS/BTW022.

57. Wiles, T.J., Norton, J.P., Russell, C.W., Dalley, B.K., Fischer, K.F., and Mulvey, M.A. (2013). Combining quantitative genetic footprinting and trait enrichment analysis to identify fitness determinants of a bacterial pathogen. PLoS Genet. 9, e1003716. https://doi.org/10.1371/JOURNAL.PGEN.1003716.

58. Santiago, M., Matano, L.M., Moussa, S.H., Gilmore, M.S., Walker, S., and Meredith, T.C. (2015). A new platform for ultra-high density *Staphylococcus aureus* transposon libraries. BMC Genomics 16, 252. https://doi.org/10.1186/S12864-015-1361-3.

59. Cain, A.K., Barquist, L., Goodman, A.L., Paulsen, I.T., Parkhill, J., and van Opijnen, T. (2020). A decade of advances in transposon-insertion sequencing. Nat. Rev. Genet. 21, 526–540. https://doi.org/10.1038/s41576-020-0244-x.

60. Valentino, M.D., Foulston, L., Sadaka, A., Kos, V.N., Villet, R.A., Maria, J.S., et al. (2014). Genes contributing to *Staphylococcus aureus* fitness in abscess- and infection-related ecologies. mBio 5, e01729–14. https://doi.org/10.1128/MBIO.01729-14.

61. Grosser, M.R., Paluscio, E., Thurlow, L.R., Dillon, M.M., Cooper, V.S., Kawula, T.H., and Richardson, A.R. (2018). Genetic requirements for *Staphylococcus aureus* nitric oxide resistance and virulence. PLoS Pathog. 14, e1006907. https://doi.org/10.1371/JOURNAL.PPAT.1006907.

62. Peyrusson, F., Nguyen, T.K., Najdovski, T., and Van Bambeke, F. (2022). Host cell oxidative stress induces dormant *Staphylococcus aureus* persisters. Microbiol. Spectr. 10, e02313–21. https://doi.org/10.1128/spectrum.02313-21.

63. Hood, M.I., and Skaar, E.P. (2012). Nutritional immunity: transition metals at the pathogen–host interface. Nat. Rev. Microbiol. 10, 525–537. https://doi.org/10.1038/nrmicro2836.

64. Flannagan, R.S., Cosío, G., and Grinstein, S. (2009). Antimicrobial mechanisms of phagocytes and bacterial evasion strategies. Nat. Rev. Microbiol. 7, 355–366. https://doi.org/10.1038/nrmicro2128.

65. Howden, B.P., Giulieri, S.G., Wong Fok Lung, T., Baines, S.L., Sharkey, L.K., Lee, J.Y.H., et al. (2023). *Staphylococcus aureus* host interactions and adaptation. Nat. Rev. Microbiol. 21, 380–395. https://doi.org/10.1038/s41579-023-00852-y.

66. Cheung, G.Y.C., Bae, J.S., and Otto, M. (2021). Pathogenicity and virulence of *Staphylococcus aureus*. Virulence 12, 547–569. https://doi.org/10.1080/21505594.2021.1878688.

67. van Opijnen, T., and Levin, H.L. (2020). Transposon insertion sequencing, a global measure of gene function. Annu. Rev. Genet. 54, 337–365. https://doi.org/10.1146/ANNUREV-GENET-112618-043838.

68. DeJesus, M.A., Ambadipudi, C., Baker, R., Sassetti, C., and Ioerger, T.R. (2015). TRANSIT – a software tool for Himar1 TnSeq analysis. PLoS Comput. Biol. 11, e1004401. https://doi.org/10.1371/JOURNAL.PCBI.1004401.

69. Christiansen, M.T., Kaas, R.S., Chaudhuri, R.R., Holmes, M.A., Hasman, H., and Aarestrup, F.M.

(2014). Genome-wide high-throughput screening to investigate essential genes involved in methicillin-resistant *Staphylococcus aureus* sequence type 398 survival. PLoS One 9, e89018. https://doi.org/10.1371/JOURNAL.PONE.0089018.

70. Abel, S., Abel zur Wiesch, P., Chang, H.H., Davis, B.M., Lipsitch, M., and Waldor, M.K. (2015). Sequence tag–based analysis of microbial population dynamics. Nat. Methods 12, 223–226. https://doi.org/10.1038/nmeth.3253.

71. Mahmutovic, A., Abel zur Wiesch, P., and Abel, S. (2020). Selection or drift: the population biology underlying transposon insertion sequencing experiments. Comput. Struct. Biotechnol. J. 18, 791–804. https://doi.org/10.1016/J.CSBJ.2020.03.021.

72. Yajjala, V.K., Widhelm, T.J., Endres, J.L., Fey, P.D., and Bayles, K.W. (2014). Generation of a transposon mutant library in *Staphylococcus aureus* and *Staphylococcus epidermidis* using bursa aurealis. Methods Mol. Biol. 1373, 103–110. https://doi.org/10.1007/7651_2014_189.

73. Bossé, J.T., Li, Y., Leanse, L.G., Zhou, L., Chaudhuri, R.R., Peters, S.E., et al. (2021). Rationally designed mariner vectors for functional genomic analysis of *Actinobacillus pleuropneumoniae* and other Pasteurellaceae species by transposon-directed insertion-site sequencing (TraDIS). Anim. Dis. 1, 29. https://doi.org/10.1186/S44149-021-00026-4.

74. Choudhery, S., Brown, A.J., Akusobi, C., Rubin, E.J., Sassetti, C.M., and Ioerger, T.R. (2021). Modeling site-specific nucleotide biases affecting Himar1 transposon insertion frequencies in TnSeq data sets. mSystems 6, e00876–21. https://doi.org/10.1128/MSYSTEMS.00876-21.

75. Ingmer, H., Gerlach, D., and Wolz, C. (2019). Temperate phages of *Staphylococcus aureus*. Microbiol. Spectr. 7, GPP3-0058-2018. https://doi.org/10.1128/MICROBIOLSPEC.GPP3-0058-2018.

76. Li, X., Koç, C., Kühner, P., Stierhof, Y.D., Krismer, B., Enright, M.C., et al. (2016). An essential role for the baseplate protein Gp45 in phage adsorption to *Staphylococcus aureus*. Sci. Rep. 6, 26455. https://doi.org/10.1038/srep26455.

77. Nygaard, R., Romaniuk, J.A.H., Rice, D.M., and Cegelski, L. (2015). Spectral snapshots of bacterial cell-wall composition and the influence of antibiotics by whole-cell NMR. Biophys. J. 108, 1380–1389. https://doi.org/10.1016/J.BPJ.2015.01.037.

78. van Dalen, R., Peschel, A., and van Sorge, N.M. (2020). Wall teichoic acid in *Staphylococcus aureus* host interaction. Trends Microbiol. 28, 985–998. https://doi.org/10.1016/J.TIM.2020.05.017.

79. Singh, V.K., Syring, M., Singh, A., Singhal, K., Dalecki, A., and Johansson, T. (2012). An insight into the significance of the DnaK heat shock system in *Staphylococcus aureus*. Int. J. Med. Microbiol. 302, 242–252. https://doi.org/10.1016/J.IJMM.2012.05.001.

80. Proctor, R.A., von Eiff, C., Kahl, B.C., Becker, K., McNamara, P., Herrmann, M., and Peters, G. (2006). Small colony variants: a pathogenic form of bacteria that facilitates persistent and recurrent infections. Nat. Rev. Microbiol. 4, 295–305. https://doi.org/10.1038/NRMICRO1384.

81. Freiberg, J.A., Reyes Ruiz, V.M., Gimza, B.D., Murdoch, C.C., Green, E.R., Curry, J.M., et al. (2024). Restriction of arginine induces antibiotic tolerance in *Staphylococcus aureus*. Nat. Commun. 15, 6734. https://doi.org/10.1038/s41467-024-51144-9.

82. Li, G., Shen, W., Gong, Y., Li, M., Rao, X., Liu, Q., et al. (2022). Essential fitness repertoire of

Staphylococcus aureus during co-infection with *Acinetobacter baumannii* in vivo. mSystems 7, e00338–22. https://doi.org/10.1128/MSYSTEMS.00338-22.

83. Kim, G.L., Hooven, T.A., Norambuena, J., Li, B., Boyd, J.M., Yang, J.H., and Parker, D. (2021). Growth and stress tolerance comprise independent metabolic strategies critical for *Staphylococcus aureus* infection. mBio 12, e00814–21. https://doi.org/10.1128/mBio.00814-21.

84. Goncheva, M.I., Chin, D., and Heinrichs, D.E. (2022). Nucleotide biosynthesis: the base of bacterial pathogenesis. Trends Microbiol. 30, 793–804. https://doi.org/10.1016/J.TIM.2021.12.007.

85. Goncheva, M.I., Flannagan, R.S., and Heinrichs, D.E. (2020). De novo purine biosynthesis is required for intracellular growth of *Staphylococcus aureus* and for the hypervirulence phenotype of a *purR* mutant. Infect. Immun. 88, e00104–20. https://doi.org/10.1128/IAI.00104-20.

86. Somerville, G.A., and Proctor, R.A. (2009). At the crossroads of bacterial metabolism and virulence factor synthesis in staphylococci. Microbiol. Mol. Biol. Rev. 73, 233–248. https://doi.org/10.1128/mmbr.00005-09.

87. Jatana, S., Homer, C.R., Madajka, M., Ponti, A.K., Kabi, A., Papay, F., and McDonald, C. (2018). Pyrimidine synthesis inhibition enhances cutaneous defenses against antibiotic resistant bacteria through activation of NOD2 signaling. Sci. Rep. 8, 8708. https://doi.org/10.1038/S41598-018-27012-0.

88. Szafranska, A.K., Oxley, A.P.A., Chaves-Moreno, D., Horst, S.A., Roßlenbroich, S., Peters, G., et al. (2014). High-resolution transcriptomic analysis of the adaptive response of *Staphylococcus aureus* during acute and chronic phases of osteomyelitis. mBio 5, e01775–14. https://doi.org/10.1128/mBio.01775-14.

89. Kofoed, E.M., Yan, D., Katakam, A.K., Reichelt, M., Lin, B., Kim, J., et al. (2016). De novo guanine biosynthesis but not the riboswitch-regulated purine salvage pathway is required for *Staphylococcus aureus* infection in vivo. J. Bacteriol. 198, 2001–2015. https://doi.org/10.1128/JB.00051-16.

90. Li, L., Bayer, A.S., Cheung, A., Lu, L., Abdelhady, W., Donegan, N.P., et al. (2020). The stringent response contributes to persistent methicillin-resistant *Staphylococcus aureus* endovascular infection through the purine biosynthetic pathway. J. Infect. Dis. 222, 1188–1198. https://doi.org/10.1093/INFDIS/JIAA202.

91. Halsey, C.R., Lei, S., Wax, J.K., Lehman, M.K., Nuxoll, A.S., Steinke, L., et al. (2017). Amino acid catabolism in *Staphylococcus aureus* and the function of carbon catabolite repression. mBio 8, e01434–16. https://doi.org/10.1128/MBIO.01434-16.

92. Troitzsch, A., Van Loi, V., Methling, K., Zühlke, D., Lalk, M., Riedel, K., et al. (2021). Carbon source-dependent reprogramming of anaerobic metabolism in *Staphylococcus aureus*. J. Bacteriol. 203, e00639–20. https://doi.org/10.1128/JB.00639-20.

93. Ledala, N., Zhang, B., Seravalli, J., Powers, R., and Somerville, G.A. (2014). Influence of iron and aeration on *Staphylococcus aureus* growth, metabolism, and transcription. J. Bacteriol. 196, 2178–2189. https://doi.org/10.1128/JB.01475-14.

94. Tan, X., Ramond, E., Jamet, A., Barnier, J.P., Decaux-Tramoni, B., Dupuis, M., et al. (2019). Transketolase of *Staphylococcus aureus* in the control of master regulators of stress response during infection. J. Infect. Dis. 220, 1967–1976. https://doi.org/10.1093/INFDIS/JIZ404.

95. Horsburgh, M.J., Clements, M.O., Crossley, H., Ingham, E., and Foster, S.J. (2001). PerR controls oxidative stress resistance and iron storage proteins and is required for virulence in *Staphylococcus aureus*. Infect. Immun. 69, 3744–3754. https://doi.org/10.1128/IAI.69.6.3744-3754.2001.

96. Ji, C.-J., Kim, J.-H., Won, Y.-B., Lee, Y.-E., Choi, T.-W., Ju, S.-Y., et al. (2015). *Staphylococcus aureus* PerR is a hypersensitive hydrogen peroxide sensor using iron-mediated histidine oxidation. J. Biol. Chem. 290, 20374–20386. https://doi.org/10.1074/jbc.M115.664961.

97. Rigby, K.M., and DeLeo, F.R. (2012). Neutrophils in innate host defense against *Staphylococcus aureus* infections. Semin. Immunopathol. 34, 237–259. https://doi.org/10.1007/S00281-011-0295-3.

98. Frank, M.W., Whaley, S.G., and Rock, C.O. (2021). Branched-chain amino acid metabolism controls membrane phospholipid structure in *Staphylococcus aureus*. J. Biol. Chem. 297, 101255. https://doi.org/10.1016/j.jbc.2021.101255.

99. Golla, R.M., Mishra, B., Dang, X., Narayana, L., Li, A., Xu, L., and Wang, G. (2020). Resistome of *Staphylococcus aureus* in response to human cathelicidin LL-37 and its engineered antimicrobial peptides. ACS Infect. Dis. 6, 1866–1881. https://doi.org/10.1021/acsinfecdis.0c00112.

100. Singh, V.K., Hattangady, D.S., Giotis, E.S, Singh, A.K., Chamberlain, N.R., Stuart, M.K., and Wilkinson, B.J. (2008). Insertional inactivation of branched-chain α-keto acid dehydrogenase in *Staphylococcus aureus* leads to decreased branched-chain membrane fatty acid content and increased susceptibility to certain stresses. Appl. Environ. Microbiol. 74, 5882–5890. https://doi.org/10.1128/AEM.00882-08.

101. Pendleton, A., Yeo, W.S., Alqahtani, S., DiMaggio, D.A., Stone, C.J., Li, Z., et al. (2022). Regulation of the Sae two-component system by branched-chain fatty acids in *Staphylococcus aureus*. mBio 13, e01472–22. https://doi.org/10.1128/mbio.01472-22.

102. Kaneda, T. (1991). Iso- and anteiso-fatty acids in bacteria: biosynthesis, function, and taxonomic significance. Microbiol. Rev. 55, 288–302. https://doi.org/10.1128/mr.55.2.288-302.1991.

103. Whaley, S.G., Frank, M.W., and Rock, C.O. (2023). A short-chain acyl-CoA synthetase that supports branched-chain fatty acid synthesis in *Staphylococcus aureus*. J. Biol. Chem. 299, 103036. https://doi.org/10.1016/j.jbc.2023.103036.

104. Matsumoto, Y., Yasukawa, J., Ishii, M., Hayashi, Y., Miyazaki, S., and Sekimizu, K. (2016). A critical role of mevalonate for peptidoglycan synthesis in *Staphylococcus aureus*. Sci. Rep. 6, 22894. https://doi.org/10.1038/SREP22894.

105. Balibar, C.J., Shen, X., and Tao, J. (2009). The mevalonate pathway of *Staphylococcus aureus*. J. Bacteriol. 191, 851–861. https://doi.org/10.1128/JB.01357-08.

106. Reichert, S., Ebner, P., Bonetti, E.J., Luqman, A., Nega, M., Schrenzel, J., et al. (2018). Genetic adaptation of a mevalonate pathway deficient mutant in *Staphylococcus aureus*. Front. Microbiol. 9, 1539. https://doi.org/10.3389/FMICB.2018.01539.

107. Michael, A.J. (2016). Polyamines in eukaryotes, bacteria, and archaea. J. Biol. Chem. 291, 14896–14903. https://doi.org/10.1074/jbc.R116.734780.

108. Lillie, I.M., Booth, C.E., Horvath, A.E., Mondragon, M., Engevik, M.A., and Horvath, T.D. (2024). Characterizing arginine, ornithine, and putrescine pathways in enteric pathobionts.

Microbiol. Open 13, e1408. https://doi.org/10.1002/mbo3.1408.

109. Seravalli, J., and Portugal, F. (2023). Putrescine detected in strains of *Staphylococcus aureus*. Pathogens 12, 881. https://doi.org/10.3390/pathogens12070881.

110. Li, B., Liang, J., Hanfrey, C.C., Phillips, M.A., and Michael, A.J. (2021). Discovery of ancestral L-ornithine and L-lysine decarboxylases reveals parallel, pseudoconvergent evolution of polyamine biosynthesis. J. Biol. Chem. 297, 101219. https://doi.org/10.1016/j.jbc.2021.101219.

111. Kwiecinski, J.M., and Horswill, A.R. (2020). *Staphylococcus aureus* bloodstream infections: pathogenesis and regulatory mechanisms. Curr. Opin. Microbiol. 53, 51–60. https://doi.org/10.1016/J.MIB.2020.02.005.

112. Malachowa, N., Whitney, A.R., Kobayashi, S.D., Sturdevant, D.E., Kennedy, A.D., Braughton, K.R., et al. (2011). Global changes in *Staphylococcus aureus* gene expression in human blood. PLoS One 6, e18617. https://doi.org/10.1371/JOURNAL.PONE.0018617.

113. Hammer, N.D., and Skaar, E.P. (2011). Molecular mechanisms of *Staphylococcus aureus* iron acquisition. Annu. Rev. Microbiol. 65, 129–147. https://doi.org/10.1146/ANNUREV-MICRO-090110-102851.

114. Kim, J., Kim, G.L., Norambuena, J., Boyd, J.M., and Parker, D. (2023). Impact of the pentose phosphate pathway on metabolism and pathogenesis of *Staphylococcus aureus*. PLoS Pathog. 19, e1011531. https://doi.org/10.1371/JOURNAL.PPAT.101153.

115. Li, J., Hou, W., Chang, J., Tian, X., He, M., Zhang, Z., and Shi, C. (2025). The pivotal role of *acnA* in linking carbon metabolism to virulence and antimicrobial resistance in methicillin-resistant *Staphylococcus aureus*. J. Antimicrob. Chemother. 80, 2934–2944. https://doi.org/10.1093/JAC/DKAF317.

116. Kehl-Fie, T.E., Zhang, Y., Moore, J.L., Farrand, A.J., Hood, M.I., Rathi, S., et al. (2013). MntABC and MntH contribute to systemic *Staphylococcus aureus* infection by competing with calprotectin for nutrient manganese. Infect. Immun. 81, 3395–3405. https://doi.org/10.1128/IAI.00420-13.

117. Chen, C., and Hooper, D.C. (2019). Intracellular accumulation of staphylopine impairs the fitness of *Staphylococcus aureus cntE* mutant. FEBS Lett. 593, 1213–1222. https://doi.org/10.1002/1873-3468.13396.

118. Wakeman, C.A., Hammer, N.D., Stauff, D.L., Attia, A.S., Anzaldi, L.L., Dikalov, S.I., et al. (2012). Menaquinone biosynthesis potentiates haem toxicity in *Staphylococcus aureus*. Mol. Microbiol. 86, 1376–1392. https://doi.org/10.1111/MMI.12063.

119. Ba, X., Matuszewska, M., Kalmar, L., Fan, J., Zou, G., Corander, D., et al. (2023). High-throughput mutagenesis reveals a role for antimicrobial resistance- and virulence-associated mobile genetic elements in *Staphylococcus aureus* host adaptation. Microbiol. Spectr. 11, e04213–22. https://doi.org/10.1128/SPECTRUM.04213-22.

120. Pané-Farré, J., Jonas, B., Förstner, K., Engelmann, S., and Hecker, M. (2006). The σB regulon in *Staphylococcus aureus* and its regulation. Int. J. Med. Microbiol. 296, 237–258.